

**PARTIAL OXIDATION OF PROPANE OVER VANADIUM-  
CONTAINING ZEOLITE CATALYSTS**

Thesis by

Lin Luo

In Partial Fulfillment of the Requirements

for the Degree of

Doctor of Philosophy

California Institute of Technology

Pasadena, California

2001

(Submitted September 22, 2000)

© 2001

Lin Luo

All rights reserved

*To my parents*

## Acknowledgements

It is with my deepest appreciation that I acknowledge my advisor, Mark Davis, for his research guidance and support over the years. The numerous discussions with him taught me to think critically and to be scientifically precise. I appreciated his faith in me and patience throughout my research. I am also greatly indebted to Dr. Jay Labinger for his valuable advice and helpful insights into my work. The true value of all I learned from Mark and Jay during my four years at Caltech goes far beyond what is presented here. I would also like to thank two other members of my thesis committee - Professor George Gavalas and Professor Richard Flagan for their interest in my thesis work.

I would like to express my appreciation to all the Davis group members for providing an excellent working environment. Chris Jones, Alex Katz, Hector Gonzalez, Paul Wagner, Wen Li, Katsuyuki Tsuji and Takahiko Takewaki were instrumental during my initiation into the Davis group and zeolite research. I am also very grateful to Masaki Okamoto for many valuable discussions on catalysis and for teaching me that patience is the number one factor for repairing instruments. My life at Caltech was made enjoyable with the presence of Patricia Andy, Nathalie Belloq, Axel Brait, Christoph Fougret, Suzie Hwang, Geraldo Nery and Patrick Piccione. I will greatly miss our enjoyable conversations at the afternoon coffee breaks and the fun we had in rock concerts in Hollywood.

I am grateful to the many technical staff at Caltech. I would like to thank Tom Dunn, for his assistance in troubleshooting of my apparatus. He and Larry Henling are my main source for questions about X-ray machine maintenance. I would also like to

thank Larry Beck and Sonjong Hwang for their assistance in solid state NMR, Shao-ching Hung in Sunny Chan Group for her assistance in EPR.

And finally, I must express my gratitude to my family, without whom this work could have never been started, let alone completely. My mother and father, to whom this work is dedicated, opened up my eyes to the world of science and taught me that nothing is beyond my reach if I only try. And while my parents are always behind me, my husband Weijun is unfailingly standing beside me. As I glanced back throughout my graduate career, there were times of failure and frustration and times of triumph. Weijun is the one who shares my darkest periods and happiness with his constant encouragement, understanding and love. Every bit of joy and agony in my student life has been a maturing experience and seems all worthwhile now.

## Abstract

Over the past few decades, significant efforts have been devoted to the development of new catalysts and processes for the partial oxidation of cheap and abundant light alkanes directly into oxygenates and olefins. One of the main challenges in the partial oxidation of light alkanes is that they are usually less reactive than the desired products, and further oxidation to total oxidation products,  $\text{CO}_x$ , is thermodynamically favored. With a few exceptions, e.g., partial oxidation of n-butane to maleic anhydride by V-P-O and ammoxidation of propane to acrylonitrile by V-Al-Sb, catalysts investigated for the partial oxidation of light alkanes consist of complicated elemental compositions of metal oxides that have less than desirable catalytic behavior.

Compared to the traditional bulk metal oxides where the active sites selective for partial oxidation of hydrocarbons are usually lattice oxygens, small metal oxide clusters that do not have lattice energies are anticipated to offer oxygen with a lower energetic barrier. Thus, by using metal oxide clusters, the reaction temperature for oxidation of hydrocarbons may possibly be lowered and total oxidation reduced. Zeolites have been shown to be able to provide an excellent matrix for stabilizing metal oxide clusters. Here, a new approach is investigated for the partial oxidation of propane that combines the tunable advantages of zeolites with possibility of high reactivity of metal oxide clusters by using zeolite supported metal oxide clusters as catalysts.

Various methods are employed to synthesize zeolite supported small metal oxide clusters, including ion-exchange-hydrolysis, liquid phase impregnation, vapor phase impregnation, and post-synthesis modification methods. Vanadium is used as the transition metal of interest and is combined with zeolite L, beta and SSZ-33. Vanadium

oxide clusters are successfully incorporated inside zeolites and they have remarkably lower reduction temperatures than the bulk metal oxide. These zeolite based catalysts are studied for propane oxidation. The influence of the locations of the vanadium, the acidity of the zeolite matrix, the hydrophobicity of the zeolite framework and the addition of a second metal (Mo and Sb) are discussed. It is found that vanadium oxide cluster catalysts ( $V_xO_y$ /zeolite L,  $V_xO_y$ /zeolite beta, V-Sb/zeolite beta, V-Mo/zeolite beta) are not particularly selective for the partial oxidation of propane at the reaction conditions investigated (contact time 2 s, reaction temperature 350-450°C, feed gas molar ratio  $C_3H_8:O_2:H_2O:He=4:2:4:5$ ), and most of the vanadium-containing zeolite beta catalysts are as active as  $V_2O_5$  (as suggested by the turnover frequency).

A considerable amount of acetic acid is produced with vanadyl ion-exchanged zeolite beta (VO-H-beta), with a selectivity to acetic acid of 21.1% at propane conversion 1.62% (350°C). It appears that more valuable oxygenates, e.g., acrylic acid, may have been produced in the reaction and overoxidized to  $CO_x$ , since feeding acrylic acid into this VO-H-beta reaction system at 350°C results in complete oxidation of the acid to  $CO_x$ . Motivated by these data, the reaction pathways for propane and propylene oxidation are investigated on this catalyst. For comparison, reaction pathways are also studied with a "Mitsubishi" type catalyst,  $Mo_1V_{0.3}Te_{0.23}Nb_{0.12}O_x$ , one of the best catalysts for propane partial oxidation to acrylic acid. With VO-H-beta, propylene is the primary product of propane oxidation and acetic acid is a sequential oxidation product of the formed propylene possibly through an acetone intermediate.  $Mo_1V_{0.3}Te_{0.23}Nb_{0.12}O_x$  also gives propylene as the primary product of propane oxidation and the propylene thus formed further oxidizes to acrylic acid and acetone. Reactions of individual oxygenate

compounds, e.g., propanal, acrolein, etc., suggest a need to further suppress the total oxidation and to improve allylic oxidation feature for the zeolite based catalysts.

## Table of Contents

Acknowledgements	iv
Abstract	vi
Table of Contents	ix
List of Tables	xii
List of Figures	xiv
List of Schemes	xvii

### Chapter One *Introduction and Objectives*

1.1 BACKGROUND .....	2
1.2 CURRENT STATUS OF SELECTIVE OXIDATION RESEARCH FOR LIGHT ALKANES .....	3
1.2.1 Oxidative Dehydrogenation .....	4
1.2.2 Oxidation to Oxygenates .....	7
1.3 ZEOLITES .....	10
1.4 METAL OXIDE CLUSTERS .....	12
1.5 OBJECTIVE .....	15
1.6 REFERENCE.....	17

### Chapter Two *Physicochemical Characterization and Propane Oxidation over Vanadium-Containing Zeolite L Catalysts*

2.1 INTRODUCTION .....	30
2.2 EXPERIMENTAL SECTION.....	31
2.2.1 Synthesis .....	31
2.2.2 Characterization .....	34
2.2.3 Propane Oxidation.....	35
2.3 RESULTS AND DISCUSSION .....	36
2.3.1 Characterization of Vanadium-Containing Zeolite L Catalysts.....	36
2.3.2 Propane Oxidation Over Vanadium-Containing Zeolite L Catalysts .....	42
2.4 SUMMARY .....	45

2.5 REFERENCE.....	46
<b>Chapter Three</b>	<b><i>Partial Oxidation of Propane over Vanadium-Containing Zeolite Beta Catalysts</i></b>
3.1 INTRODUCTION .....	66
3.2 PROPANE OXIDATION OVER VANADIUM-CONTAINING ZEOLITE BETA CATALYSTS .....	67
3.2.1 Vanadyl Ion-Exchanged and Vanadium Ion-Exchange-Hydrolyzed Zeolite Beta Catalysts .....	67
3.2.2 Vanadium Impregnated Zeolite Beta Catalysts.....	74
3.2.3 Zeolite Beta Catalysts with Vanadium in Zeolite Framework Sites .....	80
3.2.4 Ti/beta and Si/beta Based Catalysts .....	86
3.3 PROPANE OXIDATION OVER NON-ZEOLITE BETA BASED CATALYSTS.....	90
3.3.1 Introduction .....	90
3.3.2 Experimental Section .....	90
3.3.3 Results and Discussion.....	91
3.3.4 Summary .....	92
3.4 COMPARISON OF BULK V <sub>2</sub> O <sub>5</sub> AND VANADIUM-CONTAINING ZEOLITE BETA CATALYSTS .....	93
3.4.1 Introduction .....	93
3.4.2 Experimental Section .....	93
3.4.3 Results and Discussion.....	93
3.4.4 Summary .....	96
3.5 REFERENCE.....	97
<b>Chapter Four</b>	<b><i>Comparison of Reaction Pathways for the Partial Oxidation of Propane over Vanadyl Ion-exchanged Zeolite Beta and Mo<sub>1</sub>V<sub>0.3</sub>Te<sub>0.23</sub>Nb<sub>0.12</sub>O<sub>x</sub></i></b>
4.1 INTRODUCTION .....	133
4.2 EXPERIMENTAL SECTION .....	134
4.2.1 Catalysts Preparation.....	134
4.2.2 Catalytic Reactions.....	135
4.2.3 Reaction Pathway Study .....	136

4.3 RESULTS AND DISCUSSION .....	137
4.3.1 Partial Oxidation of Propane .....	137
4.3.2 Reaction Pathways: Trends in Product Selectivities .....	138
4.3.3 Reaction Pathway Method II: Oxidation of Possible Oxygenates .....	142
4.3.4 Comparison of Catalytic Behavior of Propane Oxidation over VO-H- beta and $\text{Mo}_1\text{V}_{0.3}\text{Te}_{0.23}\text{Nb}_{0.12}\text{O}_x$ .....	149
4.4 CONCLUSION .....	150
4.5 REFERENCE .....	152

**Chapter Five**      *Summary*

## List of Tables

### Chapter One

Table 1.1	Composition of natural gas (in weight percent (wt.%)) (adapted from Ref. <sup>2</sup> ).....	22
Table 1.2	C-H bond strengths in hydrocarbons and their derivatives. <sup>3</sup> .....	23
Table 1.3	Reaction results of oxidative dehydrogenation of propane over several catalytic systems. ....	24
Table 1.4	Partial oxidation of propylene (adapted from Ref. <sup>30</sup> ). ....	25

### Chapter Two

Table 2.1	Vanadium content of vanadium-containing zeolite L samples. ....	48
Table 2.2	Propane oxidation over vanadium-containing submicron L catalysts. ....	49
Table 2.3	Propane oxidation over vanadium-containing nano L catalysts.....	50
Table 2.4	Comparison of propane oxidation over submicron-sized and nano-sized zeolite L catalysts.....	51
Table 2.5	Effect of water on propane oxidation over vanadium-containing nano-sized zeolite L catalysts.....	52

### Chapter Three

Table 3.1	Composition of vanadyl ion-exchanged and ion-exchange-hydrolyzed.....	100
Table 3.2	Propane partial oxidation over vanadyl ion-exchanged zeolite beta.....	100
Table 3.3	Comparison of propane oxidation over VO-Na-beta and its base-treated forms.....	102
Table 3.4	Propane oxidation over vanadium impregnated zeolite beta catalysts.....	103
Table 3.5	Propane oxidation over V-Sb/H-beta and V-Mo/H-beta catalysts.....	104

Table 3.6	Propane oxidation over vanadium and molybdenum-containing catalysts on different supports.....	105
Table 3.7	Propane oxidation over zeolite beta catalysts with framework vanadium.....	106
Table 3.8	Propane oxidation over Ti/beta, Si/beta and AlSi/beta based catalysts.....	107
Table 3.9	Propane oxidation over non-zeolite beta based catalysts.....	108
Table 3.10a	Turnover frequency of bulk $V_2O_5$ and zeolite based catalysts.....	109
Table 3.10b	Reaction results of propane oxidation over bulk $V_2O_5$ .....	109
Table 3.11	Acrylic acid stability over VO-H-beta.....	110
Table 3.12	Desorption of possible oxygenates in partial oxidation of propane over zeolite beta.....	111

#### Chapter Four

Table 4.1	Propane oxidation over VO-H-beta.....	154
Table 4.2	Propane oxidation over $Mo_1V_{0.3}Te_{0.23}Nb_{0.12}O_x$ .....	155
Table 4.3	Propylene oxidation over VO-H-beta.....	156

## List of Figures

### Chapter One

- Figure 1.1 Network of consecutive and parallel elementary steps in catalytic oxidation of a hydrocarbon molecule (adapted from Ref.<sup>4</sup>). ..... 27
- Figure 1.2 Best yields to propylene in oxydehydrogenation of propane reported in the literature for the various catalysts (adapted from Ref.<sup>23</sup>)..... 28

### Chapter Two

- Figure 2.1 Zeolite L structure (framework viewed along [001]). Each intersection in the figure represents a silicon or aluminum atom, while the midpoint of each line represents an oxygen atom. .... 53
- Figure 2.2 Apparatus for vacuum seal in the synthesis of vapor phase impregnation samples..... 54
- Figure 2.3 Schematic of reactor system..... 55
- Figure 2.4 a) HRTEM image of nano-sized zeolite L oriented with the c axis perpendicular to the electron beam; b) SEM image of submicron-sized zeolite L..... 56
- Figure 2.5 XRD patterns of zeolite L based samples. .... 57
- Figure 2.6 TGA of an ion-exchange-hydrolysis sample (IEH(I)-ML)..... 58
- Figure 2.7 N<sub>2</sub> adsorption isotherms of nano-sized zeolite L, IE-NL and IEH-NL..... 59
- Figure 2.8 EPR spectra for IE submicron-sized zeolite L series: a) IE-ML, b) IEH(E)-ML, and c) IEH(I)-ML..... 60
- Figure 2.9 EPR spectra of IE nano-sized zeolite L series: a) IE-NL, b) IEH(E)-NL. .... 61
- Figure 2.10 EPR spectra of a) 2wt.%-VPI-ML and b) a physical mixture of VO(acac)<sub>2</sub> with 2 wt.% vanadium..... 62
- Figure 2.11 Raman spectra of modified zeolite L samples and V<sub>2</sub>O<sub>5</sub>: a) 1wt.%-VPI-NL, b) 2wt.%-VPI-NL, c) 2wt%-IEH(E)-NL, d) NL, and e) V<sub>2</sub>O<sub>5</sub>. .... 63

Figure 2.12	FT-IR spectra of VPI-Series and VO(acac) <sub>2</sub> : (a) 1wt.%-VPI-NL, (b) 2wt.%V-VPI-NL, (c) Nano L, and (d) VO(acac) <sub>2</sub> .....	64
-------------	--	----

### Chapter Three

Figure 3.1	N <sub>2</sub> adsorption isotherms for vanadyl ion-exchanged zeolite beta and its base-treated forms.....	114
Figure 3.2	Electron paramagnetic resonance spectra of vanadyl ion-exchanged zeolite beta sample and its base-treated forms.....	115
Figure 3.3	EPR spectra of as-made, O <sub>2</sub> -treated, and O <sub>2</sub> -treated then H <sub>2</sub> -reduced VO-H-beta. ....	116
Figure 3.4	UV-Vis DR spectra of vanadyl ion-exchanged zeolite beta sample and its base-treated forms. a) VO-Na-beta, b) NH <sub>3</sub> -treated VO-Na-beta (without calcination), c) NH <sub>3</sub> -treated VO-Na-beta (with calcination), d) IEH(I)-beta, and e) H-beta. ....	117
Figure 3.5	UV-Vis DR spectra of NH <sub>4</sub> VO <sub>3</sub> and V <sub>2</sub> O <sub>5</sub> .....	118
Figure 3.6	N <sub>2</sub> adsorption isotherms of H-beta, V/H-beta, VO-H-beta, V-Sb/H-beta, and V-Mo/H-beta.....	119
Figure 3.7	EPR spectra of VO-Na-beta, V-Mo/Na-beta, and V-Sb/Na-beta.....	120
Figure 3.8	TPR profiles of V/H-beta, V/Na-beta, and V/Cs-beta. ....	121
Figure 3.9	TPR results from a) Sb-V/beta(III)(Sb 1.69 wt.%, Sb/V=0.65) b) Sb-V/beta(II) (Sb 3.29 wt.%, Sb/V=1.31), c) Sb-V/beta(I) (Sb 6.38 wt.%, Sb/V=2.64), d) Sb/H-beta (2 wt.%Sb), and e) V/H-beta (1.25 wt.%V). ....	122
Figure 3.10	XRD patterns of Vbeta(I) and its starting material, Na-beta.....	123
Figure 3.11	XRD patterns of Vbeta(H) and its precursor V-MS.....	124
Figure 3.12	UV-Vis DR spectra of vanadium containing catalysts with vanadium at different positions: a) V/Silica (1.25 wt.%V), b) VO-H-beta (1.66 wt.%V), c) V/H-beta (1.25 wt.%V), d) Vbeta(I) (0.26 wt.%V). ....	125
Figure 3.13	FTIR spectra of Vbeta(I) and Na-beta samples.....	126
Figure 3.14	TPR profiles of zeolite supported, silica supported vanadium-containing catalysts and bulk V <sub>2</sub> O <sub>5</sub> : a) VO-H-beta, b) V/silica, and c) bulk V <sub>2</sub> O <sub>5</sub> . (0.1 g was used for each TPR measurement.) ....	127

Figure 3.15	TPR profiles of Sb/beta and $\text{Sb}_2\text{O}_5$ (adapted from Ref. <sup>13</sup> ). .....	128
Figure 3.16	XRD pattern of bulk $\text{SbVO}_4$ with small amounts of $\alpha\text{-Sb}_2\text{O}_4$ impurities.....	129
Figure 3.17	TPR profiles from $\text{SbVO}_4$ and $\text{Sb}_2\text{O}_5\text{-V}_2\text{O}_5$ (adapted from Ref. <sup>13</sup> ).....	130

## Chapter Four

Figure 4.1	Product selectivity profiles for propane oxidation over VO-H-beta. ....	157
Figure 4.2	Product selectivity profiles for propylene oxidation over VO-H-beta: .....	158
Figure 4.3	Product selectivity profiles for propane oxidation over $\text{Mo}_1\text{V}_{0.3}\text{Te}_{0.23}\text{Nb}_{0.12}\text{O}_x$ .....	159
Figure 4.4	Product selectivity profiles for propylene oxidation over $\text{Mo}_1\text{V}_{0.3}\text{Te}_{0.23}\text{Nb}_{0.12}\text{O}_x$ .....	160
Figure 4.5	Conversion and product distribution of 2-propanol oxidation over VO-H-beta and $\text{Mo}_1\text{V}_{0.3}\text{Te}_{0.23}\text{Nb}_{0.12}\text{O}_x$ at 250°C and 2 s contact time with a molar feed gas ratio of 2-propanol: $\text{H}_2\text{O}:\text{O}_2:\text{He}=0.4:3.6:2:9$ .....	161
Figure 4.6	Conversion and product distribution of 1-propanol oxidation over VO-H-beta and $\text{Mo}_1\text{V}_{0.3}\text{Te}_{0.23}\text{Nb}_{0.12}\text{O}_x$ at 250°C and 2 s contact time with a molar feed gas ratio of 1-propanol: $\text{H}_2\text{O}:\text{O}_2:\text{He}=0.4:3.6:2:9$ . “Other” here refers to acetic acid, acetaldehyde and acetone. ....	162
Figure 4.7	Conversion and product distribution of propanal oxidation over VO-H-beta and $\text{Mo}_1\text{V}_{0.3}\text{Te}_{0.23}\text{Nb}_{0.12}\text{O}_x$ at 250°C and 2 s contact time with a molar feed gas ratio of propanal: $\text{O}_2:\text{He}=0.4:2:12.6$ . “Other” here refers to ethylene.....	163
Figure 4.8	Conversion and product distribution of acrolein oxidation over VO-H-beta and $\text{Mo}_1\text{V}_{0.3}\text{Te}_{0.23}\text{Nb}_{0.12}\text{O}_x$ at 250°C and 2 s contact time with a molar feed gas ratio of acrolein: $\text{O}_2:\text{He}=0.4:2:12.6$ . ....	164
Figure 4.9	Conversion and product distribution of acetone oxidation over VO-H-beta and $\text{Mo}_1\text{V}_{0.3}\text{Te}_{0.23}\text{Nb}_{0.12}\text{O}_x$ at 250°C and 2 s contact time with a molar feed gas ratio of acetone: $\text{H}_2\text{O}:\text{O}_2:\text{He}=0.4:3.6:2:9$ .....	165

## List of Schemes

### Chapter One

Scheme 1.1 Structure of Faujasite. .... 26

### Chapter Three

Scheme 3.1 Formation of a metal oxide cluster with two vanadium atoms. .... 112

Scheme 3.2 Dealumination and V-insertion method for synthesizing zeolite beta with framework vanadium. .... 113

### Chapter Four

Scheme 4.1 Main reaction pathways for propane oxidation over VO-H-beta. .... 166

Scheme 4.2 Main reaction pathway scheme for propane oxidation over  $\text{Mo}_1\text{V}_{0.3}\text{Te}_{0.23}\text{Nb}_{0.12}\text{O}_x$ . .... 167

Scheme 4.3 The reaction network for the oxidation of propane and propylene proposed by Bettahar and co-workers.<sup>32</sup> .... 168

Scheme 4.4 Reaction network for propane oxidation over  $\text{Mo}_1\text{V}_{0.3}\text{Te}_{0.23}\text{Nb}_{0.12}\text{O}_x$ . Shaded arrow refers to main reaction pathway; compounds with underlines refer to the main products involved in propane and propylene oxidation reaction. .... 169

Scheme 4.5 Reaction network for propane oxidation over VO-H-beta. Shaded arrow refers to main reaction pathway; compounds with underlines refer to the main products involved in propane and propylene oxidation reaction. .... 170

# **CHAPTER ONE**

## **Introduction and Objectives**

## 1.1 BACKGROUND

Selective oxidation of light alkanes is one of the main subjects in catalysis today. This is motivated by both the potential commercial applications and the scientific challenges.

Light alkanes usually refer to C<sub>1</sub>-C<sub>6</sub> hydrocarbons. They are low cost and environmental friendly raw materials. The present enormous capacity of light alkanes comes from huge reserves of natural gas as well as the large amounts of light gases that are formed as byproducts from the production of gasoline and diesel oil. Light alkanes are less expensive than their corresponding olefins; as an example, propane is one-third the cost of propylene.<sup>1</sup> However, to date, the petrochemical industry has been dominated by extensive use of olefins and aromatics, because of their relative ease of functionalization relative to saturated compounds. Ethylene is at present the feedstock for approximately 30% of all chemicals.<sup>1</sup> The demand for olefins is increasing and the existing capacity (principally from steam-cracking of naphtha and fluid catalytic cracking in oil refining) is predicted to become insufficient to meet this demand in the future. The high cost of olefins has prompted the development of new catalysts for the direct transformation of alkanes to oxygenates through partial oxidation processes. Although methane is the most abundant hydrocarbon (Table 1.1),<sup>2</sup> its high stability requires extreme conditions to transform methane into useful products. The focus of this thesis is on the heterogeneous, partial oxidation of propane.

The main challenge for partial oxidation of light alkanes is that they are usually less reactive compared to their desired products, and further oxidation to total oxidation products, CO<sub>x</sub>, is thermodynamically favored. For most large-scale processes, molecular

oxygen is the only economical oxidant. The reaction of light alkanes with O<sub>2</sub> usually occurs via a free-radical mechanism, and C-H bond cleavage is the initial and rate-determining step. By comparing the weakest C-H bond energy of alkanes with that of their desired products (Table 1.2), it is shown that the desired products have lower C-H bond energies, i.e., higher reactivities than the reactants.<sup>3</sup> Thus, it is difficult to stop the reaction at the desired products and avoid nonselective oxidation. Further, the high C-H bond energies of the reactants require high reaction temperatures, which is detrimental to the stability of the desired products. Therefore, novel catalysts need to be developed that work at temperatures as low as possible and avoid total oxidation of the initial products.

Another challenge for partial oxidation deals with the complexity of the oxidation reaction networks. Fig. 1.1 shows an example of an oxidation network.<sup>4</sup> Since many pathways can occur with poorly established kinetics, designing catalysts turns out to be difficult. Most of the catalyst systems investigated for light alkane oxidation are based on catalysts that work for higher alkanes and/or for olefin oxidation. Although there may be some mechanistic similarities between light alkane oxidation and those of higher hydrocarbons (C<sub>5+</sub> or olefins), their difference in C-H bond energy requires that a different approach must be taken.

## **1.2 CURRENT STATUS OF SELECTIVE OXIDATION RESEARCH FOR LIGHT ALKANES**

Over the past 50 years, many examples of catalysts active for the selective oxidation of paraffins have been reported. In this section, I will briefly review systems used for ethane and propane oxidation. The products of alkane oxidation can generally

be divided into three categories: dehydrogenation products, oxygenates and total combustion products ( $\text{CO}_x$ ).

### 1.2.1 Oxidative Dehydrogenation

Conventionally practiced dehydrogenation of paraffins is commercially well established, particularly the dehydrogenation process of propane and isobutane to their respective olefins. They are endothermic processes and are thermodynamically limited. Best known are the Star (Phillips Petroleum), Catofin (Lummus), Oleflex (UOP), Linde-BASF and Snamprogetti-Yarsintez processes. The advantage of these processes is that they are net producers of byproduct hydrogen. The disadvantages are their thermodynamically limited olefin yield, high frequency of regeneration to burn off coke from the catalyst surface, and the high energy input requirements due to the inherent endothermicity of the processes.

An attractive alternative to produce olefins is the catalytic oxidative dehydrogenation (ODH) of alkanes which is thermodynamically more favorable than dehydrogenation (because of the formation of water rather than  $\text{H}_2$ ) over a large temperature range and has the advantage of no carbon deposition.<sup>5</sup> Various catalyst systems have been studied for oxidative dehydrogenation of light alkanes including molten alkali salts,<sup>6</sup> bulk mixed metal oxides,<sup>7-16</sup> heteropolyacid catalysts,<sup>17</sup> and molecular sieve based catalysts.<sup>18-22</sup>

Albonetti and co-workers summarized the recent work in oxidative dehydrogenation of propane and their results are illustrated in Fig. 1.2.<sup>23</sup> They reported that V-silicalites prepared by hydrothermal methods give the best performance for

oxidative dehydrogenation of propane (70% selectivity to propylene at 40% propane conversion near 500°C with a feed molar ratio of propane:O<sub>2</sub>:inert=2.8:8.4:88.8 and a total flow of 12.6 cc/min-gcat). Detailed information for some of the catalysts, their reaction conditions and results is summarized in Table 1.3. In most cases, the molar percentage of propane in the feed was low and the catalysts with the best yields were not necessarily the catalysts with the best productivity. Thus, care must be taken when comparing catalysis results based on yields.

A large majority of the oxidative dehydrogenation catalysts have been developed around vanadium chemistry. These V<sub>2</sub>O<sub>5</sub>-based catalysts give propylene yields between 8% and 20% and their performance is strongly dependent on the loading and the support. The upper yield range is attained with MgO supported catalysts,<sup>24</sup> while SiO<sub>2</sub>, Al<sub>2</sub>O<sub>3</sub>, TiO<sub>2</sub>, La<sub>2</sub>O<sub>3</sub>, Sm<sub>2</sub>O<sub>3</sub> or Bi<sub>2</sub>O<sub>3</sub> supported systems are inferior.<sup>25</sup> For MgO-supported V<sub>2</sub>O<sub>5</sub>, the vanadia phase provides the oxidizing properties needed, and the magnesia phase provides the base properties that suppress the propylene oxidation. Magnesium vanadates have also been investigated and found to give similar yields as V<sub>2</sub>O<sub>5</sub> on MgO.<sup>7,8</sup> Mg<sub>2</sub>V<sub>2</sub>O<sub>7</sub> has been suggested to be the active phase in the magnesium vanadates and may also play a role in V<sub>2</sub>O<sub>5</sub>/MgO. V<sub>2</sub>O<sub>5</sub>/Nb<sub>2</sub>O<sub>5</sub> catalysts have also been investigated, and V<sub>2</sub>Nb<sub>23</sub>O<sub>62</sub> is presumed to be the active phase.<sup>12</sup> Propylene yields of 12% at a relatively high selectivity of 70%, and a high productivity, are reported.<sup>12</sup>

Molecular sieve materials containing framework vanadium have been studied as catalysts for oxydehydrogenation of propane.<sup>18-22</sup> In addition to V-silicalite, vanadium-

containing aluminophosphate VAPO-5 was shown to be a selective catalyst, giving propylene with selectivities around 70% for conversions around 15% at 500°C.<sup>19</sup>

Other than vanadium-based catalysts, Co-molybdate and Ni-molybdate are the two most noteworthy catalyst systems for propane oxydehydrogenation. CoMoO<sub>4</sub>/SiO<sub>2</sub> doped with P, Ni, Mg, and/or Fe are reported to yield 15% propylene<sup>26</sup> with a high productivity and low formation of undesirable partial oxidation products. Unsupported Ni-molybdates have been studied as monophases, with β-NiMoO<sub>4</sub> yields 13.2% propylene (20.9% conv., 63.1% sel.) and α-NiMoO<sub>4</sub> yields 9.3% propylene (24% conv., 37.5% sel.).<sup>15</sup> In the latter systems, the β-phase appears to be the more selective and overall preferred catalytic phase.

It is worth noting that most catalyst systems are usually active at temperatures above 450°C. The only exception is heteropolycompounds, which are active at significantly lower temperatures (around 350°C). However, their usage is hampered by the fact that they are less robust than oxide catalysts due to their limited thermostability.

For ethane oxidative dehydrogenation, high yields of ethylene (85% sel., 70% conv.) can be obtained by adding large amounts of H<sub>2</sub> to the reaction mixture and using a platinum-tin catalyst operating at 950°C with a millisecond contact time.<sup>27</sup> With KSr<sub>2</sub>Bi<sub>3</sub>O<sub>4</sub>Cl<sub>6</sub>, Ueda and co-workers obtained a 70% yield of ethylene starting from ethane at 640°C.<sup>28</sup> Compared to the above two catalysts that are active at high temperatures, Mo<sub>0.61</sub>V<sub>0.31</sub>Nb<sub>0.08</sub>/α-alumina is active at a much lower temperature. A selectivity to ethylene of 83% has been obtained at 340°C with an ethane conversion of 25%.<sup>29</sup>

### 1.2.2 Oxidation to Oxygenates

The term oxygenates is used here to refer to oxygen-containing compounds other than  $\text{CO}_x$ , such as alcohols, aldehydes and acids, etc. Published reports for oxidation of light alkanes to oxygenates are less extensive than those for oxidative dehydrogenation.

The catalytic systems tested in the direct oxidation of propane to acrolein and acrylic acid are generally mixed metal oxides with defects. The defects are believed to promote the lattice oxygen mobility during the reaction.<sup>30</sup>

Most reported yields for propane oxidation to acrolein are less than 10%. The best obtained formulations up to now are the  $\text{BiMo(V)O}$  multicomponent catalysts developed by Moro-oka et al. (63.5% of acrolein selectivity at 13.1% propane conversion).<sup>31</sup> These results in propane oxidation are far inferior to those in propylene oxidation. A typical catalyst used in industrial acrolein production is  $\text{Fe}_4\text{BiW}_2\text{Mo}_{10}\text{Si}_{1.35}\text{K}_{0.6}$ . With this catalyst at 320°C, propylene conversion is 97% and acrolein selectivity is 93%. In addition, there is a 6% selectivity to acrylic acid making the useful selectivity 99%.<sup>32</sup>

Catalysts studied for the direct conversion of propane to acrylic acid include VPO based catalysts, Bi-Mo based catalysts, and heteropolyacids. The reported yields for propane oxidation to acrylic acid are usually around 10%, far from the economic requirements needed to build a commercial plant. For example, 7% yield to acrylic acid was reported by Ai with VPO based catalyst at 350-400°C in a large excess of oxygen (oxygen/propane=32.5) and of water (water/propane =16.25).<sup>33,34</sup> V-Zr-P oxide was reported to give 14.8% yield of acrylic acid (17.5% conversion) at 340°C with a V/Zr

ratio equal to 2.<sup>35</sup> A pyridine-treated  $\text{H}_4\text{PMo}_{11}\text{V}_1\text{O}_{40}$  gives 16% propane conversion with a 30% selectivity to acrylic acid and a 30% selectivity to acetic acid at 380°C.<sup>36</sup> An exceptionally good example appears to be the catalyst reported by Mitsubishi that has the empirical composition  $\text{MoV}_{0.3}\text{Te}_{0.23}\text{Nb}_{0.12}\text{O}_x$ , which yields 48% acrylic acid at a reaction temperature of 380°C.<sup>37</sup> This result is impressive and may serve as a basis for an eventual commercial process to convert propane to acrylic acid.<sup>5</sup>

The most effective catalysts for propane ammoxidation to acrylonitrile fall into two main classes: antimonates or molybdates. The best catalysts are  $\text{VSb}_5\text{W}_{0.5}\text{Te}_{0.5}\text{Sn}_{0.5}\text{O}_x\text{-SiO}_2/\text{Al}_2\text{O}_3$  which gives a 39% yield to acrylonitrile at 68.8% conversion, and  $\text{V}_{0.3}\text{Te}_{0.23}\text{Nb}_{0.12}\text{MoO}_x/\text{SiO}_2$  which yields 55.1% acrylonitrile (86.7% conv. and 63.5% sel.).<sup>5</sup>

For ethane oxidation to oxygenates, interesting results were obtained by Zhao and co-workers. They reported that by using  $\text{Cs-V/SiO}_2$  (Cs:V:Si=1:0.1:100), acrolein was produced with a 14.7% selectivity at 2.8% ethane conversion, while acetaldehyde was formed with a 30% selectivity.<sup>38</sup> An efficient catalyst for ethane ammoxidation to acetonitrile, Co-beta, was reported to give a 26.4% yield at 400°C by Li and Armor.<sup>39</sup>

Most of the catalysts discussed above are very complicated with multiple components and multiple phases. As an example, the catalysts for propane ammoxidation must contain paraffin activating elements (e.g., V), olefin-activating elements (e.g., Bi, Te), and NH-inserting elements (e.g., Sb, Mo). Additionally, these active sites have to be able to function in the right sequence and they must be operated at the same temperature. The different phases should also be chemically compatible so that

they do not poison one another. Moreover, the paraffin activating catalyst is required to be surrounded by ample olefin ammoxidation catalyst, because the concentration of propylene intermediate must be kept low during the process to prevent the destruction of propylene by the paraffin activating catalyst.<sup>5</sup> Although large efforts have focused on the selective oxidation of light alkanes, these complexities have resulted in low yields in the final product and, in almost all cases, productivities far from values of industrial interest. Compared to some of the catalytic systems used in the partial oxidation of propylene (Table 1.2), the performances of paraffin oxidation catalyst are significantly lower than those obtained when olefin is the feedstock.<sup>30</sup>

Despite all the difficulties mentioned above, research on partial oxidation has been encouraged by several successful processes that involve partial oxidation of light alkanes, e.g., partial oxidation of n-butane to maleic anhydride by VPO<sup>40</sup> and ammoxidation of propane to acrylonitrile by V-Al-Sb-O.<sup>41</sup> New methodologies for the synthesis and characterization of catalytic materials are also being developed, such as, *in situ* studies of the catalytic active phase<sup>42,43</sup> and the synthesis of transition metal substituted zeolites.<sup>44-47</sup> New concepts from the chemical engineering perspective have been proposed, such as membrane reactors,<sup>48</sup> and millisecond contact time reactors.<sup>27</sup> These results open up a promising future for the development of novel catalyst systems for the partial oxidation of light alkanes.

### 1.3 ZEOLITES

Zeolites are microporous, crystalline, hydrated aluminosilicates that have a three-dimensional framework structure composed of  $\text{TO}_4$  tetrahedra where  $T = \text{Si}, \text{Al}$ . These tetrahedra are the primary building units in all zeolite structures, and are linked to each other by sharing of their oxygen atoms. The result is a framework structure exhibiting regularly arrayed pores and cages. Scheme 1.1 shows the structure of a zeolite, faujasite, and illustrates how an extended three-dimensional network of silica and alumina tetrahedra can be pictured as consisting of smaller building units, which themselves can be thought of as a combination of the primary tetrahedra. Uniformly sized pores of zeolites usually range from 4-7 Å (8-membered rings to 12-membered rings). The notation of “n-member” ring here represents the number of tetrahedral atoms comprising the pore opening. The largest pore found to date in a silica-based material is in UTD-1, which has 14-member ring pore openings with a size of roughly  $7.5 \times 10.0$  Å in diameter.<sup>49</sup>

All the zeolite frameworks are negatively charged due to the substitution of aluminum for silicon in the framework. This substitution requires balancing cations for charge neutralization of the framework. When the cations are protons, the zeolites are solid acids that are capable of promoting acid catalyzed reactions within the micropores of the zeolite crystals. Through an ion-exchange process, a variety of active sites can be incorporated into the micropores of zeolites. For example, ion exchange with alkali metal cations such as sodium, potassium or cesium produces active sites with basic character. In addition, exchange with transition metals can create sites with unique catalytic capabilities, e.g., Co-beta.<sup>50</sup>

Active sites can also be created by depositing an extra-framework species within the molecular sieve micropores through methods such as impregnation. Additionally, incorporation of transition metal atoms into the framework (substitution for silicon) such as titanium<sup>51</sup> or vanadium<sup>46,52</sup> can produce sites active for oxidation and oxidative dehydrogenation, respectively.

The size of the zeolite crystal can be controlled by the synthesis procedures and conditions. For various types of reactions, the particle size preferred may be different. Zeolites with large particle size are preferred when shape-selectivity is used on the products of the reaction. The constrained environment of the micropores has the ability to sterically alter the course of a catalytic reaction pathway in order to impart “shape-selectivity.” Zeolites with small particle size have advantages over larger ones when fast diffusion of the products is needed. For example, small particle size zeolites have shown in hydrocarbon conversions an enhanced ratio of surface area to mass, high diffusion rates, and resistance to deactivation by pore plugging and surface contamination. Recently, nanometer-sized zeolites were synthesized for sodalite, zeolite A, zeolite Y, offretite, zeolite beta, ZSM-5, ZSM-11 and zeolite L.<sup>53-55</sup>

Due to their high degree of porosity and high sorption capacities, zeolites have found widespread uses in ion-exchange applications as detergents and adsorption applications for drying and physical separation of hydrocarbons. Synthetic zeolites are the most important catalysts in oil industry.<sup>56</sup> Zeolites have also been intensively investigated for fine chemical synthesis.<sup>57,58</sup> The extraordinary tunable features of

zeolites (e.g., pore size, shape, capacity, and particle size) provide a working foundation for the possibility of designer catalysts.<sup>59</sup>

#### **1.4 METAL OXIDE CLUSTERS**

Most heterogeneous oxidation catalysts for partial oxidation of light alkanes are metal oxides, where the selective sites are usually lattice oxygens. Because of the high lattice energy, bulk oxides are relatively unreactive. If metal oxide particles with smaller diameters (e.g., in nm range or less) are used instead, it is anticipated that without the high lattice energy, these metal oxide particles will release oxygen with a lower energetic barrier. These particles will be referred to as clusters to distinguish them from larger particles or crystallites. In addition to the lattice energy difference between metal oxide clusters and their corresponding bulk oxides, metal oxide clusters often possess peculiar reactivity properties because of their differences in the crystalline habits, morphology, electronic properties, etc.

The size effect mentioned above has been proven for metal particles. When metal particles are in the size range of 10-50 Å, changes in the metal particle size have been shown to lead to significant changes in properties for many catalytic reactions.<sup>60</sup> Examples include Pt/Al<sub>2</sub>O<sub>3</sub>, and Ir-Pt/Al<sub>2</sub>O<sub>3</sub>, which are used for reforming of gasoline range hydrocarbons. For supported metal particles with diameters less than 10 their catalytic behavior is strikingly different from that of the corresponding bulk metal. One example of this is finely dispersed platinum in the pores of zeolite L, which has found industrial application for selective reaction of hexane to benzene.<sup>60</sup>

Although various methodologies have been developed to synthesize metal oxide clusters, it is usually very difficult to control the characteristics of the nanocrystals obtained and especially to avoid recrystallization during catalytic runs. Both these problems can be overcome in principle, when these oxide clusters are stabilized inside an ordered solid matrix such as a zeolite that controls both the growth and crystalline habit of the guest nanooxide. Furthermore, there are other advantages to use zeolite as the matrix for metal oxide clusters, such as, the presence of a strong electrostatic field inside the zeolite channels, the possibility of synergetic cooperation between isolated transition metal ions at the charge-balancing sites of zeolites and oxide nanoparticles, and the presence of shape selectivity effects. These factors suggest that catalytic behavior of oxide nanoparticles within the cavities of host microporous materials could be significantly different from those of the same oxide, either in the form of bulk materials or conventional supported oxide materials. The inclusion (encapsulation) of oxide nanoparticles inside microporous matrices can thus be a very powerful research direction to prepare catalysts with tunable properties.

Previous work of Davis and co-workers have shown that small metal oxide cluster ( $\text{Cs}_x\text{O}_y$ ) can be prepared in zeolite void spaces with properties significantly different from bulk oxides.<sup>61,62</sup> Additionally, cesium oxide clusters supported in mordenite and nickel oxide clusters supported in zeolite Y were synthesized by ion-exchange-hydrolysis method, and these materials were investigated for p-xylene oxidation<sup>63</sup> and CO complete oxidation, respectively.<sup>64,65</sup> By using chemical vapor deposition method followed by a proper calcination procedure, Yoo and co-workers were able to synthesize uniformly dispersed small ferric molybdate clusters (2-40nm) on the surface of partially

deboronated borosilicate (Fe/Mo/DBH). This Fe/Mo/DBH material exhibited higher catalytic activity, better product selectivity, and superior stability to form terephthaldehyde and p-tolualdehyde by gas-phase O<sub>2</sub> oxidation of p-xylene than its impregnated counterpart.<sup>66</sup>

Although metal oxide clusters are expected to show a catalytic behavior different from that of the bulk state, fundamental studies on their preparation are few. This may result from a lack of methods for preparation and characterization. Only a limited number of techniques were employed to characterize metal oxide clusters including X-ray absorption fine structure measurement (XAFS), high-resolution electron microscopy (HREM), and other indirect methods such as N<sub>2</sub> adsorption. The characterization of these materials remains difficult because the metals can migrate under the electron beam during the HREM experiment and XAFS is heavily dependent on simulation parameters.

Metal oxide cluster systems have never been explored for light alkane oxidation catalysis. Theoretically, for the oxidation of paraffins, the number of oxygen atoms incorporated into the hydrocarbons is reasonably determined by the residence time of the adsorbed molecule on the active catalytic surface, the number of oxygen atoms available at the active site, and the reactivity of the oxygen at the active site.<sup>67</sup> We expect that zeolite supported metal oxide cluster catalysts may be able to have fewer oxygen atoms available at each active site and higher reactivity of the active oxygen atoms than conventional catalysts. Additionally, small zeolite particles can be chosen to reduce the residence time of the adsorbed molecules inside zeolite micropores. Thus, partial oxidation of light alkanes under mild conditions is conceivable with this approach.

## **1.5 OBJECTIVE**

The performance of almost all traditional catalysts for partial oxidation of light alkanes is far from being industrially applicable. These traditional catalysts that contain bulk metal oxides are relatively unreactive due to their high lattice energy. Small metal oxide clusters that do not have high lattice energy are anticipated to be able to offer oxygen with a lower energetic barrier. The crystalline zeolites with uniform pores provide an excellent matrix for supporting small metal oxide clusters. In this project, an approach for partial oxidation of light alkanes is developed by combining the tunable advantages of zeolites with the high reactivity of metal oxide clusters by creating zeolite supported metal oxide cluster systems.

The objective of my research is to develop a methodology to synthesize zeolite supported small metal oxide clusters and investigate their catalytic behavior for the oxidation of light alkanes. To date, few metal oxide clusters system have been reported, and their characterization is difficult. Chapter Two describes my efforts to synthesize and characterize metal oxide clusters supported in zeolite L. Various methods for zeolite modification were employed including ion exchange, liquid phase impregnation, and vapor phase impregnation methods. Metal oxide clusters were successfully formed inside zeolite by ion-exchange-hydrolysis method, in which the metal atoms are first introduced to the zeolite charge-balancing sites by ion-exchange method and these isolated metal atoms agglomerate and form larger occluded material inside zeolite after hydrolysis. The resulting catalysts did not show considerable improvement in propane oxidation. This may have resulted from the hydrophilic framework of zeolite L leading to lower

selectivities for hydrophilic products. Therefore, a more hydrophobic zeolite matrix, zeolite beta, was investigated.

Chapter Three describes a detailed study over transition metal containing zeolite beta. The main points of concern are: (i) to elucidate whether metal oxide clusters supported by a hydrophobic framework, zeolite beta, are active in propane oxidation and behave differently from the corresponding bulk metal oxide, (ii) to understand the influence of locations of transition metal, acidity of the zeolite matrix, hydrophobicity of the zeolite framework, and the presence of a second metal on propane oxidation.

As a considerable amount of acetic acid was found for a vanadyl ion-exchanged zeolite beta catalyst (VO-H-beta), Chapter Four focuses on reaction pathway investigations for propane oxidation over this catalyst. The possibility of the existence of a more valuable intermediate is addressed, and the reaction pathways are proposed. Reaction pathways have also been investigated for a “Mitsubishi” type catalyst,  $\text{Mo}_1\text{V}_{0.3}\text{Te}_{0.23}\text{Nb}_{0.12}\text{O}_x$ ; one of the best catalysts for propane partial oxidation to acrylic acid. The differences in catalytic behavior of these two catalysts are discussed, and future directions for the improvement of VO-H-beta are suggested.

## 1.6 REFERENCE

- 1) Villa, P. L.; Rapagna, S. in *Advances and challenges in the catalytic activation and functionalisation of light alkanes*; Derouane E. G. Ed.; Kluwer Academic Publishers, 1998, pp L37.
- 2) Olah, G. A.; Molnar, A. *Hydrocarbon Chemistry*; John Wiley & Sons: New York, 1995.
- 3) Lide, D. R. *CRC Handbook of Chemistry and Physics*; 80th ed.; CRC Press LLC, 1999.
- 4) Haber, J. in *Advances and challenges in the catalytic activation and functionalisation of light alkanes*; Derouane E. G. Ed.; Kluwer Academic Publishers, 1998, pp L183.
- 5) Grasselli, R. K. *Catal. Today* **1999**, *49*, 141-153.
- 6) Dahl, I. M.; Grande, K.; Jens, K. J.; Rytter, E.; Slagtern, A. *Appl. Catal.* **1991**, *77*, 163-174.
- 7) Sam, D. S. H.; Soenen, V.; Volta, J. C. *J. Catal.* **1990**, *123*, 417-435.
- 8) Kung, M. C.; Kung, H. H. *J. Catal.* **1992**, *134*, 668-677.
- 9) Michaels, J. N.; Stern, D. L.; Grasselli, R. K. *Catal. Lett.* **1996**, *42*, 135-137.
- 10) Michaels, J. N.; L., S. D.; Grasselli, R. K. *Catal. Lett.* **1996**, *42*, 139-148.
- 11) Stern, D. L.; Michaels, J. N.; DeCaul, L.; Grasselli, R. K. *Appl. Catal. A-Gen.* **1997**, *153*, 21-30.
- 12) Smits, R. H. H.; Seshan, K.; Leemreize, H.; Ross, J. R. H. *Catal. Today* **1993**, *16*, 513-523.
- 13) Fang, Z. M.; Zou, J.; Weng, W. Z.; Wan, H. L. *Stud. Surf. Sci. Catal.* **1998**, *119*, 629-634.
- 14) Ueda, W.; Lee, K. H.; Yoon, Y. S.; Moro-oka, Y. *Catal. Today* **1998**, *44*, 199-203.

- 15)Mazzocchia, C.; Aboumrad, C.; Diagne, C.; Tempesti, E.; Herrmann, J. M.; Thomas, G. *Catal. Lett.* **1991**, *10*, 181-191.
- 16)Stern, D. L.; Grasselli, R. K. *J. Catal.* **1997**, *167*, 560-569.
- 17)Mizuno, N.; Tateishi, M.; Iwamoto, M. *Appl. Catal. A-Gen.* **1995**, *128*, 165-170.
- 18)Centi, G.; Trifiro, F. *Appl. Catal. A-Gen.* **1996**, *143*, 3-16.
- 19)Concepcion, P.; Lopez Nieto, J. M.; Perez-Pariente, J. *Catal. Lett.* **1993**, *19*, 333-337.
- 20)Blasco, T.; Concepcion, P.; Lopez Nieto, J. M.; Perez-Pariente, J. *J. Catal.* **1995**, *152*, 1-17.
- 21)Okamoto, M.; Luo, L.; Labinger, J. A.; Davis, M. E. *J. Catal.* **2000**, *192*, 128-136.
- 22)Salem, G. F.; Besecker, C. J.; Kenzig, S. M.; Kowlaski, W. J.; Cirjak, L. M. : US Patent 5,306,858, 1994.
- 23)Albonetti, S.; Cavani, F.; Trifiro, F. *Catal. Rev.-Sci. Eng.* **1996**, *38*, 413-438.
- 24)Chaar, M. A.; Patel, C.; Kung, H. H. *J. Catal.* **1988**, *109*, 463-467.
- 25)Corma, A.; Lopez-Nieto, J. M.; Paredes, N.; Rajadell, M. J.; Perez, M. in *Proceedings of the XIII Symposium on Iberoamerican Catalysis*: Segovia, Spain, 1992.
- 26)Hardman, H. F. : US Patent, 4,255,284, 1981.
- 27)Bodke, A. S.; Olschki, D. A.; Schmidt, L. D.; Ranzi, E. *Science* **1999**, *285*, 712-715.
- 28)Ueda, W.; Lin, S. W.; Tohmoto, I. *Catal. Lett.* **1997**, *44*, 241-245.
- 29)Thorsteinson, E. M.; Wilson, T. P.; Young, F. G.; Kasai, P. H. *J. Catal.* **1978**, *52*, 116-132.
- 30)Bettahar, M. M.; Costentin, G.; Savary, L.; Lavalley, J. C. *Appl. Catal. A-Gen.* **1996**, *145*, 1-8.
- 31)Kim, Y. C.; Ueda, M.; Moro-oka, Y. *Catal. Today* **1992**, *13*, 673.

- 32) Wittcoff, H. A.; Reuben, B. G. *Industrial Organic Chemicals*; John Wiley & Sons: New York, 1996.
- 33) Ai, M. *Catal. Today* **1992**, *13*, 679-684.
- 34) Ai, M. *Catal. Today* **1998**, *42*, 297-301.
- 35) Han, Y. F.; Wang, H. M.; Cheng, H.; Deng, J. F. *Chem. Commun.* **1999**, 521-522.
- 36) Li, W.; Labinger, J. A.; Davis, M. E. *Submitted to J. Catal.* **2000**.
- 37) Ushikubo, T.; Nakamura, H.; Koyasu, Y.; Wajiki, S.: EP 0608838A2, 1994.
- 38) Zhao, Z.; Yamada, Y.; Teng, Y. H.; Ueda, A.; Nakagawa, K.; Kobayashi, T. *J. Catal.* **2000**, *190*, 215-227.
- 39) Li, Y. J.; Armor, J. N. *Chem. Commun.* **1997**, *20*, 2013-2014.
- 40) Hodnett, B. K. *Catal. Rev. Sci. Eng.* **1985**, *27*, 373-424.
- 41) Centi, G.; Grasselli, R. K.; Trifiro, F. *Catal. Today* **1992**, *13*, 661-666.
- 42) Hutchings, G. J.; Desmartinchomel, A.; Olier, R.; Volta, J. C. *Nature* **1994**, *368*, 41-45.
- 43) Volta, J. C.; Bere, K.; Zhang, Y. J.; Olier, R. *ACS Symp. Ser.* **1993**, *523*, 217-230.
- 44) Blasco, T.; Cambor, M. A.; Corma, A.; Esteve, P.; Guil, J. M.; Martinez, A.; Perdigon-Melon, J. A.; Valencia, S. *J. Phys. Chem. B* **1998**, *102*, 75-88.
- 45) Dartt, C. B.; Davis, M. E. *Appl. Catal. A-Gen.* **1996**, *143*, 53-73.
- 46) Dzwigaj, S.; Peltre, M. J.; Massiani, P.; Davidson, A.; Che, M.; Sen, T.; Sivasanker, S. *Chem. Commun.* **1998**, 87-88.
- 47) Takewaki, T.; Beck, L. W.; Davis, M. E. *Top. Catal.* **1999**, *9*, 35-42.
- 48) Bernstein, L. A.; Agawalla, S.; Lund, C. F. *ACS Symp. Ser.* **1993**, *523*, 427-437.

- 49)Freyhardt, C. C.; Tsapatsis, M.; Lobo, R. F.; Balkus, K. J.; Davis, M. E. *Nature* **1996**, *381*, 295-298.
- 50)Li, Y. J.; Armor, J. N. *J. Catal.* **1998**, *173*, 511-518.
- 51)Notari, B. *Catal. Today* **1993**, *18*, 163-172.
- 52)Zatorki, L. W.; Centi, G.; Lopez Nieto, J.; Trifiro, F.; Bellussi, G.; Fattore, V. in *Zeolites: Facts, Figures, Future*; Jacobs, P. A. and van Santen, R. A., Ed.; Elsevier Science: Amsterdam, 1989, pp 1243.
- 53)Tsapatsis, M.; Lovallo, M.; Okubo, T.; Davis, M. E.; Sadakata, M. *Chem. Mater.* **1995**, *7*, 1734-1741.
- 54)Cambor, M. A.; Corma, A.; Valencia, S. *Micropor. Mesopor. Mat.* **1998**, *25*, 59-74.
- 55)Johannes, P.; Machteld, M.; Marc, H: WO Pat 97/03021, 1997.
- 56)Higgins, J. B. *Reviews in Mineralogy* **1994**, *29*, 507.
- 57) Newsam, J. M. in *Solid State Chemistry: Compounds*; Cheetham, A. K. and Day, P., Ed.; Oxford University Press, 1992, pp 234-280.
- 58)Davis, M. E. *Ind. Eng. Chem. Res.* **1991**, *30*, 1675-1683.
- 59)Davis, M. E. *Chem. Eur. J.* **1997**, *3*, 1745-1750.
- 60)Gates, B. C. *Chem. Rev.* **1995**, *95*, 511-522.
- 61)Hathaway, P. E.; Davis, M. E. *J. Catal.* **1989**, *116*, 263-178.
- 62)Hathaway, P. E.; Davis, M. E. *J. Catal.* **1989**, *116*, 279-284.
- 63)Hashimoto, K.; Matzuo, K.; Kominami, H.; Kera, Y. *J. Chem. Soc. Faraday Trans.* **1997**, *93*, 3729-3732.
- 64)Sano, M.; Suzuki, M.; Niwa, M. *Bull. Chem. Soc. Jpn.* **1997**, *66*, 3511-3512.

- 65) Sano, M.; Maruo, T.; Yamatera, H.; Suzuki, M.; Saito, Y. *J. Am. Chem. Soc.* **1987**, *109*, 52-55.
- 66) Yoo, J. S. *Catal. Today* **1998**, *41*, 409-432.
- 67) Kung, H. H.; Michalakos, P.; Owens, L.; Kung, M.; Anderson, P.; Owen, O.; Jahan, I. *ACS Symp. Ser.* **1993**, *523*, 389-408.
- 68) Bellussi, G.; Centi, G.; Perathoner, S.; Trifiro, F. *ACS Symp. Ser.* **1993**, *523*, 281-297.
- 69) Parmaliana, A.; Sokolovskii, V.; Miceli, D.; Giordano, N. *Appl. Catal. A-Gen.* **1996**, *135*, L1-L5.

**Table 1.1** Composition of natural gas (in weight percent (wt.%)) (adapted from Ref.<sup>2</sup>).

Location	CH <sub>4</sub>	C <sub>2</sub> H <sub>6</sub>	C <sub>3</sub> H <sub>8</sub>	C <sub>4</sub> H <sub>10</sub>
United States	89.5-92.5	5.1-2	2.1-0.7	1.6-0.5
Algeria	86.9	9.0	2.6	1.2
Iran	74.9	13.0	7.2	3.1
North Sea	90.8	6.1	0.7	0.1

**Table 1.2** C-H bond strengths in hydrocarbons and their derivatives.<sup>3</sup>

Starting materials	C-H bond energy kJ/mol	Desired products	C-H bond energy kJ/mol
CH <sub>3</sub> -H	438.9	HOCH <sub>2</sub> -H	401.8
CH <sub>3</sub> CH <sub>2</sub> -H	423.0	CH <sub>2</sub> =CH-H	465.3
		HOCH(CH <sub>3</sub> )-H	401.4
		CH <sub>3</sub> C(=O)-H	373.8
(CH <sub>3</sub> ) <sub>2</sub> CH-H	409.1	CH <sub>2</sub> =CHCH <sub>2</sub> -H	361.9
		HOC(CH <sub>3</sub> ) <sub>2</sub> -H	381
		CH <sub>3</sub> COCH <sub>2</sub> -H	411.3

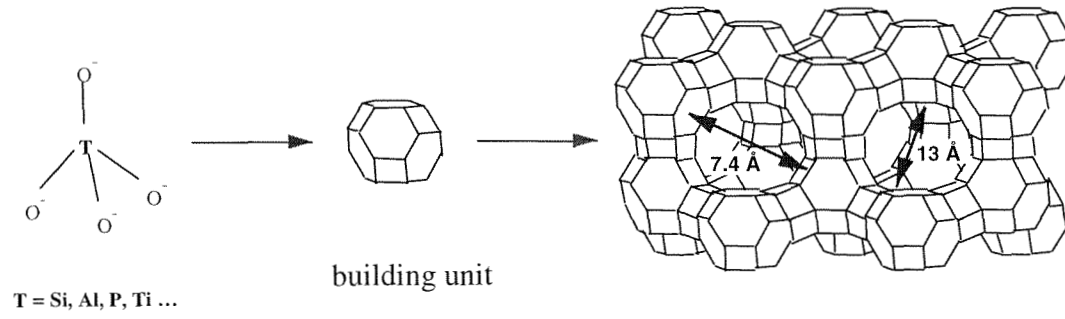
**Table 1.3** Reaction results of oxidative dehydrogenation of propane over several catalytic systems.

Catalyst	Temp (°C)	C <sub>3</sub> H <sub>8</sub> :O <sub>2</sub> :Inert (He or N <sub>2</sub> ):H <sub>2</sub> O	Total flow (cc/min-gcat)	Conv.(%)		Yield(%) C <sub>3</sub> H <sub>6</sub>	Ref.
				C <sub>3</sub> H <sub>8</sub>	C <sub>3</sub> H <sub>6</sub>		
VSil545	490-550	2.8/8.4/88.8/-	12.6	-	25	68	
VAPO-5	520	4/8/88/-	200	21	13.4	19	
NiMoO <sub>4</sub>	560	9/9/42/-	60	26.6	16	19	
5%V <sub>2</sub> O <sub>5</sub> /SiO <sub>2</sub>	650	25/15/60/-	400	33	4.95	69	
V-Mg-O	540	4/8/88/-	333	35.8	15.2	24	
V-Mo-O/SiO <sub>2</sub>	500	4/2/5/4	75	15.0	9.4	this work, Chapter 3	
Cs <sub>2.5</sub> Cu <sub>0.08</sub> H <sub>3.34</sub> PV <sub>3</sub> Mo <sub>9</sub> O <sub>40</sub> *	380	10/10/10/-	30	35	9.45	17	

\* Acetic acid, acrylic acid and acrolein were also produced. The selectivity to acetic acid was 7%, and the total selectivity to acrylic acid and acrolein was 4%.

**Table 1.4** Partial oxidation of propylene (adapted from Ref.<sup>30</sup>).

Temp(°C)	Conv.(%) propylene	Sel. (%)		
		acrolein	acrylic acid	acetic acid
Bi-Mo-O(modified by Fe, Co etc)				
350	98	95	-	-
CoMoTeO				
360	97	13.9	39.2	-
NiMoTeO				
350	97.3	20.9	58.8	-
VPTeO				
410	100	3.0	37.0	5.0



**Scheme 1.1** Structure of Faujasite.



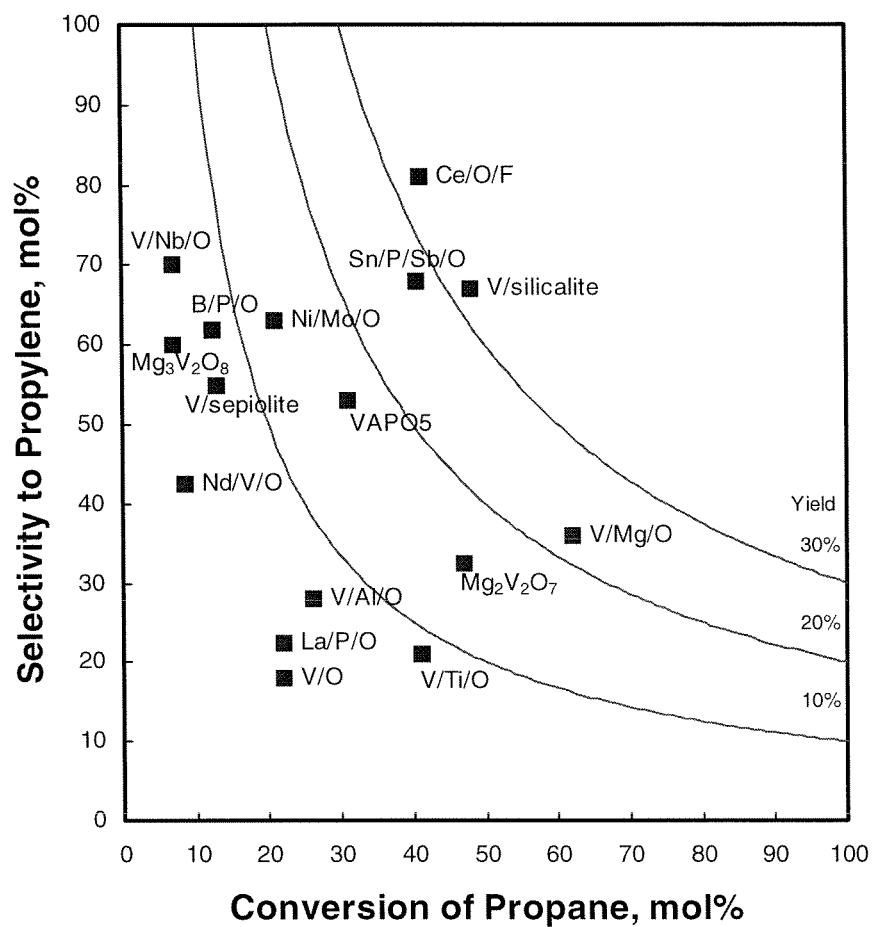


**Figure 1.2** Best yields to propylene in oxydehydrogenation of propane reported in the literature for the various catalysts (adapted from Ref.<sup>23</sup>).

## **CHAPTER TWO**

### **Physicochemical Characterization and Propane Oxidation over Vanadium- Containing Zeolite L Catalysts**

## 2.1 INTRODUCTION

Zeolite L (Linde Type L) is a type of zeolite with a one-dimensional channel system and large pore openings (12-member ring, 7.1 Å in diameter).<sup>1</sup> The internal cages of zeolite L have a diameter of roughly 13 Å. A schematic of the zeolite L structure is shown in Fig. 2.1. The composition of zeolite L is typically  $K_9[Al_9Si_{27}].21H_2O$  with potassium cations as the framework charge balance.

We first chose zeolite L as the matrix for building metal oxide clusters. This is based on several considerations as follows. First, zeolite L has a large pore size that offers sufficient space to build metal oxide clusters within. Additionally, the framework of zeolite L is highly charged as a consequence of its high silicon to aluminum ratio (~3). This charge can possibly stabilize the occluded materials and modify their surface chemistry. Furthermore, the particle size of zeolite L is tunable. Both submicrometer and nanometer size zeolite L can be synthesized. The nanometer size zeolite L (nano L) is of particular interest, because using small size particles can significantly reduce the diffusion time of the desired products inside zeolite channels, and further reduce the chance of overoxidation. As mentioned in Chapter One, overoxidation is a major challenge for partial oxidation of light alkanes. Zeolite L is one of the few zeolites that can be synthesized in nanometer size while having large pores.<sup>2</sup> Thus, zeolite L may be a good matrix for supporting metal-oxide clusters.

Vanadium is the most preferred element to activate light alkanes.<sup>3</sup> In this chapter, we focus on vanadium containing zeolite L catalysts.

## 2.2 EXPERIMENTAL SECTION

### 2.2.1 Synthesis

#### Synthesis of Zeolite L

Both nano L and submicron L have been synthesized.

Nano L was synthesized by the following literature procedure:<sup>4</sup> (1) Preparation of a silica solution: 22.5 g fumed silica (Cab-O-Sil M5) was carefully added to a KOH solution of 17 g KOH pellets (Aldrich, 85%+) and 93 g H<sub>2</sub>O under stirring. The resulting mixture was stirred and heated at 60°C until a clear solution was obtained (4-8 hours); (2) Preparation of an alumina solution: 1 g of aluminum foil (Aldrich, 0.05mm thick, 99.8%) was slowly added to a KOH solution of 7.3 g KOH pellets and 39 g H<sub>2</sub>O under stirring. The solution formed was filtered to remove the iron impurities of the aluminum foil that remained undissolved; (3) Combination of the two solutions: The alumina solution was slowly added to the silica solution under stirring at room temperature. The resulting mixture was poured into Teflon lined bombs and heated in a forced convection oven (175°C) with rotation for 8-16 hours. The solid samples were repeatedly washed (centrifuged and redispersed in water using ultrasonication) until the pH of the dispersion was below 8, and then dried at 100°C for 12 hours. The solid obtained is nano L in potassium form.

A typical synthesis for submicron L proceeds as follows: 0.511 g of Al<sub>2</sub>O<sub>3</sub>·2H<sub>2</sub>O (Vista) were added to a solution of 4.047 g of KOH (Aldrich) and 19.28 g of deionized H<sub>2</sub>O. A suspension was obtained after stirring for 15 minutes, and 15 g of Ludox AS-40 was added to the above suspension. The entire gel was stirred for 30 minutes. After aging for 2 days, the gel was heated at 175°C for 8 days under autogenous pressure in a

Teflon lined autoclave. The solid was washed with deionized water, filtered, and dried in air at 70°C. The resulting submicron L is also of potassium form.

### Modification of Zeolite L

Three approaches (ion exchange-hydrolysis method, vapor phase impregnation method, and liquid phase impregnation method) were employed to synthesize V-O clusters supported by zeolite L:

#### Method I: Ion-Exchange-Hydrolysis (IEH)

This method is based on the fact that the cations within the zeolite matrix have properties similar to those found in aqueous solution.<sup>5</sup> Thus, by soaking the transition metal ion-exchanged zeolite in an alkaline solution, metal hydroxide can be formed inside the zeolite pores. The produced metal hydroxide could be transformed into metal oxide clusters inside the zeolite matrix by calcination in air.<sup>6</sup> In our vanadium case,  $\text{VO}^{2+}$  can first be introduced to the framework charge-balancing sites of zeolite L, and base, such as KOH, can be used to precipitate  $\text{VO}^{2+}$  inside zeolite pores. More specifically, the framework charge-balancing ion  $\text{VO}^{2+}$  can be replaced by  $\text{K}^+$  ion of KOH, and the  $\text{VO}^{2+}$  ions can combine with  $\text{OH}^-$  to form  $(\text{VO})^{2+}_x(\text{OH})^-_{2x}$  inside the zeolite pores. After calcination,  $\text{V}_x\text{O}_y$  can be formed inside zeolite L in a manner consistent with metal oxide formation from dehydration of the corresponding base.

Vanadyl ion-exchanged L (both nano-sized zeolite L and submicron-sized zeolite L) was synthesized by stirring 1 g potassium form of zeolite L (K-L) with 50 mL 0.1 M  $\text{VOSO}_4$  (Aldrich) (pH = 2.2-2.8) at 60°C overnight, followed by centrifuging, washing and drying at 70°C in air. The procedure was repeated once to obtain higher vanadium

contents.<sup>7</sup> The solid obtained is denoted IE-L (IE-ML for submicron L and IE-NL for nano L).

Hydrolysis was performed by adding 0.2 M KOH to a vanadyl ion-exchanged zeolite L and H<sub>2</sub>O slurry (1 g of IE-L/12.5 g H<sub>2</sub>O). The mixture was stirred for more than 1 hour so that the pH value of the mixture was stable. The resulting solid was centrifuged and dried in a 70°C oven for 2 hours and air dried thereafter.<sup>6,8</sup> This method is referred to as IEH (E).

A second hydrolysis procedure was employed and involved incipient wetness impregnation of a KOH solution to the dehydrated vanadyl ion-exchanged zeolite L. IE-L samples were first dehydrated at 175°C for 4 hours. The volume of the KOH solution added was equal to the pore volume of zeolite and the amount of KOH was chosen to be just enough to replace the balanced VO<sup>2+</sup> ions. The resulting mixture was dried in air for 2 days. This method is referred to as IEH (I). Here “I” indicates hydrolysis by liquid phase impregnation of KOH.

#### Method II: Vapor Phase Impregnation (VPI)

VO(acac)<sub>2</sub> (vanadyl acetylacetonate, Aldrich) was impregnated into zeolites in a method similar to the reported vapor phase impregnation of Pt(acac)<sub>2</sub> to zeolite L.<sup>9</sup> Dehydrated zeolite L was physically mixed with a fixed amount of VO(acac)<sub>2</sub> according to the desired vanadium content in the zeolite (0.5 wt.%, 1 wt.%, 2 wt.% ). The mixture was then put into a glass tube with a volume of 8 mL, and sealed under a vacuum of better than 10<sup>-4</sup> Torr (Fig. 2.2). The sample (in the sealed tube) was slowly heated to

145°C and then stored at this temperature for 16-24 hours. After the heat treatment, the sample was slowly cooled down to room temperature (20°C/hour).

Method III: Liquid Phase Impregnation (LPI)

Incipient wetness impregnation of vanadium oxalate was also employed. Zeolite L samples were first dehydrated at 175°C for 4 hours and the obtained dehydrated samples were mixed with an aqueous solution of  $\text{VO}_2\text{C}_2\text{O}_4$  (GFS Chemicals, Inc.). The mixture was then dried in air for two days, and calcined at 500°C for 12 hours. The resulting powder was yellow.

For all the samples prepared above, the nomenclature used here is “vanadium wt.-%-synthesis method-size of the zeolite.” For example, a sample of submicron-sized zeolite L with 2 wt.-%V, synthesized by IEH-impregnation method is denoted as “2wt.-%-IEH(I)-ML.”

### **2.2.2 Characterization**

Transmission electron micrographs (TEM) were recorded using a Phillips 430 microscope operating at 200 kV. The scanning Electron Microscopy (SEM) images were obtained using a Camscan Series 2-LV scanning electron microscope with an accelerating voltage of 15 kv. X-ray diffraction (XRD) powder patterns were collected using  $\text{CuK}\alpha$  radiation on a Scintag XDS-2000 diffractometer equipped with a liquid  $\text{N}_2$  cooled, Germanium solid-state detector. Nitrogen adsorption isotherms were determined at 77K using an Omnisorp 100CX apparatus. Around 0.1 g of zeolite sample were used for each measurement. Thermal-gravimetric analysis (TGA) was performed on a Dupont

951 thermogravimetric analyzer. Typically 10-20 mg of sample were heated in air under a temperature ramp rate of 10°C/min. Electron paramagnetic resonance (EPR) results were recorded on an E-line Varian spectrometer at liquid helium temperature. The spectrometer was operated at X-band wavelength with 100 kHz magnetic field modulation. A typical operation was done under 2 mw of power and  $2.0 \times 10^3$  of gain with a 20 Gauss modulation and a time constant of 0.064. DPPH was used as the standard for magnetic field calibration. Raman spectra were obtained with a Nicolet Raman 950 stand-alone FT-Raman accessory using Happ-Genzel apodization. Samples were first calcined in air at 400°C for 4 hours and sealed before each measurement. FTIR spectra were obtained using a Nicolet System 800 Spectrophotometer with KBr pellet technique. Elemental analyses were performed by Galbraith Laboratories, Inc.

### **2.2.3 Propane Oxidation**

Catalytic experiments were carried out using a continuous flow system (BTRS-Jr., Autoclave Engineers) with a fixed bed stainless steel reactor. Before a reaction, samples were pelletized and sieved to 35/60 mesh size. 0.5 g catalyst with 1.0 g SiC inert were used for each run. Catalysts were pretreated under He and O<sub>2</sub> at 450°C for two hours. The reactions were carried out at temperatures from 350°C to 600°C under atmospheric pressure with a reactant molar ratio of propane: oxygen: helium = 20:10:70 and a total flow of 100 mL/min.

Product analysis was performed using a gas chromatograph (Hewlett Packard G1800A GCD system) equipped with an electron ionization detector and a capillary column (Hewlett Packard, HP Plot-Q). Gaseous products were analyzed using online

sampling, while liquid products were collected in an ice trap and analyzed separately. A detailed reaction system scheme is shown in Fig. 2.3.

## 2.3 RESULTS AND DISCUSSION

### 2.3.1 Characterization of Vanadium-Containing Zeolite L Catalysts

*Elemental Analysis* Vanadium contents of ion-exchange and ion-exchange-hydrolysis samples are reported in Table 2.1. For both IE-ML and IE-NL samples, vanadium contents are about 3 wt.% (about 1 vanadium atom per unit cell). Hydrolysis by ion-exchange with KOH results in 30% vanadium loss. For liquid impregnation and vapor phase impregnation samples, the vanadium content is assumed to be the amount of vanadium loaded.

*SEM and TEM* High resolution TEM shows that the size of the nano L particles is around 20 ~ 40 nm (Fig. 2.4a). The size of submicron L particles is slightly less than 1 micrometer as observed from SEM (Fig. 2.4b). Therefore, the size difference between these two types of zeolite L samples is about 25~40 times.

*XRD* XRD patterns of as-made and modified nano L and submicron L samples are shown in Fig. 2.5. The XRD peaks of nano L samples are much broader than those of submicron-sized L. This broadness of XRD peaks is attributed to the smaller size of the nano L particle.<sup>10</sup> After vanadium is introduced to the zeolite by ion-exchange, ion-exchange-hydrolysis, liquid phase impregnation, and vapor phase impregnation methods, most of the crystal structures are still kept, although the crystallinity appears to decrease slightly from the lowering of the XRD line intensities.

TGA TGA of IEH(I)-ML samples have derivative peaks at 57.7°C and 360°C (Fig. 2.6); TGA of IE-ML samples also have a derivative peak at 57°C, but no peak around 360°C is observed. The weight loss below 200°C is from the loss of zeolite water. The peak at 360°C for IEH-ML samples suggests that a new species is formed. This new species could be  $V_xO_y$  clusters obtained from dehydration of  $(VO)^{2+}_x(OH)^{-}_{2x}$ , which are possible products from the addition of KOH to VO-L. Fresh IEH(E)-ML and IEH samples of nano-sized zeolite L all show TGA patterns similar to that illustrated in Fig. 2.6.

$N_2$  Adsorption The  $N_2$  adsorption isotherms (Fig. 2.7) show that the volume of  $N_2$  adsorption decreases in the order of as-made, IE and IEH nano-sized zeolite L. This indicates that for the  $VO^{2+}$  ion-exchanged zeolite L samples, most  $VO^{2+}$  ions are located inside the pores. Further hydrolysis results in even larger occluded materials, suggesting possible formation of metal-oxide clusters inside zeolite pores.

A detailed calculation shows that after ion exchange the volume of  $N_2$  adsorbed decreases from 0.154 to 0.149 g  $N_2$ /g zeolite, and after hydrolysis the volume of  $N_2$  adsorbed further decreases to 0.143 g  $N_2$ /g zeolite. The volume loss of 5.2 mg  $N_2$ /g zeolite due to ion exchange corresponds to 18.1 Å<sup>3</sup> per vanadium atom; while after hydrolysis, a total volume loss of 10.7 mg  $N_2$ /g zeolite corresponds to 37.1 Å<sup>3</sup> per vanadium atom (the density of liquid nitrogen is 0.808 g/mL and both IE-NL and IEH(I)-NL have 3.02 wt.%V). The crystal lattice of the vanadium pentoxide,  $V_2O_5$ , monocystal has orthorhombic symmetry with the space group  $D_{2h}-P_{mmm}$ , and unit cell parameters are  $a=11.51$  Å,  $b=4.37$  Å,  $c=3.56$  Å.<sup>11</sup> As each unit cell contains 5 vanadium atoms, the average volume per vanadium atom is 35.8 Å<sup>3</sup>. This value is close to our observed

volume loss per vanadium atom for IEH(I)-NL sample. Therefore, the decrease of micropore volume may be due to the incorporation of  $V_2O_5$ , but other methods of investigation are necessary to prove this speculation.

No information is obtained from  $N_2$  adsorption isotherms on the difference in average pore-size among these three samples, although difference could occur after the modification procedures. Zeolite with smaller pore openings usually can have larger interactions with the adsorbate molecules (or atoms), which means a lower transition pressure will occur for microporous adsorption. However, because of the strong interactions between the quadruple of  $N_2$  molecule with the zeolite framework,<sup>12</sup> the influence of pore size on transition pressures of microporous adsorption can be neglected. Therefore, no difference observed for the transition pressures of the three materials is reasonable. Argon would be a better adsorbate for pore size study.

EPR The EPR spectrum of ion exchanged submicron-sized L (IE-ML) has two groups of eight peaks, that is typical for a well isolated vanadyl group (Fig. 2.8a). This eight-peak splitting is called hyperfine structure and is a result of the interaction of the electronic spin of a transition metal with its own nuclear spin (spin-nuclear interaction, vanadium has a nuclear spin of  $7/2$ ). The parameters (g-values with  $g_{\parallel}=1.988$  and  $g_{\perp}=2.03$ , and hyperfine constants with  $A_{\parallel}=211.8$  gauss and  $A_{\perp}=76.7$  gauss) predict that vanadium atoms have a distorted octahedral (or square pyramidal) symmetry.<sup>13</sup>

EPR spectra of ion-exchange-hydrolysis samples (both IEH(E)-ML and IEH(I)-ML) have wide bands with hyperfine structure superimposed (Fig. 2.8b, c). The observed wide bands come from strong spin-spin interaction of vanadium atoms that are close to each other. Explanations for these broad bands are given as follows. The spin-

spin interaction is generally 10-1000 times stronger than the spin-nuclear interaction. When the distance of two paramagnetic metal atoms decreases, the spin-spin interaction increases. When two spins are close enough, the local magnetic field can be highly perturbed by the magnetic dipole-dipole interaction of two spins. Thus, the actual magnetic field is a combination of the applied external field and magnetic field resulting from neighboring spins. Suppose that  $H_0$  is the resonant field of isolated paramagnetic species for which the spin-spin interactions can be ignored. Since different spins might have slightly different local environments, the actual magnetic fields for different spins may be slightly higher than  $H_0$  or lower than  $H_0$ . As a result, resonances can occur at slightly lower external fields in some situations, and slightly higher external magnetic fields in other situations. Because the magnetic field shown on the resonance spectrum only reflects the external field portion, the resulting spectrum usually contains a broad band, which is a sum of many resonances. Hyperfine structure due to spin-nuclear interaction can be obscured inside this broad band.<sup>14,15</sup>

The broad bands observed for IEH(E)-ML and IEH(I)-ML require the IEH samples to have a higher local density of vanadium relative to the ion exchange sample IE-ML, while keeping the total vanadium content the same. From  $N_2$  adsorption isotherm, we also know that most of the vanadium atoms are located inside the zeolite pores and large occluded materials are formed after hydrolysis. These results suggest that  $(VO)_x(OH)_{2x}^-$  clusters have formed in the IEH samples. When these two samples have been stored in air for a week, the broad bands disappear. This could be due to the oxidation of  $(VO)_x(OH)_{2x}^-$  in air to vanadium(V)-oxide clusters, that are EPR silent.

EPR spectra of IE-NL and IEH(E)-NL show a more complicated situation (Fig. 2.9). Even for the IE case, strong spin-spin interactions can be observed. For both IE-NL and IEH-NL samples, vanadium-oxide clusters may have been formed.

Vapor phase impregnated samples are not simple physical mixtures of VO(acac)<sub>2</sub> and zeolites as shown by EPR. The EPR spectrum of vapor phase impregnated sample 2wt.-%-VPI-ML has well separated hyperfine structures (Fig. 2.10a), indicating that vanadium is well isolated and there is no aggregated form of VO(acac)<sub>2</sub> in zeolite matrix. For comparison, a well-ground physical mixture of submicron-sized zeolite L and VO(acac)<sub>2</sub> with the same amount of vanadium (2wt.-%) was prepared. It has a broad EPR band (Fig. 2.10b) indicating that VO(acac)<sub>2</sub> is not well dispersed through physical mixing. Thus, during the vapor phase impregnation process, VO(acac)<sub>2</sub> is homogeneously sublimed and samples with isolated vanadium atoms are obtained.

EPR spectra suggest that for IEH-ML, IE-NL and IEH-NL samples vanadium oxide clusters have been formed, while for as-made VPI samples vanadium sites are well separated.

*Raman Spectroscopy* Fig. 2.11 shows Raman spectra of VPI and IEH samples along with those of zeolite L and V<sub>2</sub>O<sub>5</sub>. All of the zeolite L samples have three typical Raman bands: a broad band at ~1100 cm<sup>-1</sup> assigned to the asymmetric stretch of Si-O, a band between 600 and 800 cm<sup>-1</sup> assigned to the double ring vibration, and a strong peak at ~500 cm<sup>-1</sup> assigned to the motion of the oxygen atom perpendicular to the T-O-T bonds.<sup>16</sup>

In addition to these bands, vanadium-containing samples (1wt.-%-VPI-NL, 2wt.-%-VPI-NL and 2wt.-%-IEH(E)-NL) also show a broad band between 850 and 1000 cm<sup>-1</sup>,

that can originate from either the hydrated vanadyl group or from the terminal V=O of polyvanadate.<sup>17</sup> Since the solids had been calcined before the Raman spectra were taken, these bands suggest the possible formation of polyvanadate in the calcined IEH and VPI samples. Among these materials, only the Raman spectra of 2wt.%-VPI-NL indicates the possibility of having a crystalline V<sub>2</sub>O<sub>5</sub> phase (from the sharp peak at 995 cm<sup>-1</sup>). The V=O band is shifted to a higher frequency as the vanadium loading of VPI-NL is increased from 1 wt.%V to 2 wt.%V, which can be attributed to an increase in the average chain length of polyvanadate with loading.<sup>17</sup>

FTIR Spectroscopy From the IR spectra (Fig. 2.12) of 2wt.%-VPI-NL, certain features of VO(acac)<sub>2</sub> have been changed, supposedly via interaction with the zeolite framework. For example, a band at ~1723 cm<sup>-1</sup> is observed for VPI sample and can possibly be attributed to  $\nu(\text{C}=\text{O})$  (for pure VO(acac)<sub>2</sub> the location of  $\nu(\text{C}=\text{O})$  is at around 1560 cm<sup>-1</sup>). A band of  $\delta(\text{CH}_3)$  is shifted from 1420 cm<sup>-1</sup> in VO(acac)<sub>2</sub> to 1471 cm<sup>-1</sup> in the VPI solid. These FT-IR results suggest the absence of an aggregated state of V-O in VPI-NL sample, which is consistent with the results from EPR studies as discussed above. Having demonstrated homogeneous dispersion of VO(acac)<sub>2</sub> throughout the zeolite surface by FT-IR and EPR, one could envision forming controlled V-O clusters within the zeolites by the calcination of the VPI sample with O<sub>2</sub> (suggested by Raman spectra).

From the above results, V-O clusters are formed inside the zeolite pores for IEH samples. The well separated vanadium atoms in ion-exchange samples agglomerate after hydrolysis (EPR) and form larger occluded materials (N<sub>2</sub> adsorption); polyvanadates are

observed (Raman). For VPI samples, vanadium atoms are homogeneously dispersed (EPR) and possible polyvanadate exists after calcination by O<sub>2</sub> (Raman). During the calcination, V(IV) is oxidized to V(V) (EPR silent) and formation of V-O clusters may be observable by solid state NMR. However, we only obtained featureless NMR spectra because of the trace amounts of V(IV) that remain in all calcined samples.

### 2.3.2 Propane Oxidation Over Vanadium-Containing Zeolite L Catalysts

Comparison of IEH and IE samples The products of propane oxidation over the zeolite L samples are propylene, ethylene and the total oxidation products CO and CO<sub>2</sub>. No oxygenates are formed for any of the catalysts under our reaction conditions (Tables 2.2-2.5). For vanadyl ion-exchanged submicron-sized zeolite L catalyst (IE-ML), the propane conversion is 2.48% at 450°C with a propylene selectivity of 50.2% (Table 2.2). At a higher temperature, 550°C, the conversion increases to 12.5% and the selectivity to propylene is 47.3%. A lower conversion is observed for IEH(E)-ML sample, which could be due to the lower vanadium content in IEH(E)-ML compared to IE-ML. For IEH(I)-ML sample with the same vanadium content as that of IE-ML, the propane conversion is 1.34% at 450°C with 79.3% propylene selectivity, and 11.8% at 550°C with 57.4% propylene selectivity. Thus, introduction of KOH to IE-ML sample increases the propylene selectivity.

Propane oxidation over nano-sized zeolite L samples shows a similar trend with KOH addition to IE-NL (Table 2.3). For example, with IE-NL, the propane conversion is 2.59% with a propylene selectivity of 45.6% at 450°C; while with IEH(I)-NL, the selectivity to propylene increases to 70.5% at a propane conversion of 1.27%. A

different reaction condition is utilized, where the feed gas molar ratio is changed to propane:O<sub>2</sub>:He = 4:2:9 with a total flow rate of 15 mL/min. With this longer contact time condition, an increase of propylene selectivity is also observed as KOH is added to IE-NL. (For IE-NL, the propane conversion is 13.0% with 29.3% propylene selectivity; while for IEH(I)-NL, the conversion is 11.6% and the selectivity to propylene increases to 42.2%.)

The increase of propylene selectivity with addition of KOH can be attributed to two possibilities. One is that formation of metal-oxide clusters after addition of KOH can improve the selectivity of propylene; another possibility is that the addition of KOH increases the basicity of catalysts so that the heat of adsorption for propylene decreases resulting in a higher selectivity of propylene.<sup>18</sup> At this time the latter interpretation appears more reasonable.

Control experiments have been done for propane oxidation (Table 2.2). For pure ML, little activity is observed. Addition of KOH to ML increases the propane activity, however, with significant total oxidation. (At 450°C, a 19% propane conversion is observed with a selectivity to CO<sub>x</sub> of 99.5%.) Pure V<sub>2</sub>O<sub>5</sub> shows low activity with only 5.1% propane consumed and a 44.7% propylene selectivity at 450°C.

*Particle Size Effect* Little difference is observed for propane oxidation over nano-sized zeolite L samples and submicron-sized zeolite L samples (Table 2.4). For example, at 450°C the conversion is 2.59% for IE-NL with a 45.6% propylene selectivity, while the conversion is 2.48% for IE-ML with propylene selectivity of 50.2%. At 550°C, for IE-NL, the conversion is 13.0% and the selectivity to propylene is 52.6%; while for IE-ML,

the conversion is 12.5% and the propylene selectivity is 47.3%. These results suggest that diffusion may not be an important issue at these reaction conditions.

Effect of Contact Time A longer contact time greatly increases propane conversion. As shown in Table 2.3, for IEH(I)-NL sample, the propane conversion is 1.27% and the propylene selectivity is 70.5% at 450°C with a total flow rate of 100 mL/min (propane:O<sub>2</sub>:He = 20:10:70), while the conversion increases to 11.6% and the propylene selectivity is 42.2% with a total flow rate of 15 mL/min (propane:O<sub>2</sub>:He = 4:2:9).

Effect of Added Water Introduction of water to the reaction system has also been performed. A typical comparison is made for propane oxidation at 450°C under feed molar ratios of propane:O<sub>2</sub>:H<sub>2</sub>O:He=4:2:4:5 or 4:2:0:9 with a total flow of 15 mL/min. For IEH(I)-NL sample, the conversion is 11.6% and the propylene selectivity is 42.2% without water in the reaction stream; while with water, only 5.54% propane conversion is observed with a propylene selectivity of 57.8%. For LPI-NL sample, without water, 10% propane conversion is observed with selectivity to propylene 28.9%; while with water, the conversion is 3.38% and the selectivity increases to 47.4%. These results indicate that the addition of water produces an increase in propylene selectivity and a decrease in propane conversion.

Our reaction results show only low activity for all the vanadium-containing zeolite L catalysts we have studied thus far, as almost no reaction is observed at 350°C and significant activity is observed only at high temperatures (e.g. 550°C). Modification of the catalysts does not improve the reaction behavior significantly. The IEH(I) samples

(with V-O clusters and the same vanadium content as their IE counterparts) have a higher propylene selectivity in propane oxidation relative to the IE samples, while there is no obvious difference in catalytic behavior of the nano L and submicron L samples, suggesting that diffusion may not be an important issue at the conditions used here. The reaction conditions have a large effect on the reaction results. For example, higher contact times greatly increase propane conversion, and water in the feed stream enhances propylene selectivity but not propane conversion.

According to the above results, catalysts based on the potassium forms of zeolite L may not be effective catalysts for propane partial oxidation. Potassium was reported to be able to poison the centers of hydrocarbon activation.<sup>19</sup> Additionally, the high framework charge (Si/Al=3) of zeolite L may be too hydrophilic; therefore, the desorption of possible useful intermediates may be a problem.

## 2.4 SUMMARY

Various methods for zeolites modification are employed including ion exchange, liquid phase impregnation, and vapor phase impregnation methods. Metal oxide clusters are successfully formed inside zeolite by an ion-exchange-hydrolysis method. The isolated metal atoms introduced to the zeolite charge-balancing sites agglomerate after hydrolysis and form larger occluded material inside zeolite pores. The resulting material does not show high activity for the partial oxidation of propane. This may have resulted from the hydrophilic framework of zeolite L that has high adsorption energies for hydrophilic products thus leading to their complete oxidation. Therefore, a more hydrophobic zeolite matrix, zeolite beta, is investigated (Chapter Three).

## 2.5 REFERENCE

- 1) Meier, W. M.; Olson, D. H. *Atlas of Zeolite Structure Types*; Butterworth-Heinemann, 1996.
- 2) Lovallo, M. C.; Tsapatsis, M. in *Advanced Catalysts and Nanostructured Materials*; Moser, W. R., Ed.; Academic Press: San Diego, 1996, pp 307-343.
- 3) Cavani, F.; Trifiro, F. *Catal. Today* **1997**, *36*, 431-439.
- 4) Tsapatsis, M.; Lovallo, M.; Okubo, T.; Davis, M. E.; Sadakata, M. *Chem. Mater.* **1995**, *7*, 1734-1741.
- 5) Morrison, T. I.; Reis, A. H.; Gebert, E. *J. Chem. Phys.* **1980**, *72*, 6276.
- 6) Suzuki, M.; Tsutsumi, K.; Takahashi, H.; Saito, Y. *Zeolites* **1988**, *8*, 284-291.
- 7) Komorek, J.; Romotowski, T.; Serwicka, E. M.; Mastikhin, V. M. *Zeolites* **1994**, *14*, 629-634.
- 8) Wark, M.; Kessler, H.; Schulz-Ekloff, G. *Micropor. Mat.* **1997**, *8*, 241-253.
- 9) Hong, S.; Mielczarski, E.; Davis, M. E. *J. Catal.* **1992**, *134*, 349-358.
- 10) Bish, D. L.; Post, J. E. *Modern Powder Diffraction*; The Mineralogical Society of America, 1989; Vol. 20.
- 11) Witko, M.; Tokarz, R.; Haber, J. *Appl. Catal. A-Gen.* **1997**, *157*, 23-44.
- 12) Hathaway, P. E.; Davis, M. E. *Catal. Lett.* **1990**, *5*, 333-348.
- 13) Whittington, B. I.; Anderson, J. R. *J. Phys. Chem.* **1993**, *97*, 1032-1041.
- 14) Abragam, A.; Bleaney, B. *Electron Paramagnetic Resonance of Transition Ions*; Dover Publications, 1986.
- 15) Pilbrow, J. R. *Transition Ion Electron Paramagnetic Resonance*; Oxford University Press, 1990.
- 16) Knops-Gerrits, P.-P.; De Vos, D. E.; Feijen, E. J. P.; Jacobs, P. A. *Microporous Mater.* **1997**, *8*, 3-17.
- 17) Went, G. T.; Oyama, S. T.; Bell, A. T. *J. Phys. Chem.* **1990**, *94*, 4240-4246.

18) Grabowski, R.; Grzybowska, B.; Kozłowska, A.; Stoczyński, J.; Wcisto, K. *Top. Catal.* **1996**, *3*, 277-288.

19) Kung, M. C.; Kung, H. H. *J. Catal.* **1992**, *134*, 668-677.

**Table 2.1** Vanadium content of vanadium-containing zeolite L samples.

Sample	V/Al ratio	vanadium content (wt.%)
IE-ML	0.17	3.05
IEH(E)-ML	0.11	1.96
IEH(I)-ML	0.18	3.10
IE-NL	0.23	3.06
IEH(E)-NL	0.15	2.12
IEH(I)-NL	0.22	3.02

**Table 2.2** Propane oxidation over vanadium-containing submicron L catalysts.

Catalyst	Temp (°C)	Conv. (%)		Sel. (%)			
		C <sub>3</sub> H <sub>8</sub>	O <sub>2</sub>	C <sub>3</sub> H <sub>6</sub>	C <sub>2</sub> H <sub>4</sub>	CO	CO <sub>2</sub>
IE-ML	450	2.48	11.4	50.2	0	24.2	25.5
	550	12.5	58.6	47.3	3.5	22.0	27.2
IEH(E)-ML	450	0.71	3.91	46.0	0	0	54.0
	550	6.53	29.6	45.6	7.42	9.86	37.1
IEH(I)-ML	450	1.34	4.90	79.3	0	0	20.7
	550	11.8	45.5	57.4	3.2	19.7	19.7
	600	30.6	100	45.2	20.5	16.1	16.5
ML	450	no reaction					
	550	4.94	23.7	42.8	3.65	11.6	42.0
ML+KOH*	450	19.0	52.7	0.48	0	96.7	2.83
	550	22.6	62.9	4.58	0.49	88.6	6.3
V <sub>2</sub> O <sub>5</sub>	350	1.62	7.71	30.4	0	66.1	3.46
	450	5.10	21.3	44.7	0	40.9	14.4

0.5 g catalyst (mesh size -35/+60) together with 1.0 g SiC as the inert were used for each reaction. The feed gas molar ratio was C<sub>3</sub>H<sub>8</sub>:O<sub>2</sub>:He=20:10:70 with a total flow rate of 100 mL/min.

\* Same amounts of KOH were added to ML as that of IEH(I)-ML.

**Table 2.3** Propane oxidation over vanadium-containing nano L catalysts.

Catalyst	Temp (°C)	Conv. (%)		Sel. (%)			
		C <sub>3</sub> H <sub>8</sub>	O <sub>2</sub>	C <sub>3</sub> H <sub>6</sub>	C <sub>2</sub> H <sub>4</sub>	CO	CO <sub>2</sub>
IE-NL <sup>a</sup>	450	2.59	14.7	45.6	0	41.5	12.9
	550	13.0	60.6	52.6	3.59	27.8	16.2
IEH(I)-NL <sup>a</sup>	450	1.27	5.87	70.5	0	0	29.5
	550	11.4	55.0	52.7	3.83	21.4	22.1
IE-NL <sup>b</sup>	350	2.28	16.7	29.3	0	52.4	18.4
	450	13.0	100	29.3	0	35.1	35.6
IEH(I)-NL <sup>b</sup>	350	1.01	5.42	70.2	0	0	29.8
	450	11.6	75.6	42.2	0	27.6	30.2

0.5 g catalyst (mesh size -35/+60) together with 1.0 g SiC as the inert were used for each reaction.

a) The feed gas molar ratio was C<sub>3</sub>H<sub>8</sub>:O<sub>2</sub>:He=20:10:70 with a total flow rate of 100 mL/min.

b) The feed gas molar ratio was C<sub>3</sub>H<sub>8</sub>:O<sub>2</sub>:He=4:2:9 with a total flow rate of 15 mL/min.

**Table 2.4** Comparison of propane oxidation over submicron-sized and nano-sized zeolite L catalysts.

Catalyst	Temp (°C)	Conv. (%)		Sel. (%)			
		C <sub>3</sub> H <sub>8</sub>	O <sub>2</sub>	C <sub>3</sub> H <sub>6</sub>	C <sub>2</sub> H <sub>4</sub>	CO	CO <sub>2</sub>
IE-NL	450	2.59	14.7	45.6	0	41.5	12.9
	550	13.0	60.6	52.6	3.59	27.8	16.2
IE-ML	450	2.48	11.4	50.2	0	24.2	25.5
	550	12.5	58.6	47.3	3.5	22.0	27.2
IEH(I)-NL	450	1.27	5.87	70.5	0	0	29.5
	550	11.4	55.0	52.7	3.83	21.4	22.1
IEH(I)-ML	450	1.34	4.90	79.3	0	0	20.7
	550	11.8	45.5	57.4	3.2	19.7	19.7

0.5 g catalyst (mesh size -35/+60) together with 1.0 g SiC as the inert were used for each reaction. The feed gas molar ratio was C<sub>3</sub>H<sub>8</sub>:O<sub>2</sub>:He=20:10:70 with a total flow rate of 100 mL/min.

**Table 2.5** Effect of water on propane oxidation over vanadium-containing nano-sized zeolite L catalysts.

Catalyst	Conv. (%)		Sel. (%)		
	C <sub>3</sub> H <sub>8</sub>	O <sub>2</sub>	C <sub>3</sub> H <sub>6</sub>	CO	CO <sub>2</sub>
IEH(I)-NL <sup>a</sup>	11.6	75.6	42.2	27.6	30.2
IEH(I)-NL <sup>b</sup>	5.54	29.8	57.8	25.3	16.9
LPI-NL <sup>a*</sup>	10.0	86.5	28.9	21.1	50.0
LPI-NL <sup>b*</sup>	3.38	22.5	47.4	24.4	34.2

0.5 g catalyst (mesh size -35/+60) together with 1.0 g SiC as the inert were used for each reaction. The temperature was 450°C.

a) The feed gas molar ratio was C<sub>3</sub>H<sub>8</sub> :O<sub>2</sub>:He=4:2:9 with a total flow rate of 15 mL/min.

b) The feed gas molar ratio was C<sub>3</sub>H<sub>8</sub> :O<sub>2</sub>:H<sub>2</sub>O:He=4:2:4:5 with a total flow rate of 15 mL/min.

\*LPI-NL has 2 wt.% vanadium content.

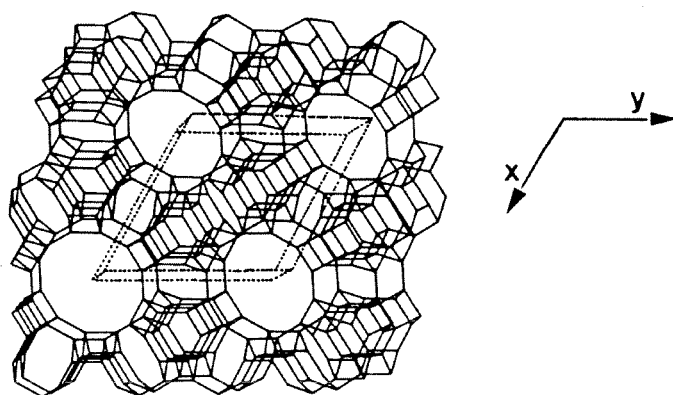


**Figure 2.1** Zeolite L structure (framework viewed along [001]). Each intersection in the figure represents a silicon or aluminum atom, while the midpoint of each line represents an oxygen atom.

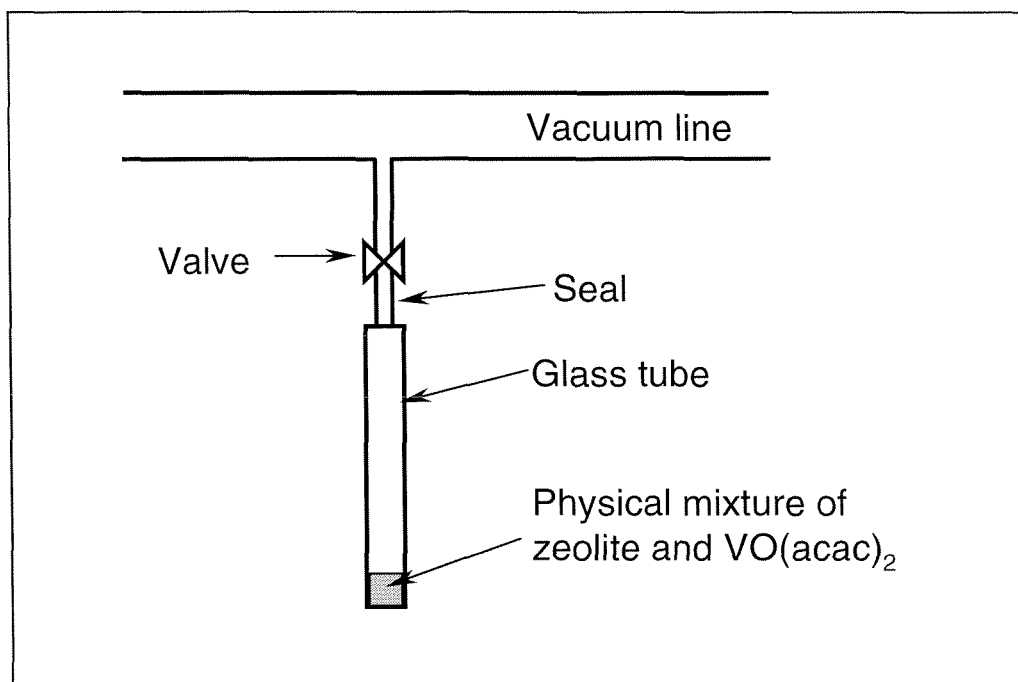


**Figure 2.2** Apparatus for vacuum seal in the synthesis of vapor phase impregnation samples.

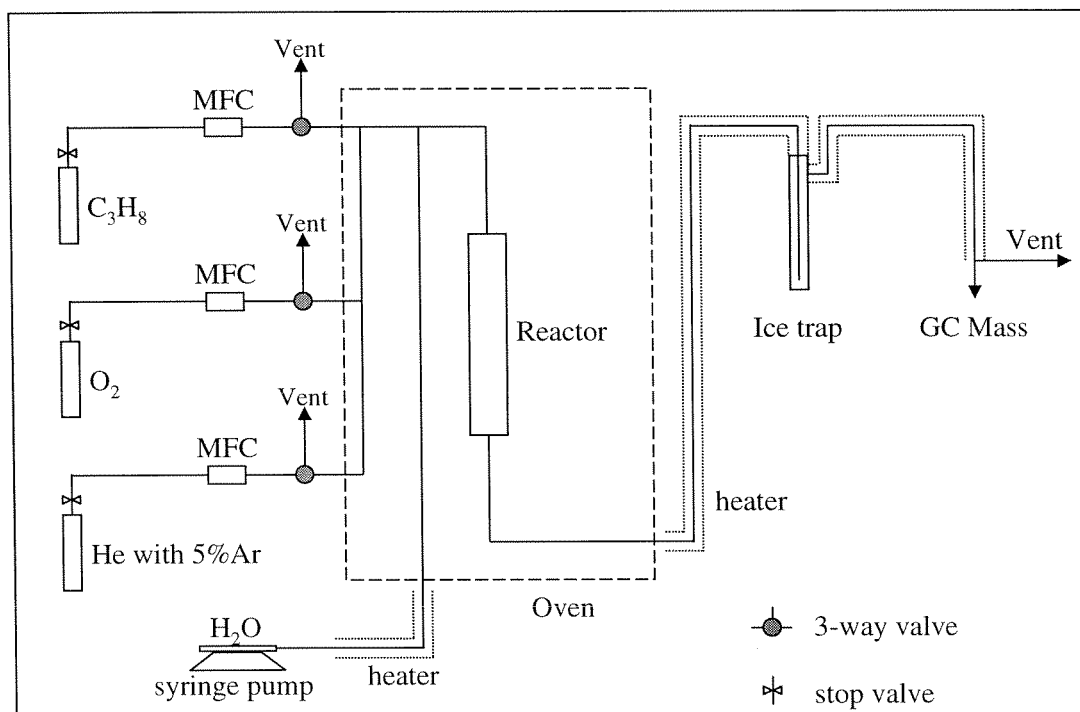


**Figure 2.3** Schematic of reactor system.

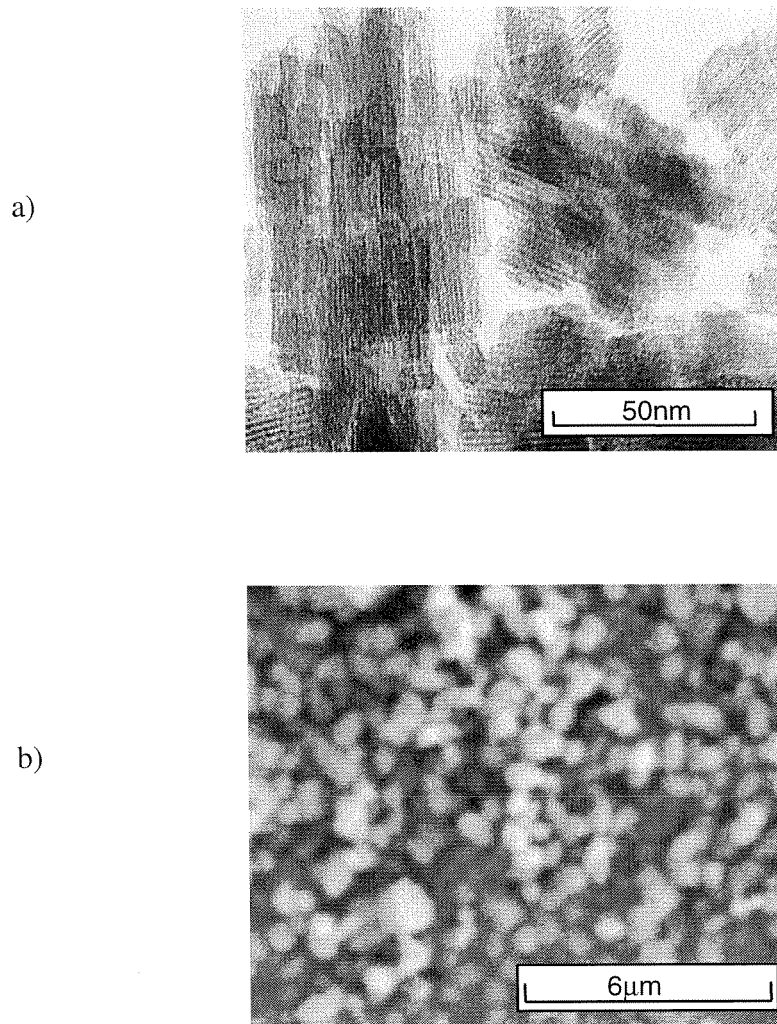


**Figure 2.4** a) HRTEM image of nano-sized zeolite L oriented with the c axis perpendicular to the electron beam; b) SEM image of submicron-sized zeolite L.

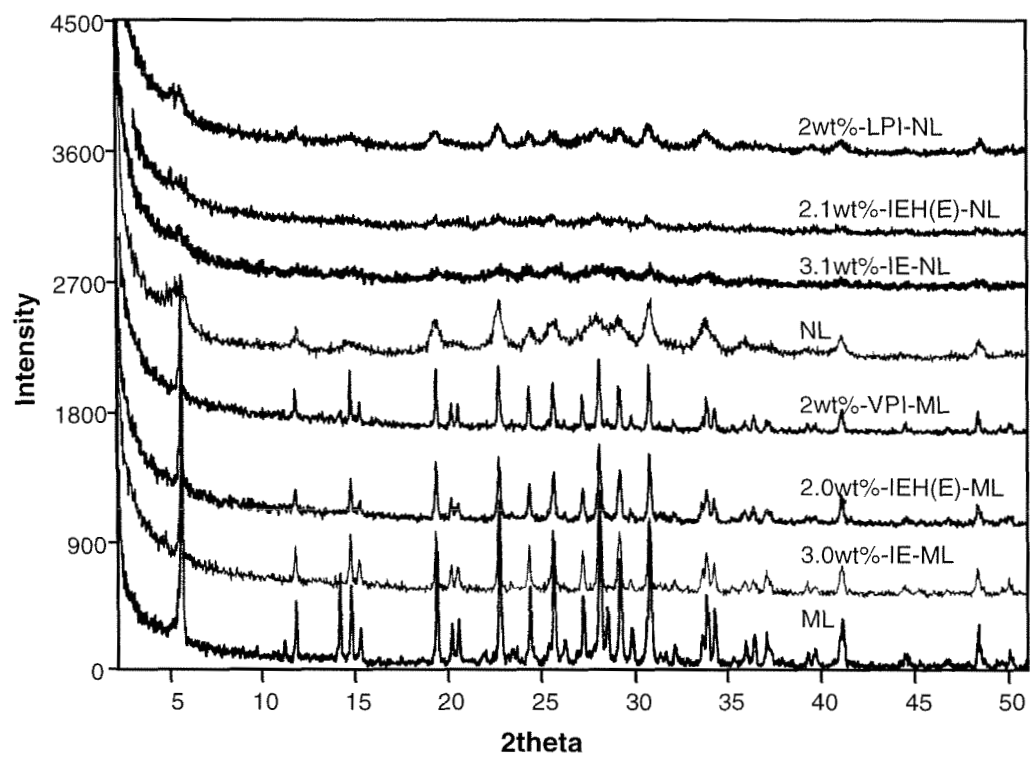


**Figure 2.5** XRD patterns of zeolite L based samples.

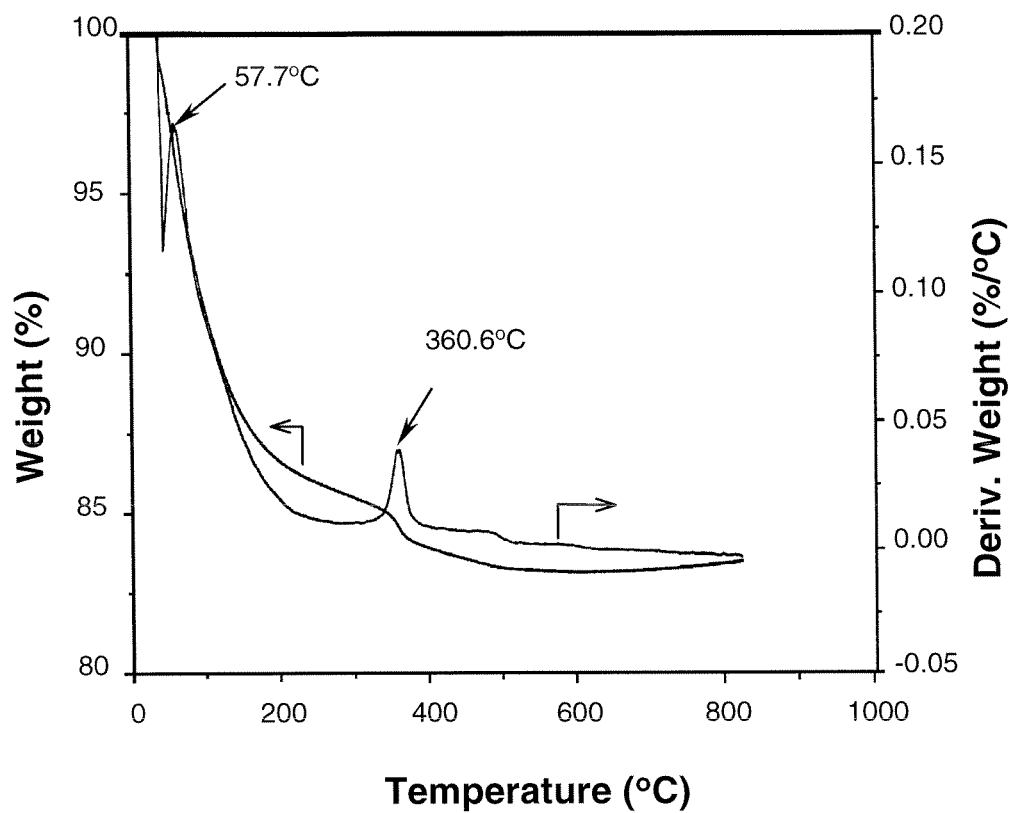


**Figure 2.6** TGA of an ion-exchange-hydrolysis sample (IEH(I)-ML).

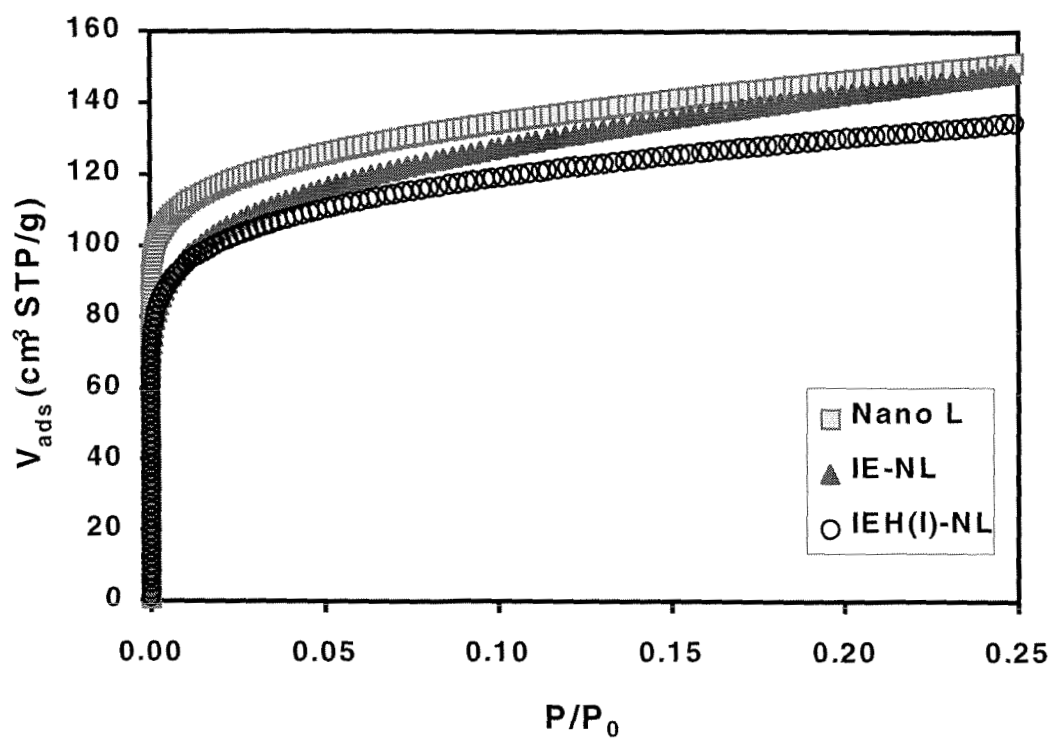


**Figure 2.7**  $N_2$  adsorption isotherms of nano-sized zeolite L, IE-NL and IEH-NL.

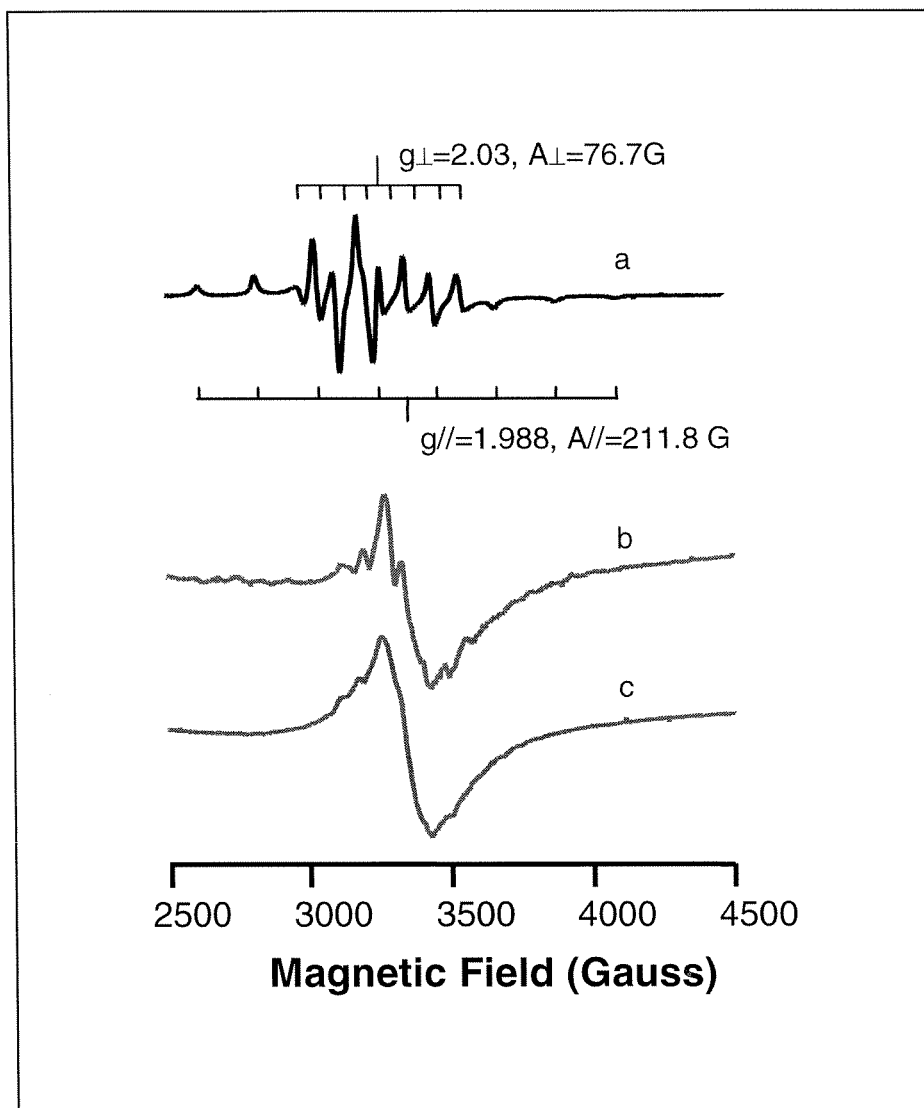


**Figure 2.8** EPR spectra for IE submicron-sized zeolite L series: a) IE-ML, b) IEH(E)-ML, and c) IEH(I)-ML.

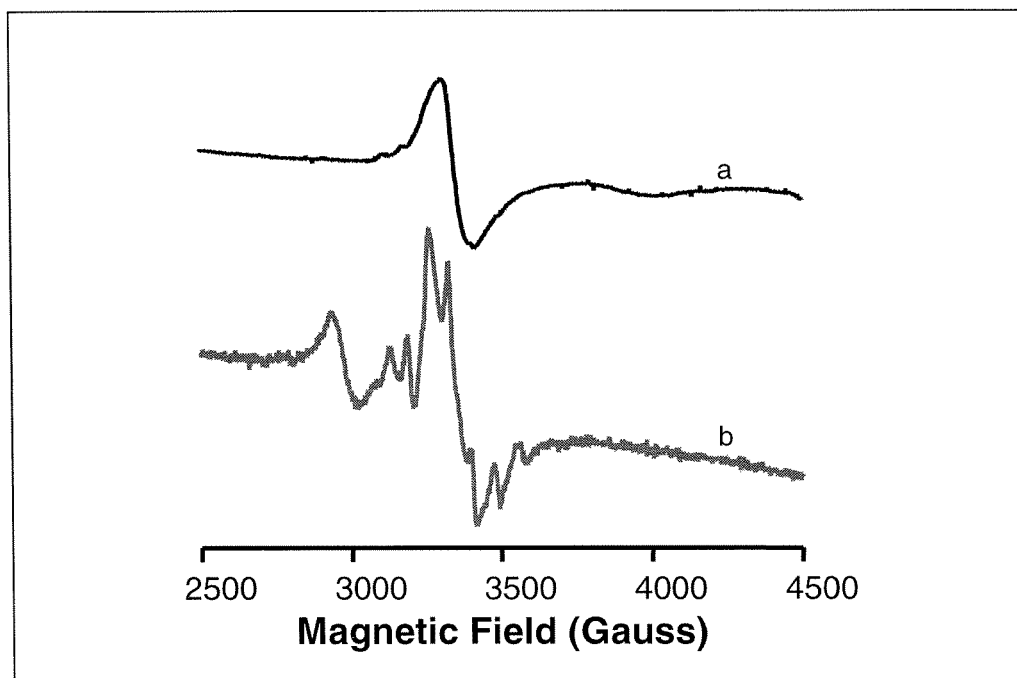


**Figure 2.9** EPR spectra of IE nano-sized zeolite L series: a) IE-NL, b) IEH(E)-NL.

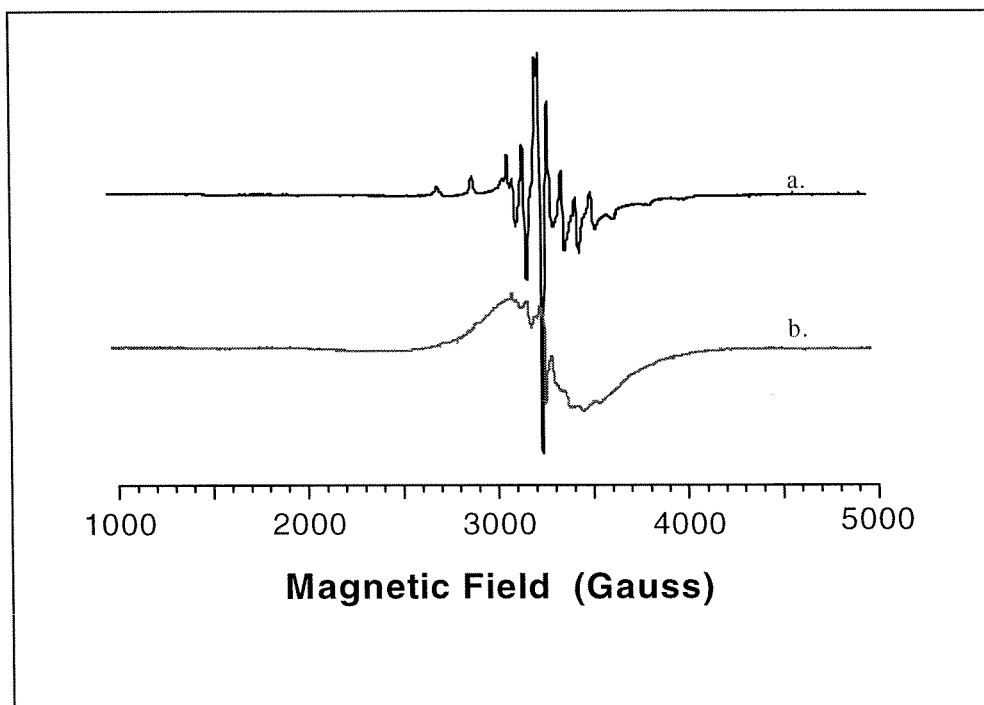


**Figure 2.10** EPR spectra of a) 2wt.%-VPI-ML and b) a physical mixture of  $\text{VO}(\text{acac})_2$  with 2 wt.% vanadium.

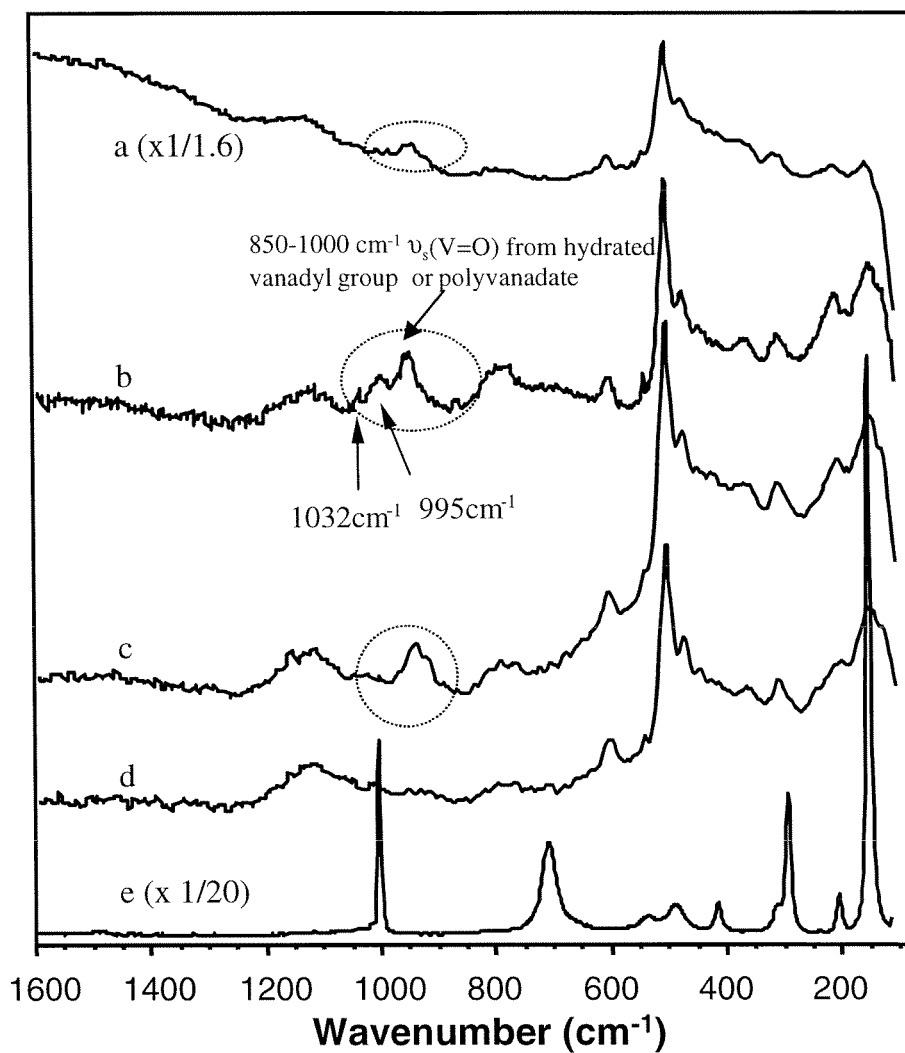


**Figure 2.11** Raman spectra of modified zeolite L samples and  $\text{V}_2\text{O}_5$ : a) 1wt.-%-VPI-NL, b) 2wt.-%-VPI-NL, c) 2wt.-%-IEH(E)-NL, d) NL, and e)  $\text{V}_2\text{O}_5$ .

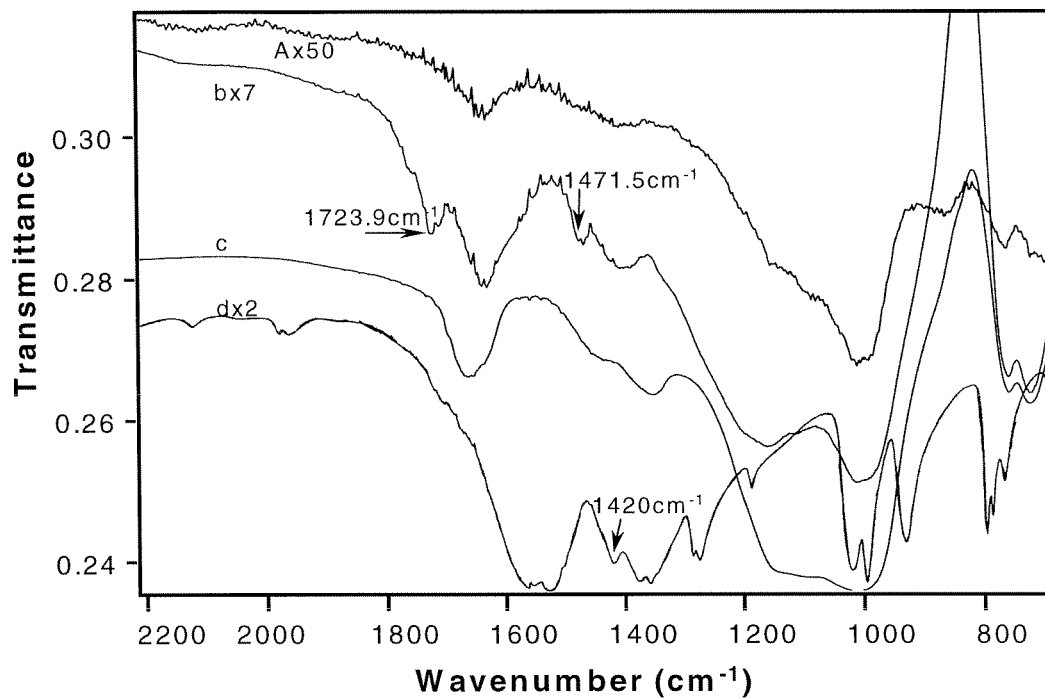


**Figure 2.12** FT-IR spectra of VPI-Series and VO(acac)<sub>2</sub>: (a) 1wt.%-VPI-NL, (b) 2wt.%V-VPI-NL, (c) Nano L, and (d) VO(acac)<sub>2</sub>.

# **CHAPTER THREE**

## **Partial Oxidation of Propane over Vanadium-Containing Zeolite Beta Catalysts**

### 3.1 INTRODUCTION

In this chapter, I report my investigation on propane partial oxidation over vanadium-containing zeolite beta catalysts. As mentioned in Chapter One, zeolites with large pores and small particle size are preferred as the matrix for propane partial oxidation catalysts because the large pores offer sufficient space to build metal-oxide clusters inside, and the smaller the particle size, the shorter the diffusion pathway away from the active sites to the bulk fluid phase. Zeolite beta has large 12 member-ring pore openings and a 3D channel system ([001]  $12\ 5.5 \times 5.5^*$   $\langle 100 \rangle$   $12\ 7.6 \times 6.4^{**}$ ).<sup>1</sup> Small particle size zeolite beta can be synthesized. Most synthesized zeolite beta has crystal sizes in the submicrometer range and nanocrystalline zeolite beta as small as 10 nm has been reported.<sup>2</sup> Besides large pores and small particle size, zeolite beta has other advantages as follows. (1) The hydrophobic framework of zeolite beta may improve selectivities to the desired hydrophilic products. The hydrophobic framework of zeolite beta is attributed to its high Si/Al ratio (a typical composition of zeolite beta is  $\text{Na}_n[\text{Al}_n\text{Si}_{64-n}\text{O}_{128}]$  ( $n < 7$ )). Compared to the hydrophilic frameworks such as zeolite L where it is difficult to desorb the hydrophilic intermediates, the hydrophobic framework of zeolite beta system may assist the desorption of hydrophilic, desired products. As a consequence, a higher activity and higher selectivities to the desired products may be obtained using zeolite beta system. (2) Zeolite beta is commercially available and tailoring of zeolite beta has been intensely investigated. The position of some transition metal inside framework and outside of the framework can be controlled. Examples of transition metal in framework position include Zn/beta (CIT-6),<sup>3,4</sup> V/beta<sup>5</sup>, and

Ti/beta,<sup>6,7</sup> etc. In this chapter, I investigated vanadium-containing zeolite beta catalysts, with emphases on: (1) understanding whether metal oxide clusters supported by a hydrophobic framework, zeolite beta, are active in propane oxidation and behave differently from the corresponding bulk metal oxide; (2) understanding the influence of the location of the transition metal, the acidity of the zeolite matrix, the hydrophobicity of the zeolite framework and the presence of a second metal on propane oxidation.

## **3.2 PROPANE OXIDATION OVER VANADIUM-CONTAINING ZEOLITE**

### **BETA CATALYSTS**

#### **3.2.1 Vanadyl Ion-Exchanged and Vanadium Ion-Exchange-Hydrolyzed Zeolite**

##### **Beta Catalysts**

###### 3.2.1.1 Introduction

In Chapter Two, ion-exchange-hydrolysis is found to be a reliable method to build metal oxide clusters inside zeolites. Here efforts are continued to synthesize metal oxide clusters within a zeolite beta matrix. As potassium may poison the centers of hydrocarbon activation,<sup>8</sup> the hydrogen, ammonium, and sodium forms of zeolite beta are used instead of the potassium form.

###### 3.2.1.2 Experimental Section

###### Sample Preparation

The starting materials used for the preparation of vanadyl ion-exchanged zeolite beta were Na-zeolite beta (PQ Corp, Si/Al=12),  $\text{NH}_4\text{NO}_3$  (Aldrich) and  $\text{VOSO}_4$  (Aldrich). The ammonium form of zeolite beta ( $\text{NH}_4$ -beta) was synthesized by ion-exchange of Na-beta with 1 M  $\text{NH}_4\text{NO}_3$  solution (50 mL  $\text{NH}_4\text{NO}_3$  solution/1 g zeolite)

overnight at 80°C three times. The resulting NH<sub>4</sub>-beta was washed with double distilled water, filtered, and dried overnight in an 80°C oven. H-beta was formed by calcination of NH<sub>4</sub>-beta at 500°C for 4 hours in N<sub>2</sub>. Vanadyl ion-exchanged zeolite beta was prepared by ion-exchange of Na-beta, NH<sub>4</sub>-beta or H-beta with 0.1 M VOSO<sub>4</sub> solution (50 mL VOSO<sub>4</sub> solution/1 g zeolite) for 10 hours at 60°C twice,<sup>9</sup> and the resulting mixture was washed with water, filtered, and dried overnight in an 80°C oven. Depending on the starting form of zeolite beta, the solids obtained were referred as VO-Na-beta, VO-NH<sub>4</sub>-beta and VO-H-beta.

Two hydrolysis methods, ammonia vapor treatment and liquid phase impregnation of NaOH, were employed to synthesize the hydrolysis samples of VO-Na-beta. The procedure for liquid phase impregnation of NaOH was similar to that described in Chapter Two. The resulting sample was denoted IEH(I)-beta. Ammonia vapor treatment was performed as follows. Vanadyl ion-exchanged sample was first dehydrated at 200°C for 2 hours in He, then cooled to room temperature in a He atmosphere. Moist ammonia vapor carried by He flow through the dehydrated samples for 48 hours was used to hydrolyze the vanadyl ions. The resulting sample was then dried for 1 hour in He at 150°C and calcined at 550°C for 5 hours in air.<sup>10</sup> White color solids were obtained.

### Characterization

The characterization procedures for vanadyl ion-exchanged and vanadium ion-exchange-hydrolyzed zeolite beta catalysts are similar to those described in Chapter Two. Diffuse reflectance UV-VIS spectra were obtained on a Cary 3G UV-VIS spectrometer

(Varian) equipped with a diffuse reflectance accessory. EPR spectra of O<sub>2</sub>-treated and O<sub>2</sub>-treated then H<sub>2</sub>-reduced VO-H-beta were recorded. The treated samples were prepared in a flow reactor, transferred into EPR tubes in the glove box and then sealed. O<sub>2</sub> treatment was conducted at 400°C for 2 hours in an O<sub>2</sub>/He flow and H<sub>2</sub> treatment was conducted under 550°C for 2 hours in H<sub>2</sub> flow.

### Propane Oxidation

Propane oxidation was carried out using a continuous flow system (BTRS-Jr., Autoclave Engineers) with a fixed bed stainless steel reactor. 0.5 mL catalyst (0.20g with mesh size -35/+60) together with 1.0 mL SiC were used for each reaction. Before a reaction, the catalyst was pretreated at 350°C in He for 1 hour. The feed gas molar ratio was propane:O<sub>2</sub>:H<sub>2</sub>O: He =4:2:4:5 with a total flow rate of 15 mL/min.

### 3.2.1.3 Results and Discussion

Elemental Analysis The composition of some of the vanadyl ion-exchanged and ion-exchange-hydrolyzed samples are shown in Table 3.1. The starting material, Na-beta, has a Si/Al ratio of 12. After ion-exchange, the Si/Al ratio of VO-Na-beta is 14.8, while for VO-H-beta this ratio is 25.2. The increase in Si/Al ratio suggests that dealumination occurs for both ion-exchanged samples and it is more severe for H-beta based samples. The vanadium content for VO-H-beta is 1.66 wt.%, corresponding to 1~2 vanadium per unit cell (average 1.3 V/unit cell).

N<sub>2</sub> Adsorption The N<sub>2</sub> adsorption isotherms reveal that the pore volumes decreased after hydrolysis (Fig. 3.1). Both IEH(I) and NH<sub>3</sub> vapor treated samples have smaller pore volumes than ion-exchanged sample VO-Na-beta. This volume loss is

similar to that observed for zeolite L samples, indicating that larger occluded material formed inside of the zeolite pores after hydrolysis.

EPR EPR spectra were taken for VO-Na-beta, and its  $\text{NH}_3$ -treated and NaOH-treated counterparts (Fig. 3.2). The EPR spectrum of VO-Na-beta has two eight-peak sets ( $g_{\parallel}=1.966$ ,  $A_{\parallel}=186.9$  Gauss,  $g_{\perp}=2.017$ ,  $A_{\perp}=81.9$  Gauss), indicating that vanadium atoms are well separated with octahedral coordination. I did not observe wide bands for the hydrolysis samples as for fresh IEH(I)-L samples, which may be due to the fact that the hydrolysis samples of zeolite beta had been stored in air for two weeks before EPR spectra were taken and during this storage period the V(IV) was oxidized to V(V) by air. This assumption is supported by the disappearance of EPR intensity for these two hydrolysis samples.

EPR spectra of as-made VO-H-beta also have two eight-peak sets ( $g_{\perp}=2.001$ ,  $A_{\perp}=80.9\text{G}$ , and  $g_{\parallel}=1.954$ ,  $A_{\parallel}=202.7\text{G}$ ), indicating that the vanadium atoms are well separated (Fig. 3.3). After calcination in oxygen, the intensity of the EPR spectra decreases, suggesting some of the V(IV) are oxidized to V(V). When the calcined sample is reduced by  $\text{H}_2$ , the intensity of EPR spectra increases and is comparable to that of the as-made VO-H-beta. Thus, it is likely that the vanadium species do not aggregate during either oxidation or reduction.

UV-VIS DR Spectroscopy UV-Vis DR spectra were recorded between 200 and 800 nm for VO-Na-beta and its base-treated forms (Fig. 3.4). The spectra of  $\text{NH}_4\text{VO}_3$  and  $\text{V}_2\text{O}_5$  are shown in Fig. 3.5 for comparison. The typical bands for  $\text{NH}_4\text{VO}_3$ , a one-dimensional polymeric metavanadate with a 4-fold coordinated  $\text{VO}_4$  unit, are 220, 290 and 350 nm. In the charge-transfer spectrum of crystalline  $\text{V}_2\text{O}_5$ , where the vanadium ion

is situated in the center of the distorted octahedron, the minimum of reflectance at 467 nm gives rise to the orange-brown color of this oxide.<sup>11</sup> The spectrum of VO-Na-beta has a small band at around 240 nm, indicating the existence of small amounts of Td V(V). In the visible region, a broad band near 600 nm is observed with the absorption intensity comparable to that of the 240 nm band. This broad band corresponds to a crystal field d-d transition of vanadyl  $\text{VO}^{2+}$  ions. Since a d-d transition is generally 10-30 times weaker than charge-transfer transition,<sup>12</sup> the comparable intensities between V(V) and V(IV) indicate that  $\text{VO}^{2+}$  ions are dominant in VO-Na-beta sample. UV-Vis DR spectrum of  $\text{NH}_3$ -treated VO-Na-beta (without calcination) sample has bands at 206, 236 and 324 nm, and a long tail in the visible region. This spectrum suggests that some of the V(IV) in the VO-Na-beta are oxidized to Td V(V) after  $\text{NH}_3$  treatment, while most of V(IV) still remain as V(IV). After calcination, the intensity of Td V(V) peak increases greatly, the broad band of the d-d transition disappears, and a shoulder at 500 nm appears. Therefore, after calcination V(IV) ions are almost completely oxidized to V(V) with a tetrahedral coordination, and some crystalline  $\text{V}_2\text{O}_5$  is present (although the contribution of  $\text{V}_2\text{O}_5$  to the total intensity is quite small). The NaOH-treated sample (IEH(I)-beta) shows only peaks for Td V(V), suggesting that after the NaOH treatment, most of the  $\text{VO}^{2+}$  ions are oxidized to V(V).

The  $\text{N}_2$  adsorption isotherms, EPR and UV-Vis DR spectra of hydrolysis samples of VO-Na-beta suggest the possible formation of V-O clusters inside zeolite beta by the ion-exchange-hydrolysis preparation method.

Propane Oxidation For propane oxidation over vanadyl ion-exchanged zeolite beta samples (VO-Na-beta, VO-NH<sub>4</sub>-beta and VO-H-beta), the products observed are propylene, acetic acid, CO<sub>x</sub>, and small amounts of acetone and ethylene (Table 3.2). The activities of these three samples are similar. Compared to VO-Na-beta, the more acidic sample VO-H-beta has a higher selectivity to acetic acid. At 350°C, the conversion for VO-H-beta is 1.6%, the selectivities to acetic acid and propylene are 21.1% and 20.9%, respectively. As the temperature is elevated to 400°C, the conversion increases to 4.27%, and the selectivity to propylene and acetic acid decreases to 13.6% and 13.9%, respectively. Considerable amounts of acetic acid are only observed for propane oxidation with water over VO-H-beta. Without feeding water, the formation of acetic acid decreases greatly. When the feed gas ratio is C<sub>3</sub>H<sub>8</sub>:O<sub>2</sub>:He = 4:2:9, the selectivity to acetic acid at 350°C is only 0.83% at 1.0% propane conversion; while with feeding water, the selectivity is 21.1% at 1.62% conversion. Thus, water has a large influence on the product distribution. VO-NH<sub>4</sub>-beta has a similar product distribution as VO-H-beta, since during the pretreatment at 350°C NH<sub>4</sub><sup>+</sup> ions decompose to H<sup>+</sup>.

Base treatment does not improve the activity of catalysts; however, a much higher selectivity to propylene is observed for ion-exchange-hydrolysis samples (Table 3.3). For example, at 350°C, the selectivity to propylene for VO-Na-beta is 9.43% at 2.16% propane conversion, while the selectivities for IEH(I)-beta and NH<sub>3</sub>-treated VO-Na-beta samples are 35.6% (1.92% conversion) and 32% (1.09% conversion), respectively. As metal oxide clusters are formed after hydrolysis, the catalysis results for VO-Na-beta and its base-treated counterparts suggest that no significant improvement of catalytic activity is made by creating metal-oxide-cluster-containing samples. A more detailed study of

the activity of zeolite-based catalysts and bulk oxide based catalysts is provided in Section 3.4.

#### 3.2.1.4 Summary

Vanadyl ion-exchanged zeolite beta samples and ion-exchange-hydrolysis samples are synthesized. Vanadium atoms in vanadyl ion-exchanged zeolite beta catalysts are well separated, and no aggregation occurs during calcination and reduction processes (EPR). After hydrolysis, occluded materials are formed inside zeolite pores ( $N_2$  adsorption) and V(IV) in vanadyl ion-exchanged samples is oxidized to V(V) with tetrahedral coordination (EPR, UV-Vis DR). No significant catalytic activity improvement is observed after hydrolysis. An active catalyst, vanadyl ion-exchanged zeolite beta (VO-H-beta), is found to produce considerable amounts of acetic acid.

### 3.2.2 Vanadium Impregnated Zeolite Beta Catalysts

#### 3.2.2.1 Introduction

The effect of the zeolite acidity and the influence of a second metal to the vanadium-zeolite beta catalyst system are studied here. The impregnation method is applied to introduce the transition metal into the zeolite beta matrix. As described in the previous section, VO-H-beta is active in propane oxidation and large amounts of acetic acid are produced. This catalyst is chosen to be the starting material for introducing a second metal by the impregnation method.

#### 3.2.2.2 Experimental Section

Vanadium impregnated zeolite beta samples were synthesized by the incipient wetness impregnation method. Zeolite beta samples with different acidity (H-beta, Na-beta, and Cs-beta) were first dehydrated at 175°C for 4 hours and cooled under a N<sub>2</sub> atmosphere. A solution of VOCl<sub>3</sub> (GFS chemical) was added to the dehydrated samples to reach the desired vanadium content 1.25 wt.%. The resulting materials were referred to as V/matrix. Here Cs-beta was synthesized by ion-exchange of Na-beta with 1 M CsNO<sub>3</sub> (Aldrich) solution at 80°C overnight twice (1 g zeolite with 50 mL solution).

A second metal was introduced by the impregnation method to vanadyl ion-exchanged zeolite beta (VO-H-beta and VO-Na-beta). An aqueous solution of (NH<sub>4</sub>)<sub>2</sub>MoO<sub>4</sub> (Aldrich) was used as the Mo source, and an ethanol solution of Sb(OAc)<sub>3</sub> (Aldrich) was used as the Sb source. The VO-beta sample was first dehydrated at 175°C, and then Mo or Sb solution was added according to the desired V/Sb and V/Mo ratios. The resulting materials were referred as V-Sb/beta or V-Mo/beta.

EPR, N<sub>2</sub> adsorption, and TPR (temperature programmed reduction) were employed to investigate the samples listed above. The samples were pretreated at 400°C in air for 4 hours before N<sub>2</sub> adsorption isotherms were recorded. TPR experiments were performed in a temperature-programmed apparatus equipped with a quartz tube reactor of 4 mm inner diameter and a thermal conductivity detector (TCD). About 100 mg sample were placed into the reactor. The sample was pretreated in air at 400°C for 2 hours and cooled to room temperature. TPR profiles were measured under a temperature ramp rate of 10°C/min from room temperature to 800°C. The reducing gas used was an 8% H<sub>2</sub>/N<sub>2</sub> mixture.

Propane oxidation over these catalysts was performed under the same condition as in Section 3.2.1.2, except a 2 hours pretreatment in O<sub>2</sub>/He at 400°C was used.

### 3.2.2.3 Results and Discussion

N<sub>2</sub> Adsorption Fig. 3.6 shows the N<sub>2</sub> adsorption isotherms of H-beta, V/H-beta (vanadium impregnated H-beta sample with 1.25 wt.%V), VO-H-beta (vanadyl ion-exchanged H-beta with 1.66 wt.%V), V- Sb/H-beta (Sb impregnated sample of VO-H-beta, V:Sb=1:1.1) and V-Mo/H-beta (Mo impregnated VO-H-beta sample with V:Mo=1.1:1). The zeolite microporous volumes decrease in the following order: H-beta > V/H-beta > VO-H-beta > V- Sb/H-beta > V-Mo/H-beta. H-beta has the largest microporous volumes. When vanadium atoms are introduced to H-beta by impregnation or ion-exchange methods, the zeolite microporous volumes decrease, indicating that most of the vanadium atoms are inside the zeolite pores. After introducing a second metal, Sb

or Mo, to VO-H-beta, the microporous volumes are further decreased, suggesting that most of Sb and Mo atoms are inside zeolite matrix.

EPR Vanadium atoms in vanadyl ion-exchanged zeolite beta samples are well separated and are in V(IV) valence state as stated in the previous section. Influence of the vanadium valence state by addition of a second metal is monitored by EPR spectroscopy. As Mo is introduced by impregnation of VO-Na-beta with  $\text{Na}_2\text{MoO}_4$ , the obtained V-Mo/Na-beta becomes EPR silent (Fig. 3.7). Therefore, V(IV) in VO-Na-beta is oxidized to V(V) possibly due to the basicity introduced. When Sb is introduced to VO-Na-beta system, most of the vanadium remains as V(IV) as indicated by the EPR pattern of V-Sb/H-beta.

TPR Temperature programmed reduction is used to investigate the reducibility of the transition metals inside the catalysts. TPR profiles of vanadium catalysts supported by H-beta, Na-beta, and Cs-beta with the same vanadium content are compared in Fig. 3.8. The reduction temperature of these three catalysts increases as the basicity of supports increases. For example, the reduction temperatures for V/H-beta and V/Na-beta are  $523^\circ\text{C}$  and  $528^\circ\text{C}$ , respectively, while that of V/Cs-beta is  $584^\circ\text{C}$ . This difference in reduction temperature may be attributed to a better vanadium dispersion for V/H-beta and V/Na-beta samples.

The reduction behavior of zeolite supported bimetal oxides, V-Sb/zeolite, is also studied. Three V-Sb/beta(I-III) samples with different Sb/V ratios were prepared. Figure 3.9 shows the TPR results from these samples together with those of Sb/H-beta and V/H-beta for comparison.<sup>13</sup> Sb/H-beta has 2 wt.%Sb and was previously calcined at  $500^\circ\text{C}$  in air for 4 hours. Two main reduction peaks at  $445^\circ\text{C}$  and  $558^\circ\text{C}$  are observed for Sb/H-

beta. The V-Sb/beta(II) sample (3.29 wt.%Sb, Sb/V=1.31) has the same Sb content as the Sb/H-beta sample. However, the TPR profile of V-Sb/beta(II) is very different from that of Sb/H-beta and the TPR profile of V-Sb/beta(II) is not formed by superimposing of the TPR profiles of V/H-beta and Sb/H-beta samples. There are two main reduction peaks: a sharp peak at 466°C and a broad peak at 720°C. The reduction temperature of the first peak is about 50°C lower than that of the reduction peak of the V/H-beta sample. These results suggest that an interaction between vanadium species and antimony species occurs, and Sb-O-V clusters could be formed after calcination in air. With increasing amounts of antimony in the V-Sb/beta samples, the sharp reduction peak shifts from 490°C to 445°C (Fig. 3.9).

Propane Oxidation Influence of acidity on propane oxidation is studied. As the acidity of the catalysts decreases from V/H-beta, V/Na-beta to V/Cs-beta, the catalyst activity decreases (Table 3.4), consistent with the increasing reduction temperature shown by TPR. Meanwhile, the selectivity to propylene increases while the selectivity to acetic acid decreases. For example, at 350°C, the conversion for V/H-beta is 2.39% and the selectivities to propylene and acetic acid are 14.3% and 19.0%, respectively; while at 400°C, the conversion is 5.43% and the selectivities to propylene and acetic acid are 16.3% and 3.0%, respectively. For V/Cs-beta, the conversion is 0.66% at 350°C with the selectivities to propylene and acetic acid 58.9% and 0.85%, respectively; while at 400°C, the conversion is 4.20% and the selectivities to propylene and acetic acid are 38.8% and 0.38%, respectively. Similar trend of propylene selectivity was reported by Grabowski *et al.* on the effect of alkali metals additives to V<sub>2</sub>O<sub>5</sub>/TiO<sub>2</sub> catalyst.<sup>14</sup> They believe that as basicity increases, the heat of adsorption of propylene decreases, which results in a

higher selectivity of propylene. The propane oxidation results of V/H-beta are very similar to those of vanadyl ion-exchanged zeolite beta (VO-H-beta).

A second metal is introduced to VO-H-beta. As observed from olefin oxidation, multicomponent systems are required for functionalization.<sup>15</sup> I expect that the addition of a second metal to VO-H-beta system may help in the formation of oxygenates. Sb and Mo are chosen as the second metal since Mo is a well-known component in olefin oxidation catalysts<sup>15</sup> and Sb has been reported to be a major component in propane ammoxidation catalysts.<sup>16</sup> The addition of Sb and Mo do help the activity; unfortunately, no other oxygenate except acetic acid is observed after the addition of Sb or Mo (Table 3.5). For VO-H-beta, the propane conversion is 1.62% and the selectivities to propylene and acetic acid are 20.9% and 21.1%, respectively. After addition of Mo, the propane conversion for V-Mo/H-beta (V:Mo=2:1, 1.6 wt.%V) is 2.25% and the selectivities to propylene and acetic acid are 26.9% and 22.0%, respectively. As Mo is further added (the ratio of V/Mo reached 1), the propane conversion decreases slightly to 2.18% and the selectivities to propylene and acetic acid are 27.0% and 19.2%, respectively. Addition of Sb to VO-H-beta results in a complicated change of catalytic behavior. When small amounts of antimony are added to VO-H-beta, the catalyst activity increases. No obvious change in propylene selectivity is observed, and the selectivity to acetic acid decreases. When large amounts of antimony are added, e.g., V:Sb=1:1.7, a decrease in catalyst activity is observed, possibly due to antimony blocking the access to some of the vanadium atoms.

An increase of propylene selectivity is observed when introducing moderate amounts of Mo to other supports such as Na-beta and silica (Table 3.6). With the

addition of the same amounts of Mo to V/Na-beta (V:Mo=1:1), the propane conversion decreases and a large increase of propylene selectivity is observed. At 350°C, the selectivity to propylene is 16.7% for V/Na-beta system (2.67% conversion), while the selectivity increases to 41.2% (1.68% conversion) as Mo is introduced (Mo:V=1:1). Similar results are observed for V/silica and V-Mo/silica systems (V:Mo=1:1) where dehydrogenation is almost the only reaction occurring for propane oxidation. With the addition of Mo, the selectivity to propylene reaches 78.0% at 1.83% propane conversion at 400°C and 62.9% at 15.0% propane conversion at 500°C.

#### 3.2.2.4 Conclusion

Vanadium impregnated catalysts with different matrices are synthesized and their catalytic behaviors are compared. Catalysts with basic supports show higher reduction temperatures, as indicated by TPR experiments. During the oxidation of propane, the acidity of the matrix assists the formation of acetic acid, while basicity improves the selectivity to propylene.

VO-H-beta catalyst is used as a starting material for the introduction of a second metal using the incipient wetness impregnation method. Most metals impregnated are located inside zeolite pore system, and the interaction between different metals (V-Sb) has been observed by TPR. Influence of the second metal on propane oxidation is dependent on the loading. Addition of small amounts of the second metal (Mo or Sb) can increase the catalyst activity and propylene selectivity. No obvious improvement on the selectivity to acetic acid is observed. When large amounts of the second metal (Mo or Sb) are added, the catalyst activity decreases likely due to the blocking of the access to some of the vanadium atoms.

### 3.2.3 Zeolite Beta Catalysts with Vanadium in Zeolite Framework Sites

#### 3.2.3.1 Introduction

Molecular sieve materials containing framework vanadium have been reported as catalysts for the oxydehydrogenation of propane.<sup>17-19</sup> Vanadium-containing aluminophosphate VAPO-5 was shown to be a selective catalyst, giving propylene with selectivities around 70% for conversions around 15% at 500°C.<sup>17,20</sup> Additionally, Centi and Trifiro have reported that vanadium-containing zeolites (VS-1 and VS-2) prepared by hydrothermal methods can have high selectivity for propylene (76% at 408°C with a 4% conversion).<sup>19</sup>

One of the motivations for studying materials with framework vanadium is to synthesize metal oxide clusters with two vanadium atoms (dimer). Introduction of vanadium to the zeolite framework results in new charge-balancing sites so that introduction of a second vanadium atom nearby is made possible by ion-exchange method. By calcination of the materials formed we could obtain vanadium dimers with one vanadium atom as an anchor inside of the framework and another vanadium atom outside of the framework. A scheme for this idea is shown in Scheme 3.1. Okamoto and co-workers attempted the ion-exchange of VAPO-5 with vanadyl oxalate.<sup>21</sup> Unfortunately, this treatment was found only to incorporate vanadium into the AFI framework by filling lattice vacancies. Thus, the idea of dimer formation has yet to be realized. In this section, vanadium in the framework of zeolite beta catalysts is investigated. The catalysis results of framework vanadium-containing catalysts are compared to those catalysts with vanadium in the extraframework positions.

### 3.2.3.2 Experimental Section

Two synthesis methods were employed to prepare zeolite beta containing framework vanadium. One was a two-step post-synthesis method.<sup>5</sup> Na-beta (PQ, Si/Al= 12) was first dealuminated with 13 M HNO<sub>3</sub> (JT-Baker) for 4 hours at 80°C to generate vacant T-sites associated with silanol groups. The resulting mixture was centrifuged, washed, and dried in an 80°C oven overnight. The obtained dealuminated zeolite beta (Siβ) has a Si/Al= 235, suggesting that 95% of the aluminum in the starting material had been removed. Siβ was then contacted with an aqueous solution of NH<sub>4</sub>VO<sub>3</sub> (Aldrich) at room temperature for three days (V/Si atomic ratio in the suspension was within the range 0.0007-0.021). The solids were then centrifuged, washed with H<sub>2</sub>O and dried overnight. After washing out the non-framework vanadium by contact with a 1 M NH<sub>4</sub>OAc (Aldrich) solution for 12 hours at room temperature, the obtained solids were then washed with water, dried, and calcined in O<sub>2</sub> at 450°C for 4 hours. The final product had a vanadium content of 0.26 wt.% (Si 36.6 wt.%, Al 0.15 wt.%) and is denoted Vbeta(I). “T” refers here to the post-synthesis vanadium insertion method. A representation of the de-Al and V-insertion method is shown in Scheme 3.2.

The second method of synthesizing zeolite beta containing framework vanadium was a hydrothermal method.<sup>22</sup> A mesoporous material with vanadium in its framework (V-MS) was synthesized as the following: (1) A solution of 6.24 g TEOS (tetraethyl orthosilicate, Alrich), 9 g ethanol (EM), 1.8 g isopropyl alcohol (EM) and 0.16 g VO(acac)<sub>2</sub> (vanadyl acetylacetonate, Aldrich) was slowly added under vigorous stirring to a second solution with 1.5 g dodecylamine (Aldrich), 19.4 g H<sub>2</sub>O and 0.6 g 1 M HCl

(JT-Baker); (2) The reaction mixture had a composition of  $\text{SiO}_2:0.02\text{VO}(\text{acac})_2:0.27\text{C}_{12}\text{A}:0.02\text{HCl}:36\text{H}_2\text{O}:10.5\text{EtOH}:1\text{iPrOH}$  and was stirred overnight at room temperature, then filtered and washed; (3) The solids obtained were calcined at  $550^\circ\text{C}$  for 6 hours and had a Si/V ratio of 48.5. The resulting mesoporous material was then impregnated with tetraethyl ammonium hydroxide (35 wt.% aqueous solution, Aldrich) (0.15 g V-MS/ 0.45 g TEAOH), and dried at room temperature for overnight. The TEAOH-impregnated mesoporous materials were then put into a Teflon lined bomb and heated in a  $150^\circ\text{C}$  oven for 1-2 weeks. V-MS was transformed to zeolite beta with vanadium at framework sites (Vbeta(H)), and was calcined at  $550^\circ\text{C}$  for 4 hours to remove the organic template. The resulting Vbeta(H) has a composition of Si:V=80.4 with 0.98 wt.% vanadium.

Vanadyl impregnated samples of Vbeta were also synthesized. Vanadyl oxalate was used as the vanadium source and the resulting samples have a vanadium content of 1.25 wt.%.

XRD, FTIR, UV-Vis, and TPR were employed to characterize these materials and propane oxidation was conducted under the “standard” conditions (catalyst 0.2 g together with 1.0 mL SiC, molar feed ratio of propane: $\text{O}_2$ : $\text{H}_2\text{O}$ :He=4:2:4:5, and a total flow of 15 mL/min).

### 3.2.3.3 Results and Discussion

XRD patterns of Vbeta(I) show that most of the crystallinity of the starting material is maintained even after the harsh dealumination process (Fig. 3.10). Fig. 3.11

shows XRD patterns of the nice crystalline Vbeta(H) sample formed by heating V-MS with proper organic template.

The UV-Vis spectrum of Vbeta(I) exhibits three bands at 207, 233 and 333 nm (Fig. 3.12), associated with pseudotetrahedral  $O_{3/2}V=O$  species, which are anchored to the zeolitic walls by three Si-O-V bridges while possessing a V=O double bond.<sup>23</sup> The absence of d-d transition within the range of 600-800 nm clearly indicates that no reduced V(IV) species are formed, and oxidized V(V) species are mainly present. The UV-Vis spectra of several other vanadium-containing samples are also shown in Fig. 3.12 for comparison. Most of the vanadium atoms in VO-H-beta are in the V(IV) valence state, and small amounts of V(V) exist with tetrahedral coordination. V/H-beta has only Td V(V), and V/silica has both V(V) atoms in tetrahedral coordination and octahedral coordination.

The Vbeta(I) sample has a vanadium content of 0.26 wt.% (Si 36.6 wt.%, Al 0.15 wt.%), while the Si/Al ratio of the starting material Na-beta for synthesizing Vbeta(I) is 12. Therefore, large amounts of defect sites with silanol groups are present in Vbeta(I). This is confirmed by a characteristic FT-IR peak near  $960\text{ cm}^{-1}$  (Fig. 3.13) assigned to the stretching vibration of Si-O vibrators belonging to uncoupled  $(SiO_4)$  tetrahedra with a hydroxyl group.<sup>24,25</sup> This  $960\text{ cm}^{-1}$  peak is more intense with Vbeta(I) compared to Na-beta sample. Dzwigaj and co-workers also observed this phenomena, and they believed that this peak at  $960\text{ cm}^{-1}$  reveals the presence of vacant T-sites associated with silanol groups generated upon dealuminating the beta framework.<sup>24</sup> Several other authors have taken the FT-IR peak at  $960\text{ cm}^{-1}$  in silica-based matrices containing transition metal

species, as evidence for the isomorphous substitution of Si atoms by metal atoms.<sup>26-28</sup> Thus, this  $960\text{ cm}^{-1}$  peak of Vbeta(I) sample can also be attributed to the incorporation of vanadium atoms in beta framework.

From the above discussion, both UV-Vis DR spectroscopy and FTIR spectroscopy suggest that vanadium atoms in Vbeta(I) are inside the framework of zeolite beta.

The reducibility of vanadium in Vbeta is studied by TPR. TPR profiles of Vbeta(H) and Vbeta(I) have reduction peaks at  $540$  and  $533^\circ\text{C}$ , respectively. These values are within the temperature range for the reduction of other zeolite supported samples. For example, the reduction peaks for VO-H-beta and V/H-beta are at  $539$  and  $523^\circ\text{C}$ , respectively. Thus, no obvious difference is found from TPR for the reducibility of vanadium at different positions within zeolite beta.

Propane oxidation over Vbeta samples and vanadyl-impregnated Vbeta samples (1.25 wt.%V) are reported in Table 3.7. The activity for Vbeta samples is low with a less than 1% conversion at  $400^\circ\text{C}$ , and propylene is a major product. For example, for Vbeta(I) at  $400^\circ\text{C}$ , the propane conversion is 0.71% and the selectivity to propylene is 54.4%. As the temperature is elevated to  $500^\circ\text{C}$ , the conversion increases to 5.49% and the selectivity to propylene is 46.8%. The activity is increased with the impregnation of vanadium. Acetic acid was observed for vanadyl-impregnated Vbeta samples (V/Vbeta). V/Vbeta(I) has a propane conversion of 6.49% at  $400^\circ\text{C}$ , and the selectivities to propylene and acetic acid are 45.6% and 2.5%, respectively. Trace amounts of acrolein are also observed.

Okamoto and co-workers reported that framework vanadium is the most active and selective species for propane oxidative dehydrogenation and extraframework vanadium species are less active and selective.<sup>21</sup> For zeolite beta case, Vbeta samples with vanadium in the zeolite framework behave very different from VO-H-beta, V/H-beta and V/Na-beta that have vanadium at the extraframework sites (Table 3.4 & 3.6). However, the catalytic behavior of Vbeta(I) resembles that of V/Cs-beta. Thus, the difference in acetic acid formation and activity between these catalysts may not simply be attributed to the position of vanadium atoms (framework sites or extraframework sites). The acidity of catalysts may also play a significant role.

#### 3.2.3.4. Summary

Catalysts with vanadium in the framework of zeolite beta are synthesized. Vanadium is incorporated into the framework of zeolite beta, as indicated by UV-Vis and FTIR. TPR shows no obvious difference in reducibility between catalysts with vanadium at framework or extraframework sites of the zeolite. Propane oxidation over Vbeta reveals that Vbeta is a selective oxidative dehydrogenation catalyst and its catalytic behavior is close to that of V/Cs-beta. It is suggested that the position of vanadium atoms is not as influential in propane oxidation as the acidity of the catalysts.

### 3.2.4 Ti/beta and Si/beta Based Catalysts

#### 3.2.4.1 Introduction

I also investigated other zeolite beta matrices such as pure-silica beta (Si/Beta) and titanium containing beta (Ti/beta). Recently Takewaki and co-workers found that pure-silica beta with very few defect sites can be synthesized by extraction of Zn from CIT-6 (Zn/beta).<sup>4</sup> Adsorption isotherms for water at 25°C reveals that the water adsorption capacity for typical calcined zeolite beta is four times higher than that of Si/beta ( $P/P_0=0.2$ ). Thus, pure-silica beta is an excellent hydrophobic matrix for the incorporation of vanadium. Ti-containing zeolites are known for their remarkable catalytic activity in various selective oxidations such as the hydroxylation of aromatics, the epoxidation of olefins, the ammoxidation of carbonyl compounds, the oxidation of alcohols, the sulfoxidation of thioethers and the oxidation of amines.<sup>29</sup> Here the combination of both vanadium and titanium inside zeolites is investigated.

#### 3.2.4.2 Experimental Section

Pure-silica beta (Si/beta) was synthesized by extraction of Zn from Zn/beta with acetic acid solution.<sup>4</sup> Chemical reagents used for synthesizing Zn/beta(CIT-6) were tetraethylammonium hydroxide (TEAOH, 35 wt.% aqueous solution, Aldrich), colloidal silica (HS-30, Dupont), zinc acetate dihydrate (Fisher), LiOH(Fisher), NaOH (EM), and  $\text{Al}(\text{NO}_3)_3 \cdot 9\text{H}_2\text{O}$  (JT-Baker). Zn/beta was synthesized by the following method.<sup>3</sup> 0.12 g LiOH was added to a solution of 27.3 g 35% TEAOH(aq.) and 27.2 g  $\text{H}_2\text{O}$  under stirring. 0.66 g  $\text{Zn}(\text{OAc})_2 \cdot 2\text{H}_2\text{O}$  was then added to the above solution and stirred until dissolved.

Next, 15 g HS-30 ( $\text{SiO}_2$ ) was added and the mixture was stirred for 2 hours to get a clear solution. The reaction mixture had the following composition: 0.05LiOH/0.65TEAOH/0.03Zn(CH<sub>3</sub>COO)<sub>2</sub>·2H<sub>2</sub>O/SiO<sub>2</sub>/30H<sub>2</sub>O. This mixture was charged into Teflon-lined, stainless steel autoclaves and heated statically at 150°C for 4 days in convection ovens. The as-made Zn/beta product was collected by vacuum filtration, washed with double distilled water, and dried in air at room temperature. The obtained Zn/beta contains Si/Zn = 32, Si/Li = 35 and Si/TEA<sup>+</sup> = 10.7 by elemental analysis. 0.2 g as-made Zn/beta was then added to a solution of 12 mL acetic acid (Fisher, Glacial) and 20 ml H<sub>2</sub>O. The mixture was put into a Teflon-lined stainless steel autoclave and heated in a 135°C oven for 2 days. The solids were filtered, washed, dried in an 80°C oven overnight, and calcined at 540°C for 4 hours. After this treatment, Zn was almost completely extracted, as indicated by a Si/Zn ratio of greater than 2000, and the resulting defects had been annealed. The obtained Si/beta is highly hydrophobic, as indicated by water adsorption experiments, and has very few defects, as indicated by <sup>29</sup>Si MAS NMR.<sup>4</sup>

Silica beta with small amounts of aluminum (AlSi/beta) was prepared by Zn-extraction from Al-containing Zn/beta. A similar procedure for synthesizing CIT-6 (Zn/beta) was used here for synthesizing Al-containing Zn/beta. The gel composition was 0.05LiOH/0.01Al(NO<sub>3</sub>)<sub>3</sub>/0.65TEAOH/0.03Zn(CH<sub>3</sub>COO)<sub>2</sub>·2H<sub>2</sub>O/HS-30/30H<sub>2</sub>O. Instead of heating at 150°C for 4 days as in the case of Zn/beta, heating at 150°C for 5 days was used here for Al-containing Zn/beta (AlZn/beta). Zn-extraction procedure for AlZn/beta is the same as that for Zn/beta. The resulting AlSi/beta has a composition of Si:Al=43.8.

Vanadium impregnated pure Si/beta and AlSi/beta were obtained by vacuum impregnation of Si/beta and AlSi/beta with vanadyl oxalate solution. 1.25 wt.% of vanadium was impregnated into each sample.

Ti/beta with Si/Ti ratio equal to 46 was kindly provided to us by Dr. Hiromi Yamashita. Vanadium impregnated Ti/beta sample was synthesized with a vanadium content of 1.25 wt.% (V/Ti ~1).

#### 3.2.4.3 Results and Discussion

Acrolein is observed for propane oxidation over V/Ti/beta (Table 3.8). Since no acrolein is observed from either Ti/beta or V/beta, the formation of acrolein here indicates that combination of V and Ti has created active sites for acrolein production. At 350°C, the conversion is 1.40% for V/Ti/beta, and the selectivities to propylene and acrolein are 65.0% and 1.26%, respectively. At 400°C, the conversion increases to 5.18%, the selectivity to propylene decreases to 48.6% and the selectivity to acrolein slightly increases to 1.69%. Small amounts of acetic acid are also detected in the propane reaction over V/Ti/beta.

The activities for V/Si/beta and V/AlSi/beta are much higher than that for V/H-beta (Table 3.8). At 350°C, the propane conversion for V/Si/beta is 5.65%, while the conversion for V/H-beta is 2.39%; at a higher temperature 400°C, the conversion for V/Si/beta is 13.2%, while the conversion for V/H-beta is 5.43%. These results suggest that the propane activity can be improved by using hydrophobic frameworks. Compared to V/Si/beta, V/AlSi/beta has a higher selectivity to acetic acid due to the improved acidity resulting from incorporation of Al in the framework of Si/beta. At 350°C, the

conversion for V/AlSi/beta was 5.17%, the selectivities to propylene and acetic acid were 12.8% and 13.3%, respectively.

#### 3.2.4.4 Summary

Vanadium-containing Si/beta, AlSi/beta, and Ti/beta catalysts are synthesized and their catalytic behavior is investigated. Acrolein is formed using V/Ti/beta. The use of highly hydrophobic frameworks like Si/beta and AlSi/beta is able to improve propane activity.

### 3.3 PROPANE OXIDATION OVER NON-ZEOLITE BETA BASED CATALYSTS

#### 3.3.1 Introduction

In Section 3.2, I showed that vanadium-containing zeolite beta catalysts are active in propane oxidation and a considerable amount of acetic acid is obtained. To understand whether zeolite beta is the only zeolite for these observations, SSZ-33 with pore sizes and channel structure close to those of zeolite beta is investigated. (SSZ-33 has a CON type structure, [001] **12** 6.4 x 7.0\* <-> [100] **12** 6.8\* <-> [010] **10** 5.1 x 5.1\*; zeolite beta has a BEA structure, [001] **12** 5.5 x 5.5\* <-> <100> **12** 7.6 x 6.4 \*\*.)<sup>1</sup> Amorphous materials, MCM-41 and silica, are also used as the supports for propane oxidation catalysts for comparison reasons.

#### 3.3.2 Experimental Section

SSZ-33 was kindly provided by Chevron. The composition of the aluminum-containing SSZ-33 was Si:Al=48. Vanadyl ion-exchanged SSZ-33 (VO-SSZ-33) was prepared by ion-exchange of SSZ-33 with 0.1 M VOSO<sub>4</sub> as described in Section 3.2.1 and vanadium impregnated SSZ-33 sample (V/SSZ-33) was prepared by impregnation with vanadyl oxalate solution. The compositions of VO-SSZ-33 and V/SSZ-33 were Si:Al:V= 60.7:1:0.32 with 0.39 wt.%V and Si:Al:V =48:1:0.83 with 1.20 wt.%V, respectively.

MCM-41 was synthesized as reported previously.<sup>30</sup> 2.4 g of 29 wt.% NH<sub>4</sub>OH solution (EM) were added to 26.4 g of 29 wt.% C<sub>16</sub>TMACl solution (hexadecyltrimethyl ammonium chloride, Pfaltz and Bauer). 0.37 g of sodium aluminate (54 wt.% Al<sub>2</sub>O<sub>3</sub> 41 wt.% Na<sub>2</sub>O 5 wt.% H<sub>2</sub>O, Riedel-de Haen) were added and the solution was combined

with 2.3 g TMAOH.5H<sub>2</sub>O (tetramethylammonium hydroxide pentahydrate, Aldrich), 20 g of tetramethylammonium silicate solution (10 wt.% SiO<sub>2</sub>, TMA/Si=0.5, Sachem) and 4.5 g of fumed silica (Cab-O-Sil M-5, Cabot) under stirring. The gel composition was SiO<sub>2</sub>:0.02Al<sub>2</sub>O<sub>3</sub>:0.02Na<sub>2</sub>O:0.11(C<sub>16</sub>TMA)<sub>2</sub>O:0.13(TMA)<sub>2</sub>O:0.09(NH<sub>4</sub>)<sub>2</sub>O:0.22HCl:19.3 H<sub>2</sub>O. The reaction mixture was charged into a Teflon-lined, stainless steel autoclave and heated statically at 135°C for 3 days. The product, MCM-41, was collected by vacuum filtration, washed with water, dried in air at room temperature and calcined in air at 550°C for 6 hours to remove organic template molecules. Both vanadyl ion-exchanged and vanadium impregnated MCM-41 samples were prepared. The resulting VO-MCM-41 has a composition of Si:Al:V=56:1:1.17 with 1.46 wt.% vanadium and V/MCM-41 has a vanadium content of 1.25 wt.%.

Vanadium impregnated silica gel with a surface area of 300 m<sup>2</sup>/g (Aldrich) was also prepared (1.25 wt.%V). A sample containing both vanadium and molybdenum (V-Mo/silica) was synthesized with a V/Mo ratio equal to 1 (1.25 wt.% vanadium).

### 3.3.3 Results and Discussion

V/SSZ-33 and VO-SSZ-33 are active for propane oxidation. Similar to VO-H-beta, VO-Na-beta, V/H-beta and V/Na-beta, acetic acid is a main product of propane oxidation over SSZ-33 based catalysts (Table 3.9). At 350°C, the conversion for V/SSZ-33 is 1.68%, and the selectivities to propylene and acetic acid are 21.1% and 10.6%, respectively. Thus, the product distribution for V/SSZ-33 is similar to that for V/H-beta. These results suggest that zeolite beta is not the only zeolite matrix active for propane oxidation and acetic acid is a general product for zeolite based catalysts with acidity.

V/MCM-41 and VO-MCM-41 have lower activities and propylene and  $\text{CO}_x$  are the only products detected.

Compared to zeolite-based catalysts with acidity, V/silica (with the same vanadium content) has a lower propane conversion (Table 3.9). For example, the conversion is 0.62% at 400°C. When temperature is elevated to 500°C, the conversion increases to 15.5% with a propylene selectivity of 48.9%. For silica based catalysts, the propylene selectivity is comparatively higher than that for zeolite based catalysts at higher temperatures. This higher propylene selectivity could be due to the shorter product diffusion time for silica based catalysts, since the micropores of zeolite based catalysts could result in burning of the useful products to  $\text{CO}_x$  during the transport process back to the fluid phase. With the addition of Mo to V/silica, the selectivity to propylene is further improved (78.0% at 1.83% propane conversion at 400°C and 62.9% at 15.0% propane conversion at 500°C).

### 3.3.4 Summary

The catalytic behavior of SSZ-33 based catalysts suggest that zeolite beta is not the only zeolite matrix active for propane oxidation and acetic acid is a general product for zeolite based catalysts with acidity. An active catalyst V-Mo/silica is found to have 62.9% propylene selectivity at 15% propane conversion at 500°C.

## 3.4 COMPARISON OF BULK $V_2O_5$ AND VANADIUM-CONTAINING ZEOLITE BETA CATALYSTS

### 3.4.1 Introduction

One of my targets for this project is to understand whether metal oxide clusters supported in zeolites behave differently from the corresponding bulk metal oxide. In this section, I compare the catalytic behavior of zeolite-based catalysts to bulk  $V_2O_5$ .

### 3.4.2 Experimental Section

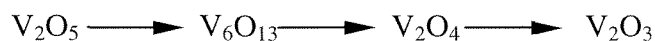
Bulk  $SbVO_4$  was synthesized according to the literature.<sup>31</sup> Firstly, 100 mL solution of anhydrous  $SbCl_5$  (Aldrich) in an absolute ethyl alcohol was prepared; then vanadyl acetylacetonate ( $VO(acac)_2$ ) was dissolved in the solution, in order to obtain a 1:1 ratio of Sb/V. The solution was added dropwise to 200 mL of a 2M aqueous solution of  $CH_3COONH_4$ , having an initial pH of around 7.0. During the precipitation of the oxohydrates, the pH, which decreases due to the release of HCl, was kept constant by the addition of ammonia solution. The resulting precipitate was filtered, washed and dried overnight at 120°C. It was then calcined at 350°C for 1 hour and at 700°C for 3 hours.

TPR was employed for zeolite based catalysts and bulk metal oxide. The TPR profiles were recorded according to procedures described in Section 3.2.2.2.

### 3.4.3 Results and Discussion

The TPR profiles of transition metal supported by zeolites and bulk metal oxides are very different. Fig. 3.14 shows the TPR profiles of zeolite supported, silica supported vanadium-containing catalysts and bulk  $V_2O_5$ . Both VO-H-beta (1.66 wt.%V) and

V/silica (1.25 wt.%V) have similar vanadium contents. The reduction peak of VO-H-beta sample is located at 539°C, while that of V/silica is located at 549°C. The reason for the ten degree difference in reduction temperatures of VO-H-beta and V/silica could be attributed to a better dispersion of vanadium in zeolite. TPR profile of bulk V<sub>2</sub>O<sub>5</sub> was also shown here for comparison. Bulk V<sub>2</sub>O<sub>5</sub> exhibits multiple major reduction peaks at much higher temperatures (673°C, 708°C, 815°C and 921°C). Bosch and co-workers have reported a similar observation,<sup>32</sup> and they have attributed the multiple reduction peaks to the reduction sequence:



Thus, the reduction temperatures of V<sub>2</sub>O<sub>5</sub> are considerably higher than those of VO-H-beta and V/silica.

Similar to the TPR difference for zeolite supported vanadium and bulk V<sub>2</sub>O<sub>5</sub>, Sb/zeolite and bulk Sb<sub>2</sub>O<sub>5</sub> have very different TPR profiles (Fig. 3. 15).<sup>13</sup> Two main reduction peaks for Sb/H-beta at 445°C and 558°C are observed for Sb/H-beta (with 2 wt.% of Sb), while two main reduction peaks for Sb<sub>2</sub>O<sub>5</sub> occurs at 520°C and 620°C.

The reduction behavior of zeolite supported bimetal oxides, V-Sb/zeolite, and bulk oxide SbVO<sub>4</sub> is also investigated.<sup>13</sup> It is difficult to synthesize single phase SbVO<sub>4</sub>. The XRD pattern of our SbVO<sub>4</sub> sample indicates that small amounts of α-Sb<sub>2</sub>O<sub>4</sub> impurity exist (Fig. 3.16). The TPR profile for SbVO<sub>4</sub> has two reduction peaks, one at 581°C and another one at 675°C (Fig. 3.17). The reduction behavior of SbVO<sub>4</sub> is different from that of Sb<sub>2</sub>O<sub>3</sub>, Sb<sub>2</sub>O<sub>5</sub>, and V<sub>2</sub>O<sub>5</sub>, indicating an interaction occurs between antimony and vanadium in SbVO<sub>4</sub>; while the TPR profile of SbVO<sub>4</sub> is close to the TPR results of a

physical mixture of antimony and vanadium oxides (Sb:V=1:1) (Fig. 3.17), since  $\text{SbVO}_4$  can be obtained by calcining a physical mixture of  $\text{V}_2\text{O}_5$  and  $\text{Sb}_2\text{O}_5$  with a Sb/V ratio of one below  $800^\circ\text{C}$ .<sup>33</sup> The reduction temperatures for V-Sb/beta samples are considerably lower than that of bulk  $\text{SbVO}_4$  (Fig. 3.9). For example, the major reduction peak for V-Sb/beta(II) is located at  $466^\circ\text{C}$ .

Turnover frequencies (TOF) for propane oxidation over bulk  $\text{V}_2\text{O}_5$  and vanadium-containing zeolite catalysts are compared in Table 3.10. Several considerations have been involved in the calculation of turnover frequency. (1) For the zeolite-based catalysts and V/silica, all the vanadium atoms are assumed to be accessible because the vanadium contents for these samples are relatively low (less than 2 wt.%). (2) The estimated number of the active sites for bulk  $\text{V}_2\text{O}_5$  is based on the surface area of  $\text{V}_2\text{O}_5$  ( $16.5 \text{ m}^2/\text{g}$ ) and a surface density of  $7 \text{ VO}_x/\text{nm}^2$ .<sup>34</sup> The results suggest that most of the zeolite-based catalysts are as active, or more active than bulk  $\text{V}_2\text{O}_5$ . The highest TOF is observed for the highly hydrophobic Si/beta based catalyst ( $3.43 \times 10^{-3} \text{ s}^{-1}$  at  $350^\circ\text{C}$  and  $8.01 \times 10^{-3} \text{ s}^{-1}$  at  $400^\circ\text{C}$  under our reaction condition); while for  $\text{V}_2\text{O}_5$ , the TOF is  $1.34 \times 10^{-3} \text{ s}^{-1}$  at  $350^\circ\text{C}$  and  $2.50 \times 10^{-3} \text{ s}^{-1}$  at  $400^\circ\text{C}$ .

The apparent turnover frequencies for catalysts containing metal oxide clusters (IEH(I)-beta and  $\text{NH}_3$ -treated VO-beta) are slightly lower than that of VO-Na-beta. Since no information on the size of the clusters is available, these values could be underestimated. Therefore, I could not conclude that metal oxide clusters are not as active as isolated vanadium.

From these turnover frequency results, zeolites could be possible supports for oxidation catalysts. However, thus far acetic acid is the only oxygenate obtained from

propane oxidation over zeolite-based catalysts. It appears possible that more valuable oxygenates, e.g., acrylic acid, were produced and overoxidized to  $\text{CO}_x$ , since feeding acrylic acid into this reaction system results in complete oxidation of the acid to  $\text{CO}_x$  at  $350^\circ\text{C}$ , and some acetic acid at lower reaction temperatures (Table 3.11). Therefore desorption experiments were performed over zeolite beta catalysts.<sup>35</sup> It is found that oxygenates only desorb from the zeolite support at relatively high temperatures (Table 3.12). Because of the limitation of these experiments (no Mass Spectrometer is connected to the TGA machine), we do not know whether the desorbed oxygenates were oxidized or not. It is possible that the reaction temperature we used could be detrimental for their survival under oxygen atmosphere. In order to understand whether more useful oxygenates are involved in propane oxidation over zeolite-based catalysts, a reaction pathway analysis was performed and is presented in the next chapter.

#### 3.4.4 Summary

A comparison of metal oxides supported in zeolites with bulk metal oxides reveals that metal oxides supported in zeolites have lower reduction temperatures than their corresponding bulk oxides. However, the zeolite supported oxide clusters do not provide significant differences in their ability to react propane with oxygen than bulk metal oxides. The comparison of TOF of propane oxidation of vanadium-containing zeolite beta catalysts and  $\text{V}_2\text{O}_5$  suggest that most of the zeolite-based catalysts are as active as bulk  $\text{V}_2\text{O}_5$ .

### 3.5 REFERENCE

- 1)Meier, W. M.; Olson, D. H. *Atlas of Zeolite Structure Types*; Butterworth-Heinemann, 1996.
- 2)Cambor, M. A.; Corma, A.; Valencia, S. *Micropor. Mesopor. Mat.* **1998**, *25*, 59-74.
- 3)Takewaki, T.; Beck, L. W.; Davis, M. E. *Top. Catal.* **1999**, *9*, 35-42.
- 4)Takewaki, T.; Beck, L. W.; Davis, M. E. *J. Phys. Chem. B* **1999**, *103*, 2674-2679.
- 5)Dzwigaj, S.; Peltre, M. J.; Massiani, P.; Davidson, A.; Che, M.; Sen, T.; Sivasanker, S. *Chem. Commun.* **1998**, 87-88.
- 6)Blasco, T.; Cambor, M. A.; Corma, A.; Esteve, P.; Guil, J. M.; Martinez, A.; Perdigon-Melon, J. A.; Valencia, S. *J. Phys. Chem. B* **1998**, *102*, 75-88.
- 7)Dartt, C. B.; Davis, M. E. *Appl. Catal. A-Gen.* **1996**, *143*, 53-73.
- 8)Kung, M. C.; Kung, H. H. *J. Catal.* **1992**, *134*, 668-677.
- 9)Komorek, J.; Romotowski, T.; Serwicka, E. M.; Mastikhin, V. M. *Zeolites* **1994**, *14*, 629-634.
- 10)Hashimoto, K.; Matzuo, K.; Kominami, H.; Kera, Y. *J. Chem. Soc. Faraday Trans.* **1997**, *93*, 3729-3732.
- 11)Schraml-Marth, M.; Wokaun, A.; Pohl, M.; L., K. H. *J. Chem. Soc. Faraday Trans.* **1991**, *87*, 2635-2646.
- 12)Luan, Z.; Kevan, L. *J. Phys. Chem. B* **1997**, *101*, 2020-2027.
- 13)Li, W.; Luo, L.; Yamashita, H.; Labinger, J. A.; Davis, M. E. *Micropor. Mesopor. Mat.* **2000**, *37*, 57-65.
- 14)Grabowski, R.; Grzybowska, B.; Koztowska, A.; Stoczynski, J.; Wcisto, K. *Top. Catal.* **1996**, *3*, 277-288.

- 15)Grasselli, R. K. *J. Chem. Edu.* **1986**, *63*, 216-221.
- 16)Grasselli, R. K. *Catal. Today* **1999**, *49*, 141-153.
- 17)Concepcion, P.; Lopez Nieto, J. M.; Perez-Pariente, J. *Catal. Lett.* **1993**, *19*, 333-337.
- 18)Blasco, T.; Concepcion, P.; Lopez Nieto, J. M.; Perez-Pariente, J. *J. Catal.* **1995**, *152*, 1-17.
- 19)Centi, G.; Trifiro, F. *Appl. Catal. A-Gen.* **1996**, *143*, 3-16.
- 20)Salem, G. F.; Besecker, C. J.; Kenzig, S. M.; Kowlaski, W. J.; Cirjak, L. M. : US Patent 5,306,858, 1994.
- 21)Okamoto, M.; Luo, L.; Labinger, J. A.; Davis, M. E. *J. Catal.* **2000**, *192*, 128-136.
- 22)Takewaki, T.; J., H. S.; Yamashita, H.; Davis, M. E. *Micropor. Mesopor. Mat* **1999**, *32*, 265-278.
- 23)Das, N.; Eckert, H.; Huo, H.; Wachs, I. E.; Wolzer, J. F.; Feher, J. G. *J. Phys. Chem.* **1989**, *93*, 6786.
- 24)Dzwigaj, S.; Massiani, P.; Davidson, A.; Che, M. *J. of Mole. Catal. A: Chem.* **2000**, *155*, 169-182.
- 25)Cambor, M. A.; Costantini, M.; Corma, A.; Gilbert, L.; Esteve, P.; Martimez, A.; Valencia, S. *J. Chem. Soc., Chem. Commun.* **1996**, *11*, 1339-1340.
- 26)Sen, T.; Rajamohanan, P. R.; Ganapathy, S.; Sivasanker, S. *J. Catal.* **1996**, *163*, 354-364.
- 27)Tuel, A.; Taarit, Y. B. *Appl. Catal. A-Gen.* **1993**, *102*, 201-214.
- 28)Chien, S. H.; Ho, J. C.; Mon, S. S. *Zeolites* **1997**, *18*, 182-187.
- 29)Perego, G.; Bellussi, G.; Corno, G.; Taramasso, M.; Buonomo, F.; Esposito, A. *Stud. Surf. Sci. Catal.* **1986**, *28*, 129.

- 30)Chen, C. Y.; Li, H. X.; Davis, M. E. *Micropor. Mesopor. Mat.* **1993**, *2*, 17.
- 31)Albonetti, S.; Blanchard, G.; Burattin, P.; Cassidy, T. J.; Masetti, S.; Trifiro, F. *Catal. Lett.* **1997**, *45*, 119-213.
- 32)Bosch, H.; Kip, B. J.; van Ommen, J. G.; Gellings, P. J. *J. Chem. Soc. Faraday Trans. I* **1984**, *80*, 2479-2488.
- 33)Birchall, T.; Sleight, A. W. *Inorg. Chem.* **1976**, *15*, 868.
- 34)Khodakov, A.; Olthaf, B.; Bell, A. T.; Iglesia, E. *J. Catal.* **1999**, *181*, 205-216.
- 35)Li, W. *Davis Group, Group Talk* **1998**.

**Table 3.1** Composition of vanadyl ion-exchanged and ion-exchange-hydrolyzed zeolite beta samples.

Catalyst	Si:Al:V:Na	vanadium content (wt.%)
VO-Na-beta	14.8:1:0.16:0.65	0.7
NH <sub>3</sub> treated*	14.3:1:0.16:0.65	0.7
IEH(I)-beta*	14.3:1:0.16:0.65	0.7
H-beta**	13.7:1:0	0.0
VO-H-beta	25.2:1:0.61:0	1.66

\* Treated VO-Na-beta samples.

\*\* Precursor for VO-H-beta.

**Table 3.2** Propane partial oxidation over vanadyl ion-exchanged zeolite beta.

Catalyst	Temp. °C	Conv.(%)		Sel. (%)					
		C <sub>3</sub> H <sub>8</sub>	O <sub>2</sub>	C <sub>3</sub> H <sub>6</sub>	C <sub>2</sub> H <sub>4</sub>	acetone	acetic acid	CO	CO <sub>2</sub>
VO-Na-beta <sup>a)</sup>	350	2.16	19.6	9.43	0	0.17	3.12	43.5	43.8
	400	4.23	35.4	18.9	0	0.11	0.02	37.5	43.5
VO-NH <sub>4</sub> -beta <sup>a)</sup>	350	2.49	14.3	20.1	0	0	16.8	33.6	29.4
	400	7.14	42.7	12.3	0.98	0	11.6	40.0	35.1
VO-H-beta <sup>a)</sup>	350	1.62	9.12	20.9	0	0	21.1	28.3	29.7
	400	4.27	25.4	13.6	1.2	0	13.9	38.0	33.4
VO-H-beta <sup>b)</sup>	350	1.0	7.8	24.7	0	0	0.83	41.5	33.0
	400	4.3	28.4	14.6	1.95	0	0.43	46.8	36.3

0.5 mL (0.20 g) catalyst together with 1.0 mL SiC were used for each reaction. Before a reaction, the catalyst was pretreated at 350°C in He for 1 hour. The feed gas molar ratio was a) propane:O<sub>2</sub>:H<sub>2</sub>O:He=4:2:4:5, b) propane:O<sub>2</sub>:H<sub>2</sub>O:He=4:2:-:9 with a total flow rate of 15 mL/min.

**Table 3.3** Comparison of propane oxidation over VO-Na-beta and its base-treated forms.

Catalyst	Temp. °C	Conv.(%)		Sel. (%)					
		C <sub>3</sub> H <sub>8</sub>	O <sub>2</sub>	C <sub>3</sub> H <sub>6</sub>	C <sub>2</sub> H <sub>4</sub>	acetone	acetic acid	CO	CO <sub>2</sub>
VO-Na-beta	350	2.16	19.6	9.43	0	0.17	3.12	43.5	43.8
	400	4.23	35.4	18.9	0	0.11	0.02	37.5	43.5
IEH(I)-beta	350	1.92	12.2	35.6	0	0	2.49	27.0	34.8
	400	5.37	32.3	23.4	3.5	0	0.64	32.1	40.3
NH <sub>3</sub> -treated	350	1.09	8.24	32.0	0	0	0.99	34.5	32.5
	400	2.81	23.1	28.3	0	0	1.93	37.2	32.6

0.5 mL (0.20 g) catalyst together with 1.0 mL SiC were used for each reaction. Before a reaction, the catalyst was pretreated at 350°C in He for 1 hour. The feed gas molar ratio was propane:O<sub>2</sub>:H<sub>2</sub>O:He=4:2:4:5 with a total flow rate of 15 mL/min.

**Table 3.4** Propane oxidation over vanadium impregnated zeolite beta catalysts.

Catalyst	Temp. °C	Conv. (%)		Sel. (%)				
		C <sub>3</sub> H <sub>8</sub>	O <sub>2</sub>	C <sub>3</sub> H <sub>6</sub>	C <sub>2</sub> H <sub>4</sub>	acetic acid	CO	CO <sub>2</sub>
V/H-beta	350	2.39	15.1	14.3	0.60	19.0	33.0	33.1
	400	5.43	37.4	16.3	1.62	3.00	36.6	42.5
V/Na-beta	350	2.69	18.7	16.7	0.85	7.97	36.1	38.4
	400	8.01	52.4	12.1	1.52	4.12	35.6	46.7
V/Cs-beta	350	0.66	2.59	58.9	0	0.85	24.8	15.5
	400	4.20	21.6	38.8	5.33	0.38	35.3	20.2
VO-H-beta	350	1.62	9.12	20.9	0	21.1	28.3	29.7
	400	4.27	25.4	13.6	1.2	13.9	38.0	33.4

0.5 mL (0.20 g) catalyst together with 1.0 mL SiC were used for each reaction. Before a reaction, the catalyst was pretreated at 400°C in O<sub>2</sub>/He for 2 hours. The molar feed ratio was C<sub>3</sub>H<sub>8</sub>:O<sub>2</sub>:H<sub>2</sub>O:He = 4:2:4:5 with a total flow rate of 15 mL/min.

**Table 3.5** Propane oxidation over V-Sb/H-beta and V-Mo/H-beta catalysts.

Temp. °C	Conv.(%)		Sel.(%)				Composition Si:Al:V:M <sub>2</sub> *	
	C <sub>3</sub> H <sub>8</sub>	O <sub>2</sub>	C <sub>3</sub> H <sub>6</sub>	C <sub>2</sub> H <sub>4</sub>	acetic acid	CO		CO <sub>2</sub>
VO-H-beta								
350	1.62	9.12	20.9	0	21.1	28.3	29.7	25.2:1:0.61:-
400	4.27	25.4	13.6	1.2	13.9	38.0	33.4	
V-Sb/H-beta (V:Sb=1:1.1)								
350	2.35	14.1	19.9	0	15.2	35.4	29.6	21.8:1:0.53:0.58
400	5.86	39.3	13.2	1.6	6.10	45.5	33.6	
V-Sb/H-beta (V:Sb=1:1.7)								
350	1.29	6.79	33.4	0	7.36	33.8	25.4	21.8:1:0.52:0.88
400	4.11	26.8	18.9	0	4.48	42.7	33.9	
V-Mo/H-beta (V:Mo=1.1:1)								
350	2.18	13.0	27.0	0	19.2	26.0	27.8	21.8:1:0.53:0.5
400	6.45	38.2	16.0	1.61	8.49	38.2	35.8	
V-Mo/H-beta (V:Mo=2:1)								
350	2.26	12.3	26.9	0	22.0	24.9	26.1	21.8:1:0.53:0.27
400	4.76	28.1	23.4	2.0	6.70	38.7	29.3	
Mo/H-beta								
350	1.61	8.84	32.2	0	4.96	29.8	33.0	13.1:1:-:0.5
400	3.31	17.0	35.2	1.61	3.80	29.3	30.1	
Sb/H-beta								
350	0.97	5.4	35.0	0	7.14	30.1	27.8	13.1:1:-:0.49
400	2.73	15.0	34.5	0	2.20	31.4	31.9	

\* M<sub>2</sub>: 2<sup>nd</sup> metal

0.5 mL (0.20g) catalyst together with 1.0 mL SiC were used for each reaction. Before a reaction, the catalyst was pretreated at 400°C in O<sub>2</sub>/He for 2 hours. The molar feed ratio was C<sub>3</sub>H<sub>8</sub>:O<sub>2</sub>:H<sub>2</sub>O:He = 4:2:4:5 with a total flow rate of 15 mL/min.

**Table 3.6** Propane oxidation over vanadium and molybdenum-containing catalysts on different supports.

Temp. °C	Conv.(%)		Sel. (%)								
	C <sub>3</sub> H <sub>8</sub>	O <sub>2</sub>	C <sub>3</sub> H <sub>6</sub>	C <sub>2</sub> H <sub>4</sub>	acetone	acetic CH <sub>3</sub> CHO	acid	acrolein	acrylic acid	CO	CO <sub>2</sub>
V-Mo/Na-beta (V:Mo=1:1, V 1.25wt.%)											
350	1.68	10.5	41.2	0	0.10	0.64	5.74	0	0	18.5	33.8
400	4.66	36.7	28.4	0	0.09	0.45	3.36	0	0	21.8	46.0
V/Na-beta (V 1.25wt.%)											
350	2.69	18.7	16.7	0.85	0	0	7.97	0	0	36.1	38.4
400	8.01	52.4	12.1	1.52	0	0	4.12	0	0	35.6	46.7
V-Mo /H-beta (V:Mo=1:1, V 1.66 wt.%)											
350	2.18	13.0	27.0	0	0.04	0	19.2	0	0	26.0	27.8
400	6.45	38.2	16.0	1.61	0	0	8.49	0	0	38.2	35.8
V/H-beta (V 1.25 wt.%)											
350	2.39	15.1	14.3	0.60	0	0	19.0	0	0	33.0	33.1
400	5.43	37.4	16.3	1.62	0	0	2.99	0	0	36.6	42.5
V-Mo/silica (V:Mo=1:1, V 1.25 wt.%)											
400	1.83	6.71	78.0	0	0.02	0.03	0.15	0.07	0	9.88	11.9
500	15.0	64.8	62.9	0	0.00	0.05	0.08	0.41	0.22	16.1	20.2
V/silica* (V 1.25 wt.%)											
400	0.62	1.77	72.8	0	0.07	0	0	0	0	19.5	7.68
500	15.5	70.0	48.9	1.00	0.06	0	0.93	1.40	0	26.7	21.0

0.20 g catalyst together with 1.0 mL SiC were used for each reaction. Catalysts were pretreated at 400°C for 2 hours in a He/O<sub>2</sub> flow. The molar feed ratio was C<sub>3</sub>H<sub>8</sub>:O<sub>2</sub>:H<sub>2</sub>O:He = 4:2:4:5 with a total flow rate of 15 mL/min.

\*Trace amounts of propanal were also observed.

**Table 3.7** Propane oxidation over zeolite beta catalysts with framework vanadium.

Temp. °C	Conv.(%)		Sel.(%)						
	C <sub>3</sub> H <sub>8</sub>	O <sub>2</sub>	C <sub>3</sub> H <sub>6</sub>	C <sub>2</sub> H <sub>4</sub>	acetone	acetic acid	acrolein	CO	CO <sub>2</sub>
Vbeta(I)									
400	0.71	3.29	54.4	1.40	0	0	0	22.8	21.4
500	5.49	24.4	46.8	4.43	0	0	0	28.0	20.9
V/Vbeta(I)									
350	1.30	4.71	60.5	0	0.15	4.54	0	25.8	9.09
400	6.49	27.33	45.6	2.38	0.10	2.46	0.66	28.4	20.4
Vbeta(H)									
400	0.81	2.78	61.9	0	0	0	0	25.3	12.8
450	3.31	11.47	63.9	0.57	0	0	0	20.0	15.8
V/Vbeta(H)									
350	0.81	3.18	55.1	0	0	2.17	0	34.7	8.00
400	1.89	8.12	49.6	0	0.02	0.30	0.10	35.5	14.5

0.20 g catalyst together with 1.0 mL SiC were used for each reaction. Catalysts were pretreated at 400°C for 2 hours in a He/O<sub>2</sub> flow. The molar feed ratio was C<sub>3</sub>H<sub>8</sub>:O<sub>2</sub>:H<sub>2</sub>O:He = 4:2:4:5 with a total flow rate of 15 mL/min.

**Table 3.8** Propane oxidation over Ti/beta, Si/beta and AlSi/beta based catalysts.

Temp. °C	Conv. (%)		Sel. (%)						
	C <sub>3</sub> H <sub>8</sub>	O <sub>2</sub>	C <sub>3</sub> H <sub>6</sub>	C <sub>2</sub> H <sub>4</sub>	acetone	acetic acid	acrolein	CO	CO <sub>2</sub>
V/Ti/beta (1.25wt.%V)									
350	1.40	4.73	65.0	0	0.04	2.49	1.26	19.7	11.5
400	5.18	21.5	48.6	1.71	0.20	2.18	1.69	26.0	19.6
Ti/beta									
400	0.52	2.59	47.4	0	0	0	0	34.4	18.2
450	2.24	9.73	46.7	2.09	0	0	0	29.0	22.3
V/Si/beta									
350	5.65	33.4	16.0	0.64	0.08	9.48	0	38.5	35.2
400	13.2	74.5	13.7	1.07	0.04	2.62	0	44.6	38.0
V/AlSi/beta									
350	5.17	35.7	12.8	0	0.10	13.3	0	30.3	43.4
400	11.6	73.3	12.8	0.81	0.07	3.65	0	34.1	48.5
V/H-beta									
350	2.39	15.1	14.3	0.60	0	19.0	0	33.0	33.1
400	5.43	37.4	16.3	1.6	0	2.99	0	36.6	42.5

0.20 g catalyst together with 1.0 mL SiC were used for each reaction. Catalysts were pretreated at 400°C for 2 hours in a He/O<sub>2</sub> flow. The molar feed ratio was C<sub>3</sub>H<sub>8</sub>:O<sub>2</sub>:H<sub>2</sub>O:He = 4:2:4:5 with a total flow rate of 15 mL/min. The vanadium content is 1.25 wt.% for all the above impregnated catalysts.

**Table 3.9** Propane oxidation over non-zeolite beta based catalysts.

Temp. °C	Conv.(%)		Sel. (%)							
	C <sub>3</sub> H <sub>8</sub>	O <sub>2</sub>	C <sub>3</sub> H <sub>6</sub>	C <sub>2</sub> H <sub>4</sub>	acetone	acetic acid	acrolein	acrylic acid	CO	CO <sub>2</sub>
V/SSZ-33 (1.20 wt.%V)										
350	1.68	11.2	21.1	0	0.10	10.6	0	0	33.1	35.1
400	5.65	33.3	21.3	1.63	0.03	6.27	0	0	34.5	36.3
VO-SSZ-33(0.39 wt.%V)										
350	1.52	8.76	22.5	2.81	0	10.8	0	0	32.7	30.7
400	3.54	19.3	25.8	3.52	0	4.96	0	0	31.9	33.8
VO-MCM-41 (1.46wt.%V)										
350	0.83	5.72	23.6	0	0	0	0	0	29.6	46.8
400	1.53	8.94	30.8	0	0	0	0	0	41.0	28.1
V/MCM-41(1.25wt.%V)										
350	0.14	0.37	83.4	0	0	0	0	0	0	16.6
400	0.45	0.94	88.4	0	0	0.8	0	0	0	10.9
V/silica* (1.25 wt.%V)										
400	0.62	1.77	72.8	0	0.07	0	0	0	19.5	7.68
500	15.5	70.0	48.9	1.00	0.06	0.93	1.40	0	26.7	21.0
V-Mo/silica (V:Mo=1:1, 1.25 wt.%V)										
400	1.83	6.71	78.0	0	0.02	0.15	0.07	0	9.88	11.9
500	15.0	64.8	62.9	0	0.00	0.08	0.41	0.22	16.1	20.2

0.20 g catalyst together with 1.0 mL SiC were used for each reaction. Catalysts were pretreated at 400°C for 2 hours in a He/O<sub>2</sub> flow. The molar feed ratio was C<sub>3</sub>H<sub>8</sub>:O<sub>2</sub>:H<sub>2</sub>O:He = 4:2:4:5 with a total flow rate of 15 mL/min.

\* Trace amounts of propanal were also observed.

**Table 3.10a** Turnover frequency of bulk V<sub>2</sub>O<sub>5</sub> and zeolite based catalysts.

Catalyst	TOF at 350°C (S <sup>-1</sup> )	TOF at 400°C(S <sup>-1</sup> )
VO-Na-beta	2.34x10 <sup>-3</sup>	4.59x10 <sup>-3</sup>
IEH(I)-beta	2.08x10 <sup>-3</sup>	5.82x10 <sup>-3</sup>
NH <sub>3</sub> -treated	1.18x10 <sup>-3</sup>	3.05x10 <sup>-3</sup>
VO-H-beta	7.41x10 <sup>-4</sup>	1.95x10 <sup>-3</sup>
V/H-beta	1.45x10 <sup>-3</sup>	3.30x10 <sup>-3</sup>
V/Cs-beta	4.01x10 <sup>-4</sup>	2.55x10 <sup>-3</sup>
Vbeta(I)	N/A	2.07x10 <sup>-3</sup>
V/Si/beta	3.43x10 <sup>-3</sup>	8.01x10 <sup>-3</sup>
V/AlSi/beta	3.14x10 <sup>-3</sup>	7.04x10 <sup>-3</sup>
V <sub>2</sub> O <sub>5</sub> *	1.34x10 <sup>-3</sup>	2.50x10 <sup>-3</sup>
V/silica	N/A	3.76x10 <sup>-4</sup>

Reaction condition: 0.5 mL (0.20 g) catalyst together with 1.0 mL SiC were used for each reaction. Before a reaction, the catalyst was pretreated at 350°C in He for 1 hour. The feed gas molar ratio was propane:O<sub>2</sub>:H<sub>2</sub>O:He=4:2:4:5 with a total flow rate of 15 mL/min.

\* 0.67 g V<sub>2</sub>O<sub>5</sub> were used.

**Table 3.10b** Reaction results of propane oxidation over bulk V<sub>2</sub>O<sub>5</sub>.

Catalyst	Temp. °C	Conv.(%)		Sel. (%)					
		C <sub>3</sub> H <sub>8</sub>	O <sub>2</sub>	C <sub>3</sub> H <sub>6</sub>	acetone	acetic acid	acrolein	CO	CO <sub>2</sub>
V <sub>2</sub> O <sub>5</sub>	350	5.77	26.8	31.1	0	14.5	0	40.8	13.5
	400	10.8	54.9	24.2	0	15.8	0	44.0	15.9

0.5 mL (0.67 g) catalyst together with 1.0 mL SiC were used for this reaction. Reaction was conducted under standard condition.

**Table 3.11** Acrylic acid stability over VO-H-beta.

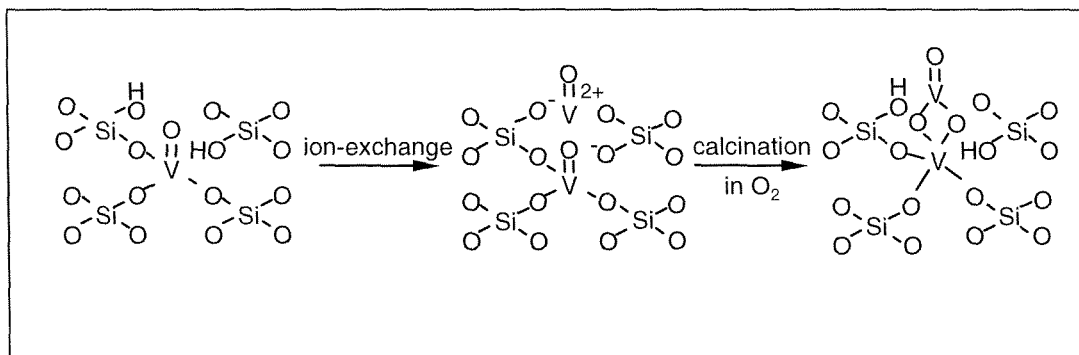
Temp °C	Conv.(%)		Sel.(%)			
	acrylic acid	O <sub>2</sub>	acetic acid	C <sub>2</sub> H <sub>4</sub>	CO	CO <sub>2</sub>
Acrylic acid solution(10 volume%):O <sub>2</sub> :He = 4:2:9 (2.0 s)						
350	100	18.3	0	0	43.8	56.2
300	100	14.4	4.30	0	34.7	61.0
250	24.6	7.39	21.1	0	15.3	52.1
200	20.6	2.55	0	0	0	100

0.5 g catalyst together with 1.0 mL SiC were used for this study. No pretreatment was done before the reaction.

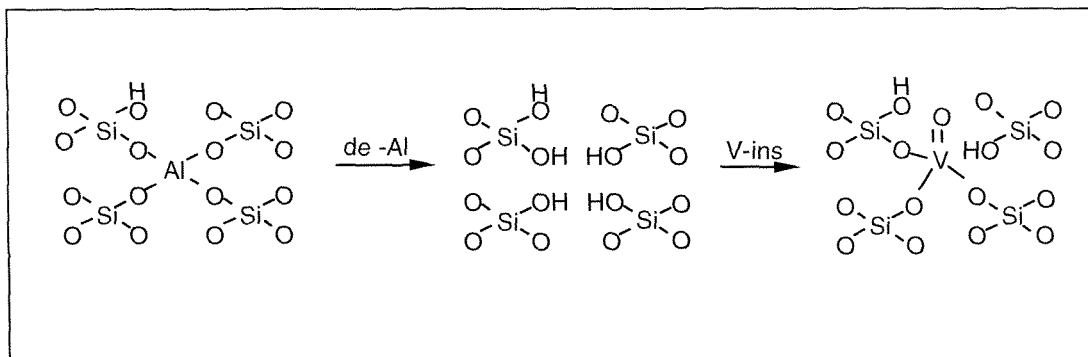
**Table 3.12** Desorption of possible oxygenates in partial oxidation of propane over zeolite beta.

Material	Adsorbate	Desorption Temperature (°C)
Beta (Si/Al=12)	Acrylic acid	332
	Propanoic acid	368
	Propanol	190
	Acetic Acid	294

Zeolite beta (0.1 g) was suspended in 10 ml diluted adsorbate solution for 2 hours, then filtered and dried at 130°C for 3 hours. The desorption temperature was recorded at the end of desorption of adsorbate from use of a TGA.



**Scheme 3.1** Formation of a metal oxide cluster with two vanadium atoms.



**Scheme 3.2** Dealumination and V-insertion method for synthesizing zeolite beta with framework vanadium.

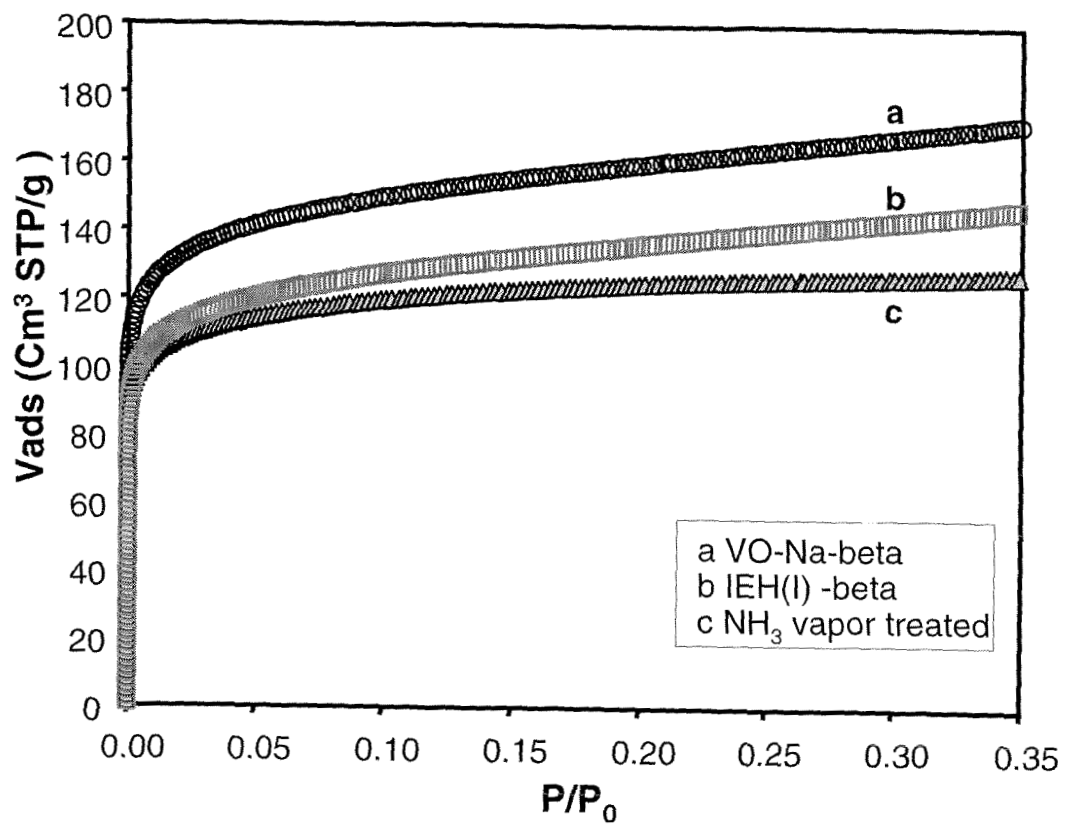


**Figure 3.1** N<sub>2</sub> adsorption isotherms for vanadyl ion-exchanged zeolite beta and its base-treated forms.

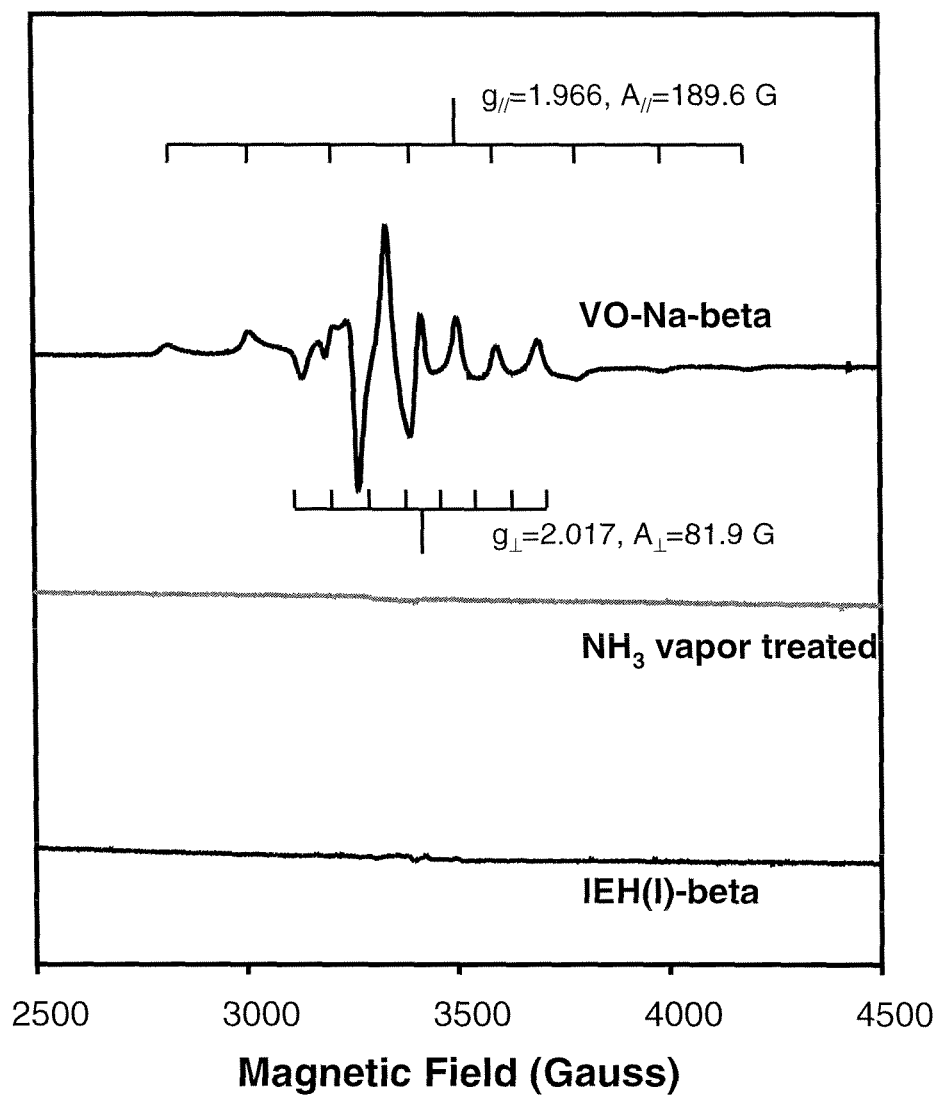


**Figure 3.2** Electron paramagnetic resonance spectra of vanadyl ion-exchanged zeolite beta sample and its base-treated forms.

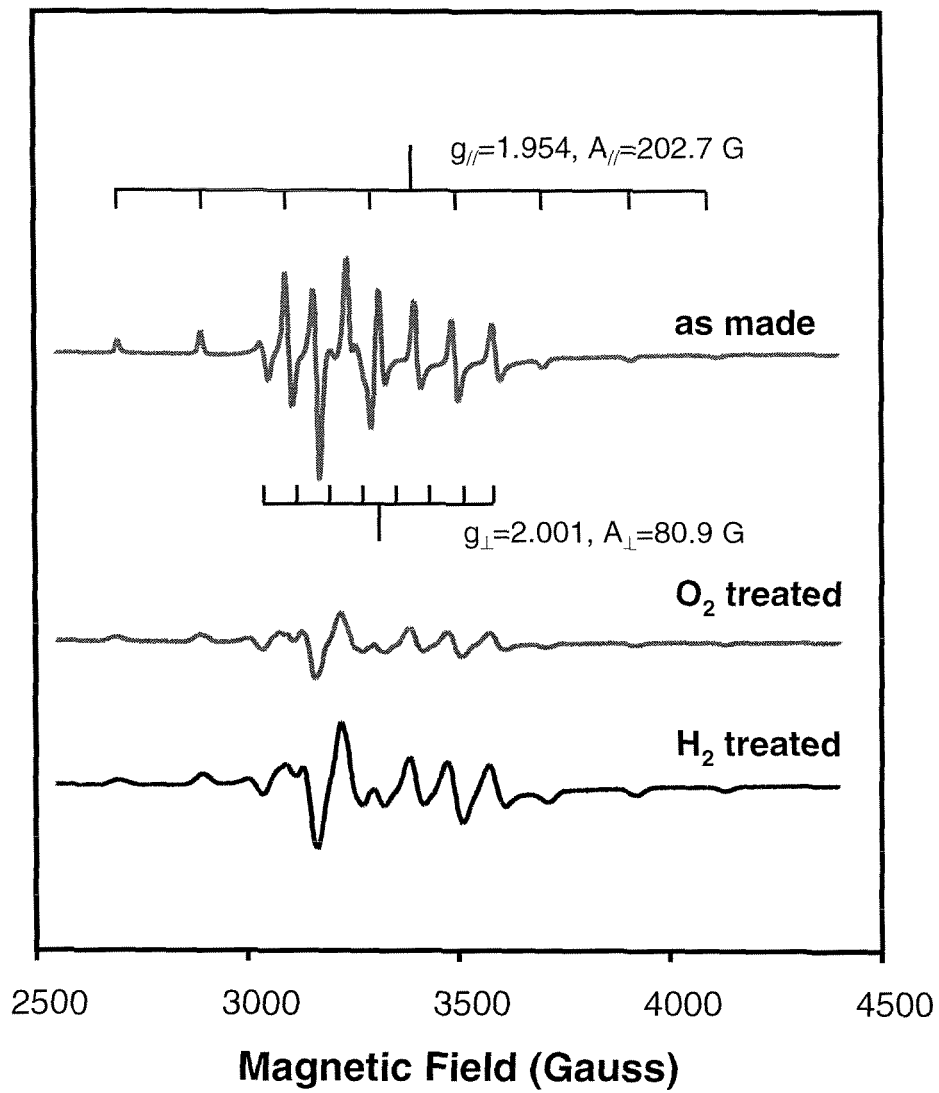


**Figure 3.3** EPR spectra of as-made, O<sub>2</sub>-treated, and O<sub>2</sub>-treated then H<sub>2</sub>-reduced VO-H-beta.

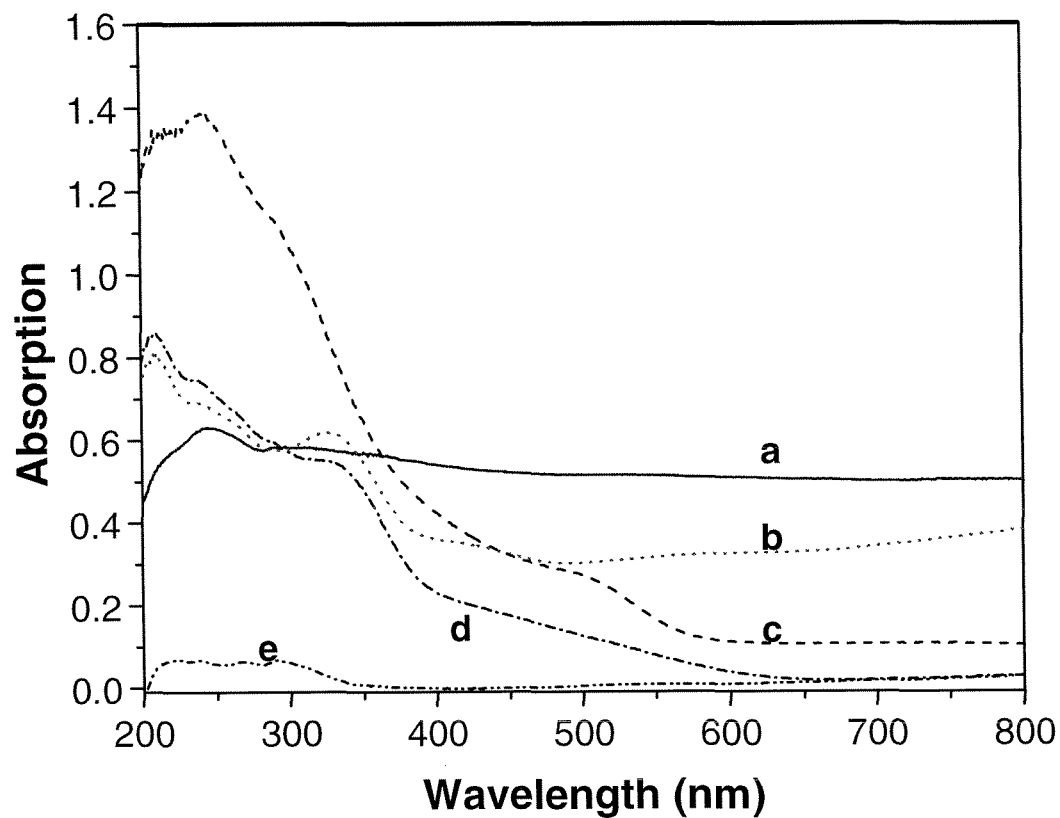


**Figure 3.4** UV-Vis DR spectra of vanadyl ion-exchanged zeolite beta sample and its base-treated forms. a) VO-Na-beta, b) NH<sub>3</sub>-treated VO-Na-beta (without calcination), c) NH<sub>3</sub>-treated VO-Na-beta (with calcination), d) IEH(I)-beta, and e) H-beta.

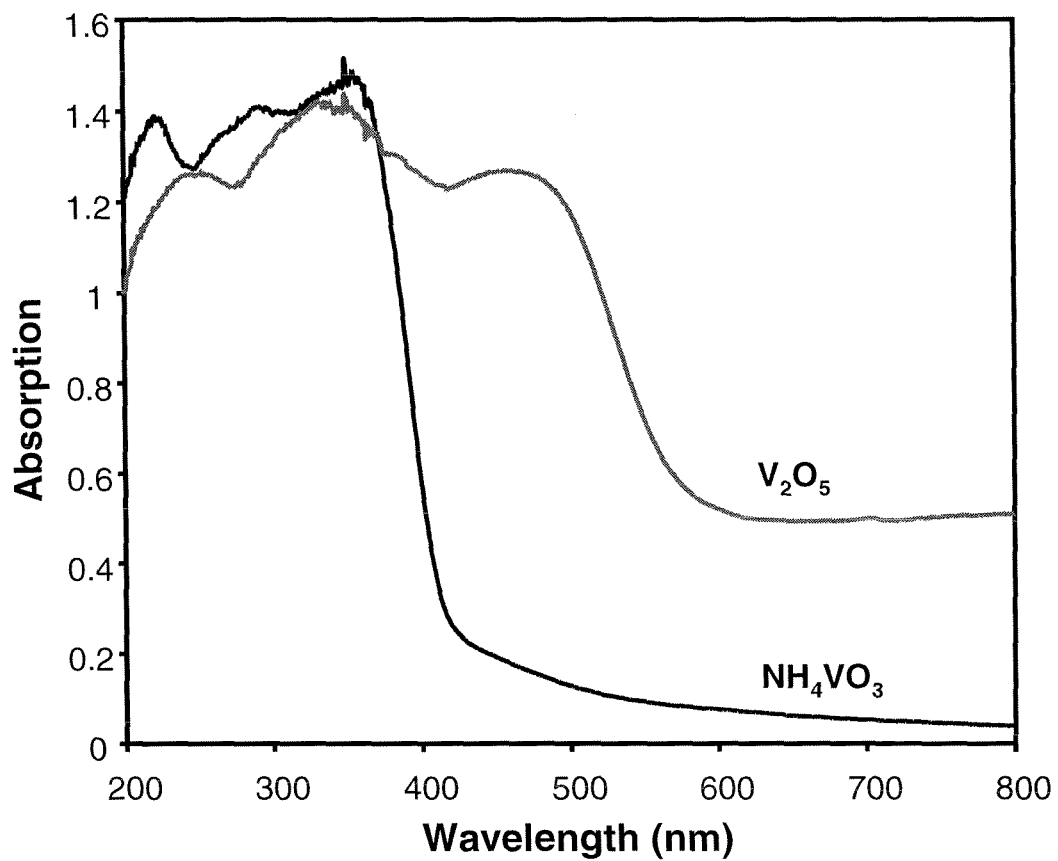


**Figure 3.5** UV-Vis DR spectra of  $NH_4VO_3$  and  $V_2O_5$ .

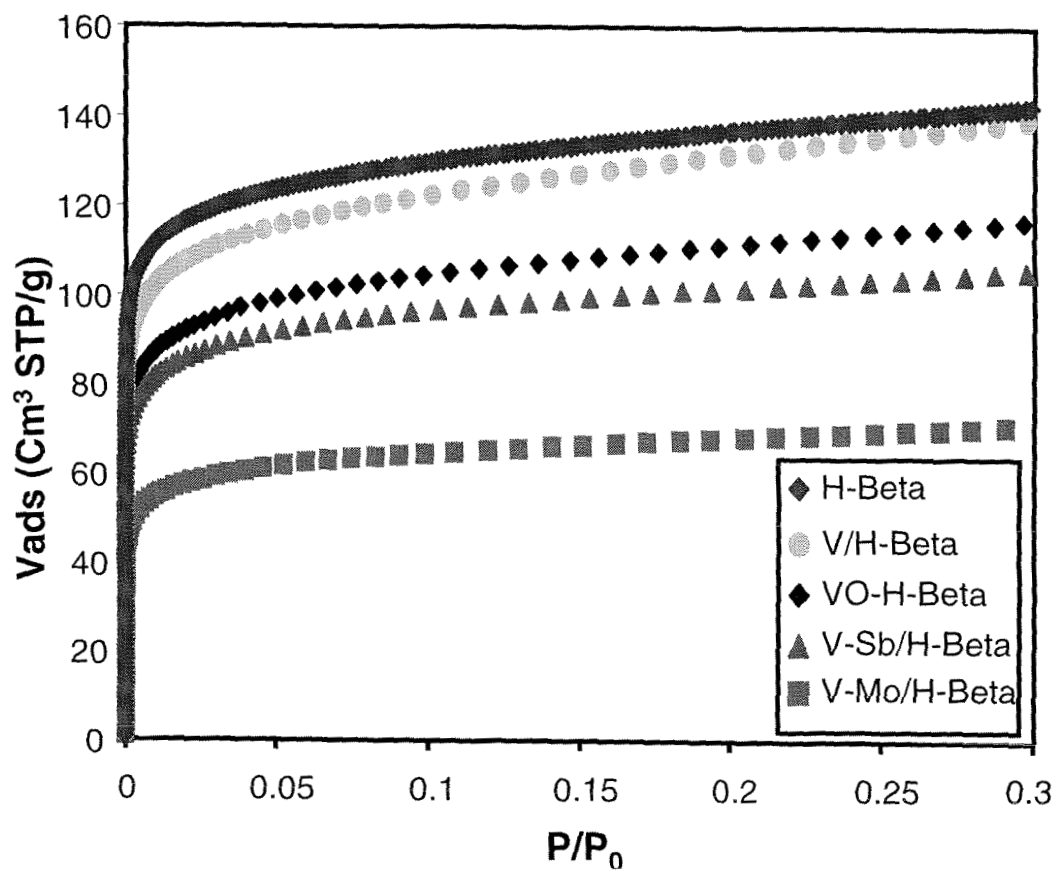


**Figure 3.6**  $\text{N}_2$  adsorption isotherms of H-beta, V/H-beta, VO-H-beta, V-Sb/H-beta, and V-Mo/H-beta.

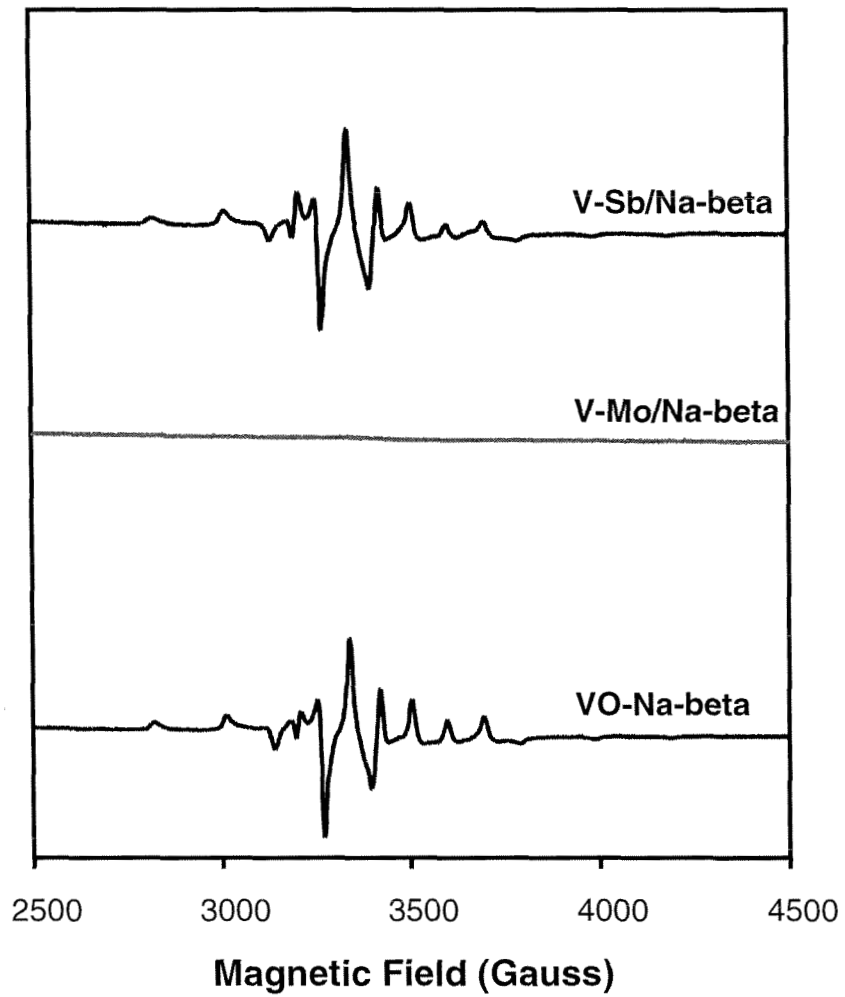


**Figure 3.7** EPR spectra of VO-Na-beta, V-Mo/Na-beta, and V-Sb/Na-beta.

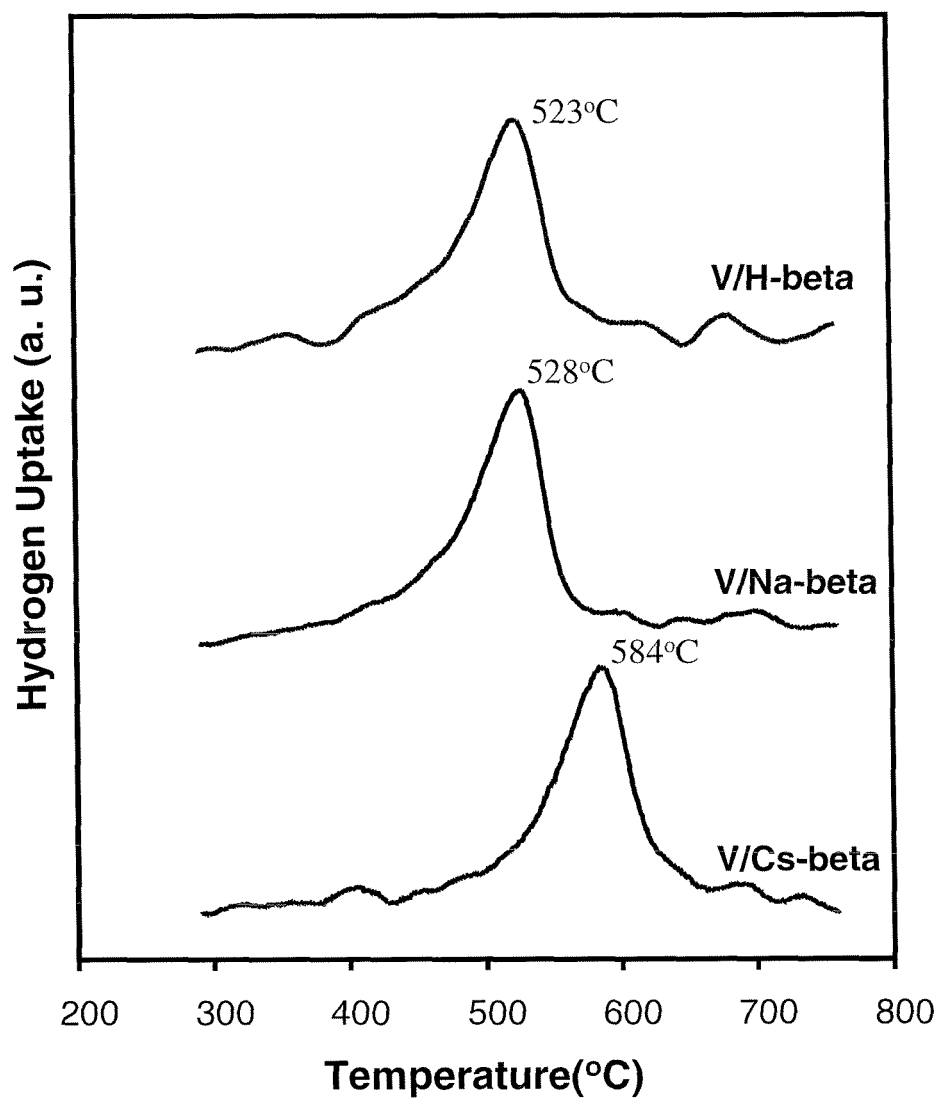


**Figure 3.8** TPR profiles of V/H-beta, V/Na-beta, and V/Cs-beta.

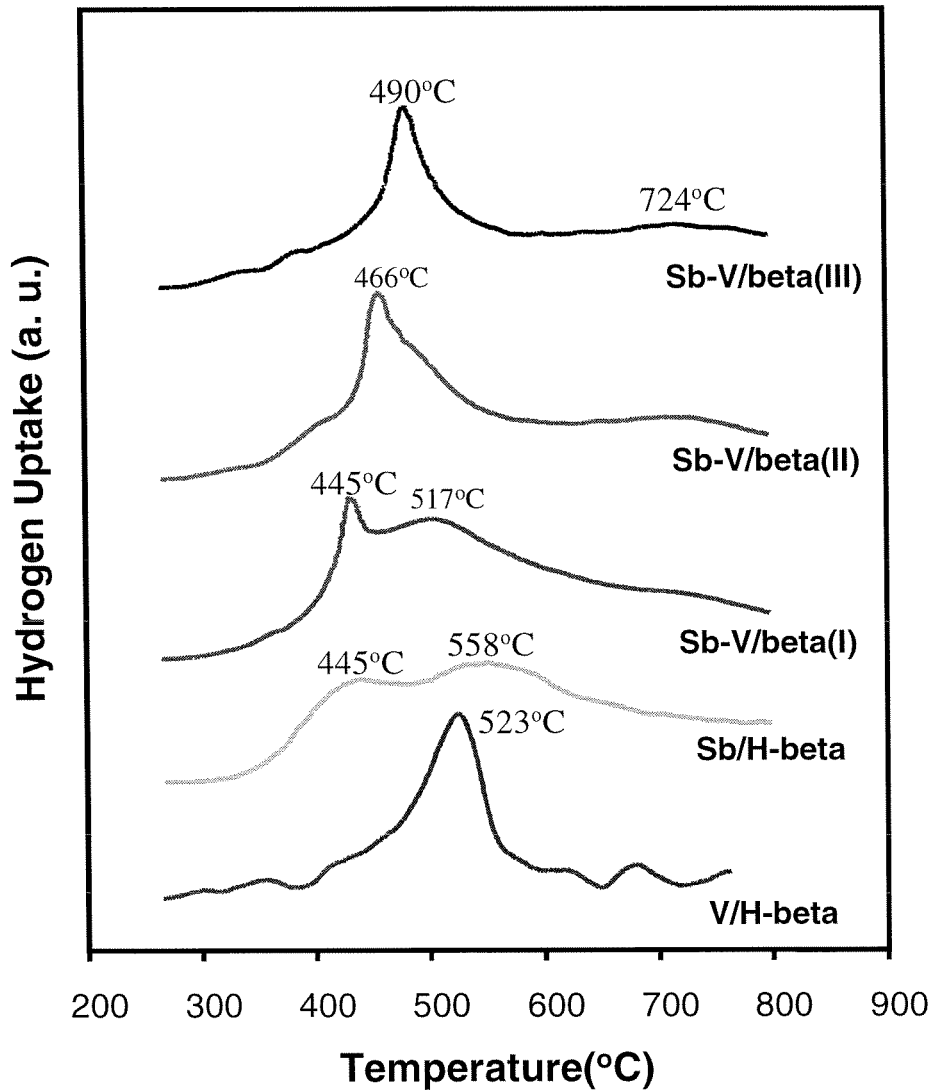


**Figure 3.9** TPR results from a) Sb-V/beta(III)(Sb 1.69 wt.%, Sb/V=0.65) b) Sb-V/beta(II) (Sb 3.29 wt.%, Sb/V=1.31), c) Sb-V/beta(I) (Sb 6.38 wt.%, Sb/V=2.64), d) Sb/H-beta (2 wt.%Sb), and e) V/H-beta (1.25 wt.%V).

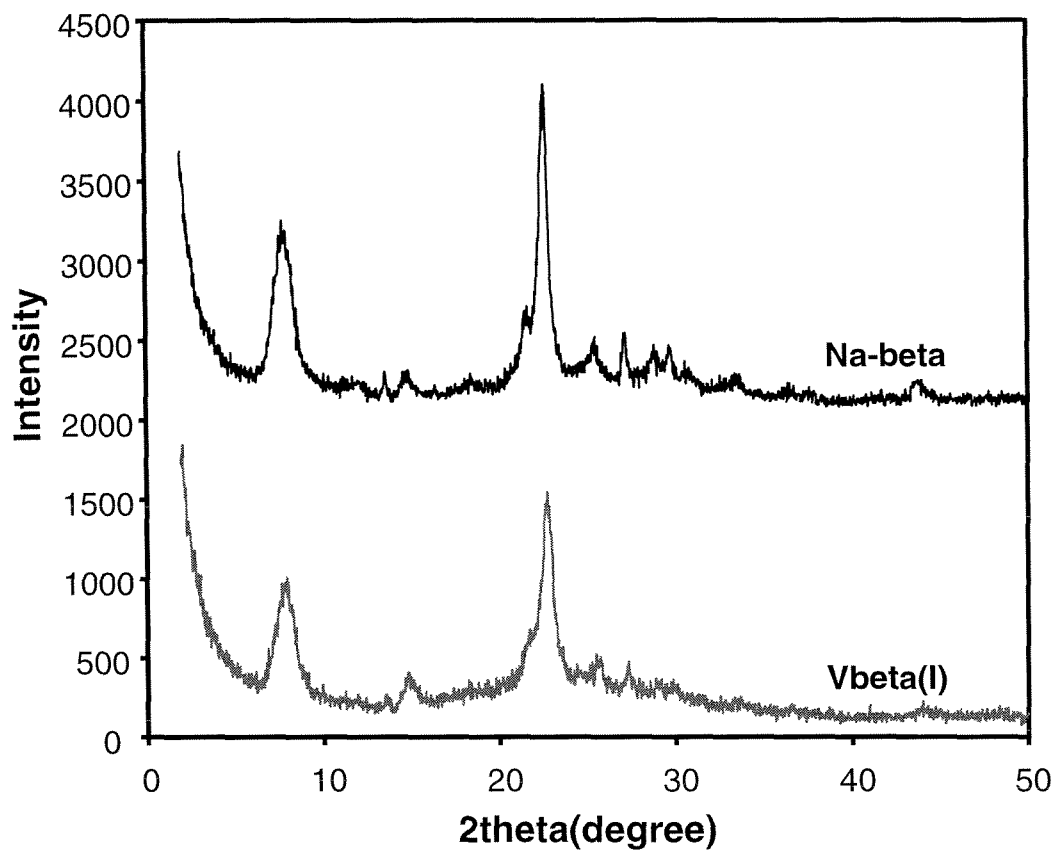


**Figure 3.10** XRD patterns of Vbeta(I) and its starting material, Na-beta.

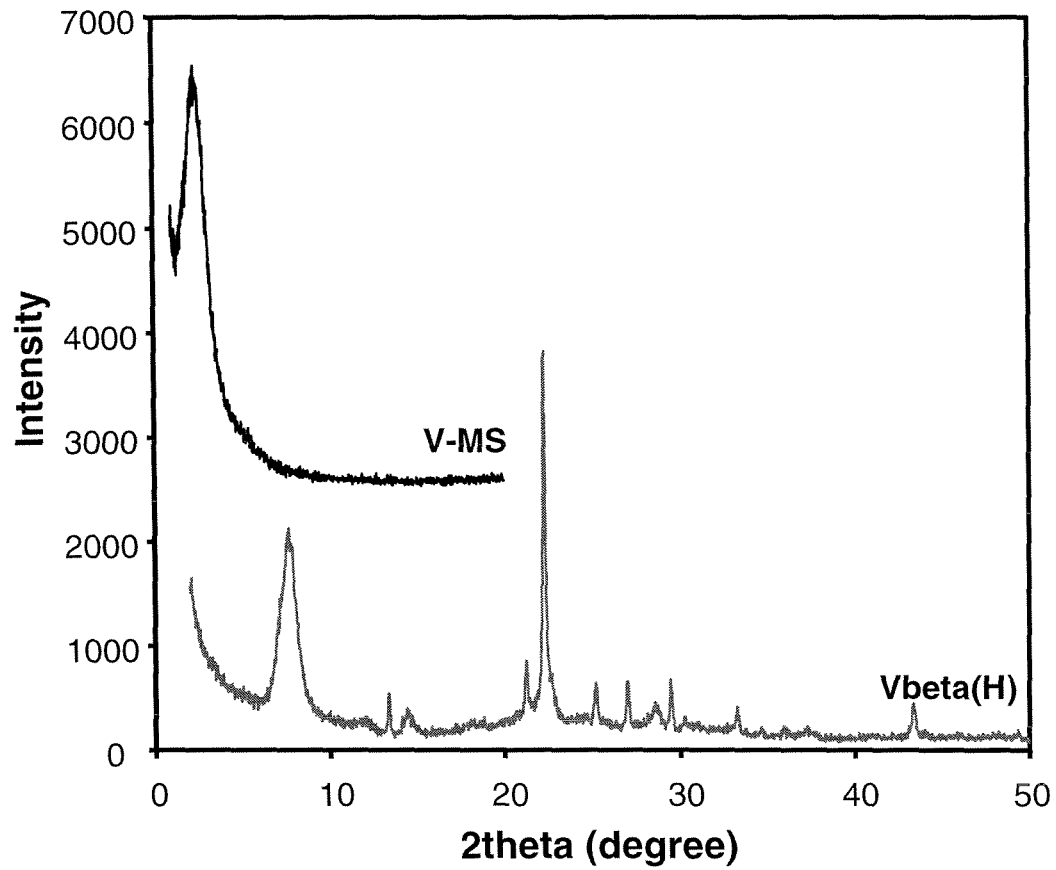


**Figure 3.11** XRD patterns of Vbeta(H) and its precursor V-MS.

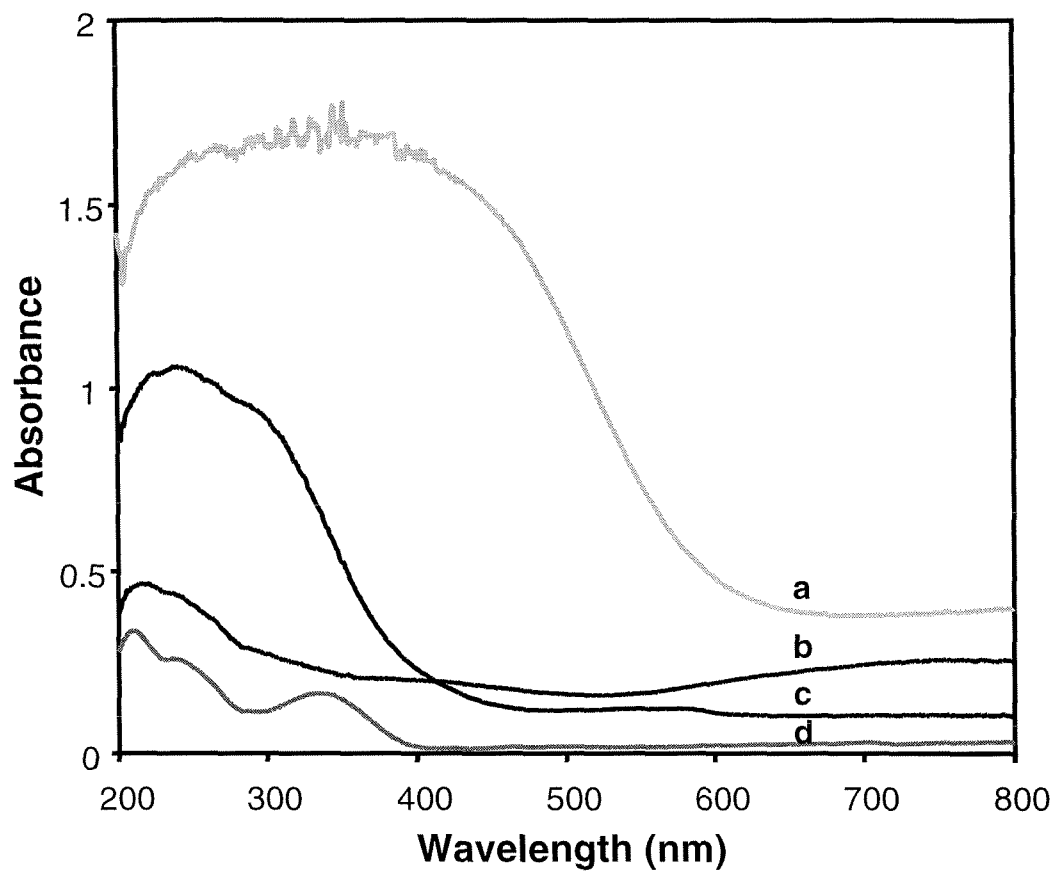


**Figure 3.12** UV-Vis DR spectra of vanadium containing catalysts with vanadium at different positions: a) V/Silica (1.25 wt.%V), b) VO-H-beta (1.66 wt.%V), c) V/H-beta (1.25 wt.%V), d) Vbeta(I) (0.26 wt.%V).

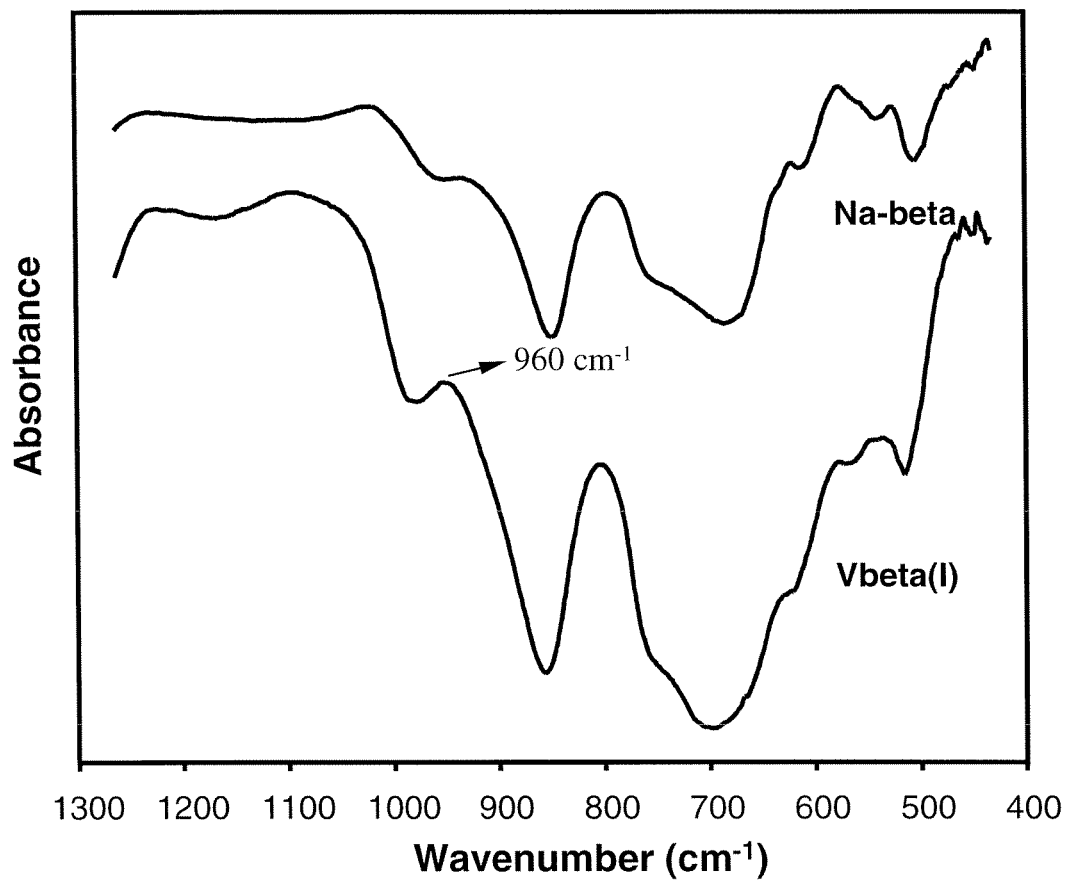


**Figure 3.13** FTIR spectra of Vbeta(I) and Na-beta samples.

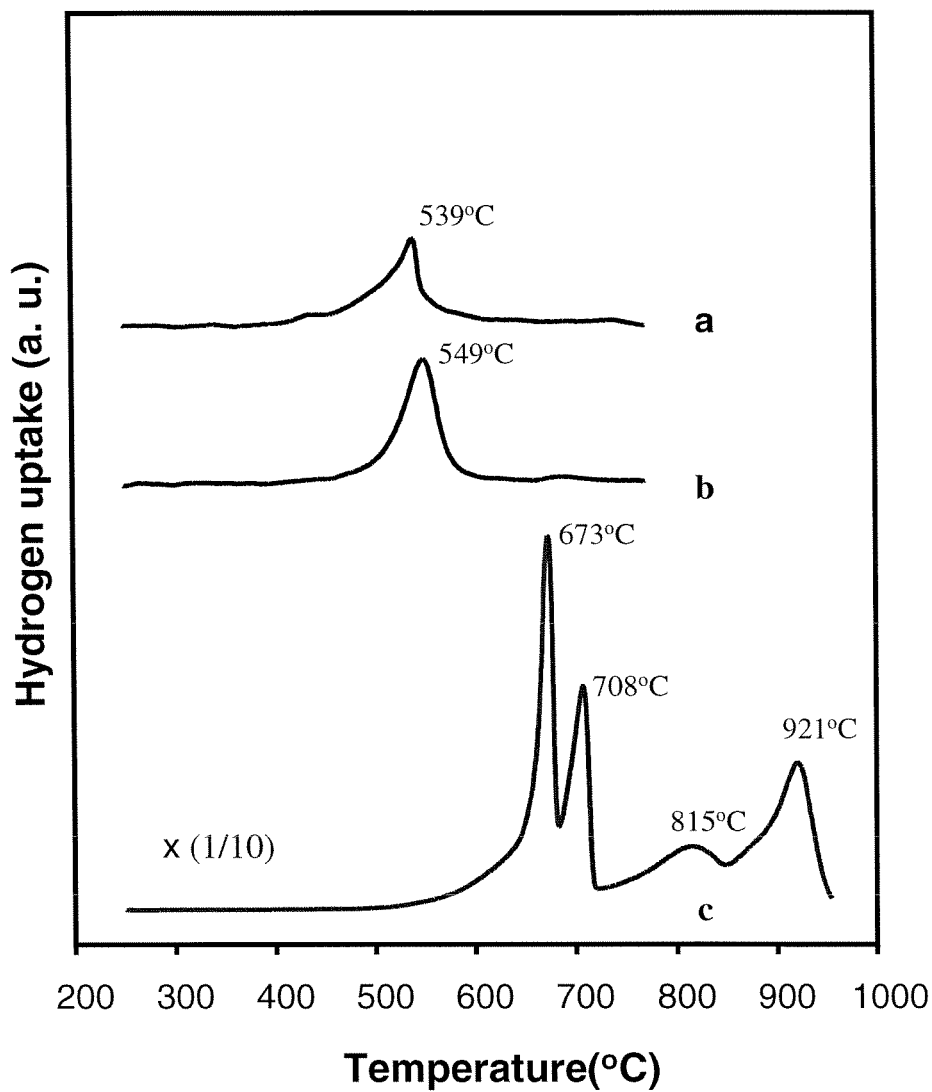


**Figure 3.14** TPR profiles of zeolite supported, silica supported vanadium-containing catalysts and bulk V<sub>2</sub>O<sub>5</sub>: a) VO-H-beta, b) V/silica, and c) bulk V<sub>2</sub>O<sub>5</sub>. (0.1 g was used for each TPR measurement.)

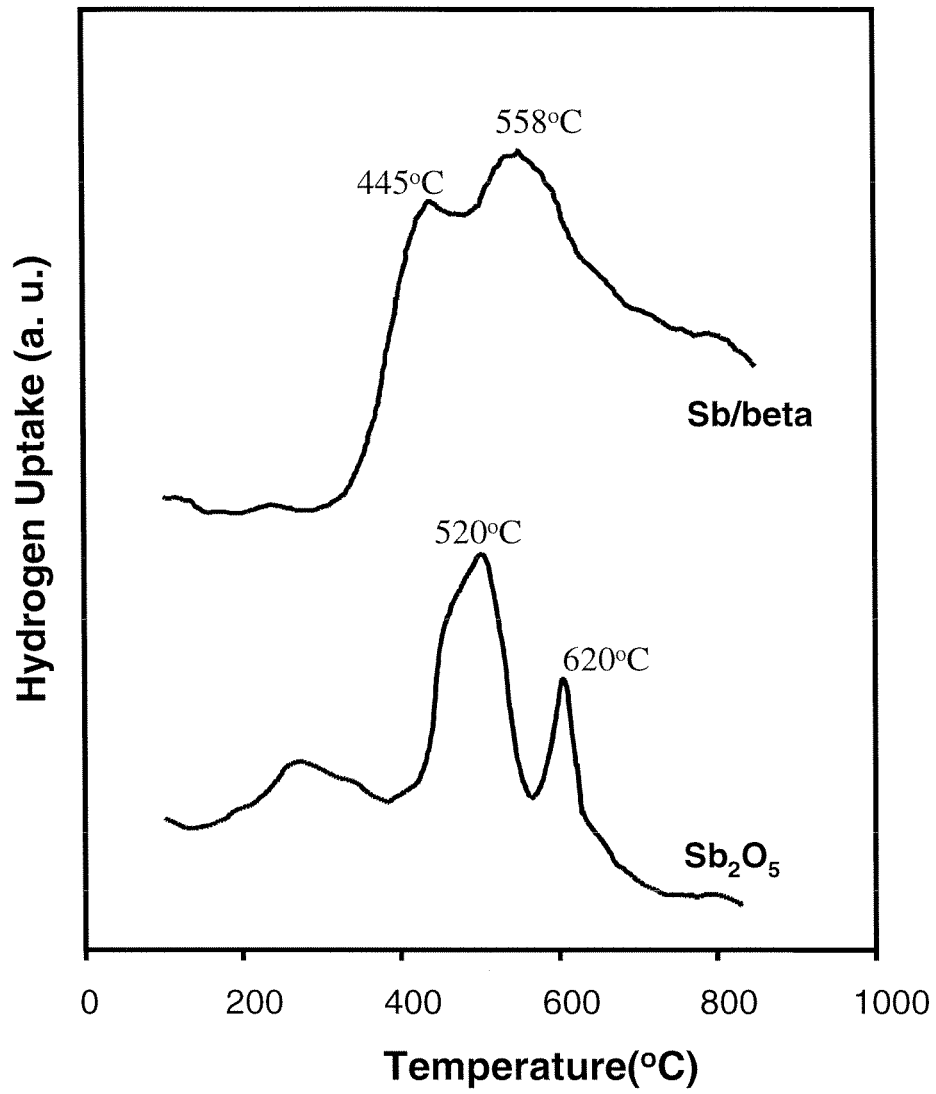


**Figure 3.15** TPR profiles of Sb/beta and Sb<sub>2</sub>O<sub>5</sub> (adapted from Ref.<sup>13</sup>).

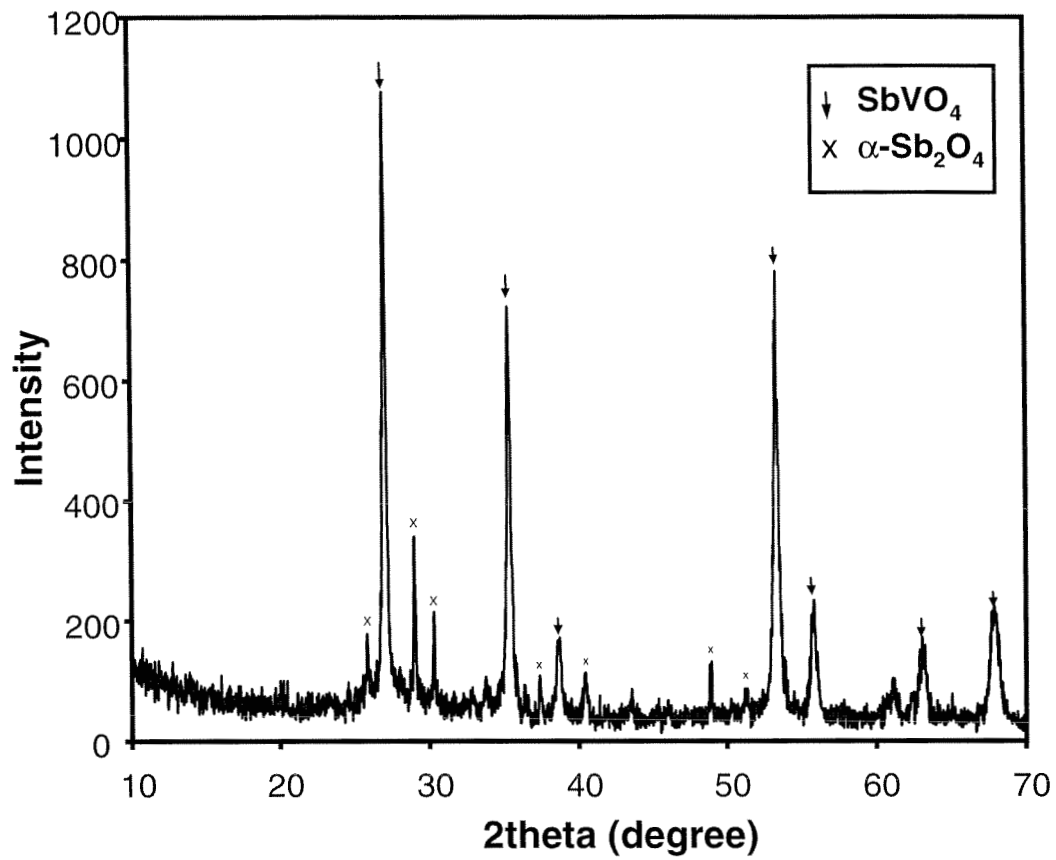


**Figure 3.16** XRD pattern of bulk  $\text{SbVO}_4$  with small amounts of  $\alpha\text{-Sb}_2\text{O}_4$  impurities.

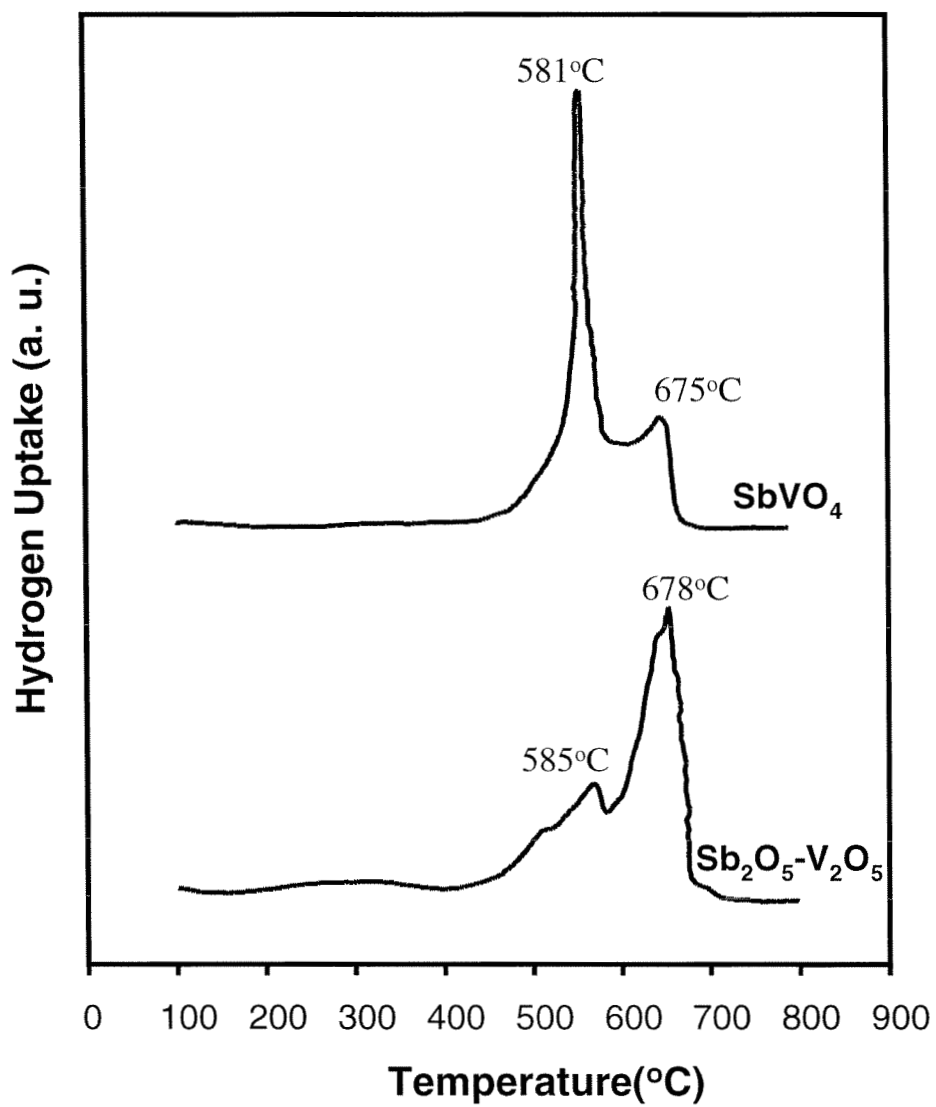


**Figure 3.17** TPR profiles from  $\text{SbVO}_4$  and  $\text{Sb}_2\text{O}_5\text{-V}_2\text{O}_5$  (adapted from Ref.<sup>13</sup>).

## **CHAPTER FOUR**

**Comparison of Reaction Pathways for the  
Partial Oxidation of Propane over Vanadyl  
Ion-exchanged Zeolite Beta and  
 $\text{Mo}_1\text{V}_{0.3}\text{Te}_{0.23}\text{Nb}_{0.12}\text{O}_x$**

**ABSTRACT**

The reaction pathways for the oxidation of propane over VO-H-beta and  $\text{Mo}_1\text{V}_{0.3}\text{Te}_{0.23}\text{Nb}_{0.12}\text{O}_x$  are investigated. Two methods are used in this study: (i) overall product selectivities are recorded as a function of conversion and (ii) those species observed or speculated to exist are reacted individually over the catalysts. With VO-H-beta, propylene is the primary product of propane oxidation and acetic acid is a sequential oxidation product of the propylene, possibly forming through an acetone intermediate.  $\text{Mo}_1\text{V}_{0.3}\text{Te}_{0.23}\text{Nb}_{0.12}\text{O}_x$  also gives propylene as the primary product of propane oxidation, and the propylene thus formed oxidizes further to acrylic acid and acetone. Reactions of individual oxygenate compounds, e.g., propanal, acrolein, etc., confirm the superior oxidation features of the mixed metal oxide catalyst relative to the zeolite-based catalyst.

*Key words:* propane oxidation; vanadium-containing zeolites; Mo-V-Te-Nb-oxide catalyst; reaction pathway.

## 4.1 INTRODUCTION

Traditional industrial production of oxygenates, such as acids, alcohols and unsaturated nitriles, is achieved by oxidation of olefins.<sup>1</sup> A potentially less costly alternative to the use of olefins is the direct transformations of light alkanes into oxygenates through a partial oxidation process. The main challenge for partial oxidation is that light alkanes are usually less reactive compared to the desired products, and further oxidation to total oxidation products,  $\text{CO}_x$ , is thermodynamically favored. Despite this thermodynamical limitation, research on partial oxidation has yielded several successful processes that involve the partial oxidation of light alkanes, e.g., partial oxidation of n-butane to maleic anhydride by  $\text{VPO}$ <sup>2</sup> and ammoxidation of propane to acrylonitrile using  $\text{V-Al-Sb-O}$ .<sup>3</sup>

Various catalyst systems have been studied for the partial oxidation of light alkanes including bulk mixed metal oxides,<sup>4-11</sup> heteropolyacids,<sup>12-14</sup> and molecular sieves.<sup>15-19</sup> Zeolite-based catalysts have been investigated for the partial oxidation of propane and were found to be suitable matrices for isolating transition metals.<sup>15,18</sup> Moreover, the uniform pore structure of zeolite can be used as a host for stabilizing small metal oxide clusters.<sup>20-24</sup> During initial oxidation studies with zeolite-based catalysts, we found that vanadyl ion-exchanged zeolite beta (VO-H-beta) produced a considerable amount of acetic acid when reacting propane with oxygen. It appeared possible that more valuable oxygenates, e.g., acrylic acid, were produced and overoxidized to  $\text{CO}_x$ , since feeding acrylic acid into this reaction system results in complete oxidation of the acid to  $\text{CO}_x$  at 350°C, and some acetic acid at lower reaction temperatures. These findings

motivated us to study the reaction pathways for propane oxidation over VO-H-beta. For comparison, we also report reaction pathways of propane partial oxidation over a “Mitsubishi type” catalyst,  $\text{Mo}_1\text{V}_{0.3}\text{Te}_{0.23}\text{Nb}_{0.12}\text{O}_x$ , one of the best catalysts for propane partial oxidation to acrylic acid.<sup>25</sup>

## 4.2 EXPERIMENTAL SECTION

### 4.2.1 Catalysts Preparation

The starting materials used for the preparation of vanadyl ion-exchanged zeolite beta (VO-H-beta) were Na-zeolite beta (PQ Corp, Si/Al=12),  $\text{NH}_4\text{NO}_3$  (Aldrich) and  $\text{VOSO}_4$  (Aldrich). VO-H-beta was synthesized in three steps as follows: (1) Na-zeolite beta was ion-exchanged with 1 M  $\text{NH}_4\text{NO}_3$  solution (50 mL  $\text{NH}_4\text{NO}_3$  solution/1 g zeolite) overnight at 80°C three times, and the resulting  $\text{NH}_4$ -beta was washed with double distilled water, filtered, and dried overnight in an 80°C oven; (2) H-beta was formed by calcination of  $\text{NH}_4$ -beta at 500°C for 4 hours in  $\text{N}_2$ ; (3) VO-H-beta was prepared by ion-exchange of H-beta with 0.1 M  $\text{VOSO}_4$  solution (50 mL  $\text{VOSO}_4$  solution/1 g zeolite) for 10 hours at 60°C twice,<sup>26</sup> and the resulting mixture was washed with double distilled water, filtered, and dried overnight in an 80°C oven. The composition of the VO-H-beta sample is Si:Al:V=25.2:1:0.61 giving 1.66 wt.%V (the elemental analysis of VO-H-beta was done by Galbraith Laboratories, Inc.).

$\text{Mo}_1\text{V}_{0.3}\text{Te}_{0.23}\text{Nb}_{0.12}\text{O}_x$  was synthesized according to a Mitsubishi patent<sup>25</sup> and provided to us by BP Amoco. The XRD pattern of this catalyst is in good agreement with that described in the patent.<sup>25</sup>

#### 4.2.2 Catalytic Reactions

The catalytic reactions were carried out using a continuous flow system (BTRS-Jr., Autoclave Engineers) with a fixed bed stainless steel reactor. Before a reaction, the catalyst samples were pelletized and sieved to -35/+60 mesh size. A mixture of 0.5 mL catalyst (0.20 g VO-H-beta, or 0.70 g  $\text{Mo}_1\text{V}_{0.3}\text{Te}_{0.23}\text{Nb}_{0.12}\text{O}_x$ ) and 1 mL silicon carbide was used for each run. Catalysts were pretreated at 350°C for one hour in a He flow. The reactions were carried out at temperatures from 250°C to 450°C under atmospheric pressure with a reactant molar ratio of propane: oxygen:  $\text{H}_2\text{O}$ : helium = 4:2:4:5 and a total flow of 15 mL/min.

Propane oxidation over  $\text{Mo}_1\text{V}_{0.3}\text{Te}_{0.23}\text{Nb}_{0.12}\text{O}_x$  was also conducted under conditions more similar to those of Example One in the Mitsubishi patent.<sup>25</sup> 1.75 g  $\text{Mo}_1\text{V}_{0.3}\text{Te}_{0.23}\text{Nb}_{0.12}\text{O}_x$  together with 2.5 mL SiC were used for the reaction with a feed molar ratio of propane:  $\text{O}_2$ : He = 1:3.15:11.85 and a total flow rate of 36.2 mL/min (space velocity of 1,734  $\text{hour}^{-1}$  with a catalyst density of 1.4  $\text{g}/\text{cm}^3$ ); in the Mitsubishi Patent,<sup>25</sup> the amount of catalyst used was 0.37 g and the feed gas molar ratio was propane: air = 1:15 with a space velocity of 1,734  $\text{hour}^{-1}$ .

Product analysis was performed using a gas chromatograph (Hewlett Packard G1800A GCD System) equipped with an electron ionization detector and a capillary column (Hewlett Packard, HP Plot-Q). Gaseous products were analyzed using online sampling, while liquid products were collected in an ice trap and analyzed separately.

The conversion was defined as the fraction of consumed hydrocarbon of the moles of hydrocarbon fed to the reaction. Selectivities are the fractions of consumed

hydrocarbon converted for each product. The contact times provided are the ratios of the catalyst volumes to the total flow rates of gaseous feeds.

#### 4.2.3 Reaction Pathway Study

The reaction pathways were first studied by following the trends in product selectivities with respect to the reactant conversion. Both propane oxidation and propylene oxidation were employed in this investigation. An amount of 0.20 g (0.5 mL) VO-H-beta with 1.0 mL SiC were used for this study, while only 17.5 mg to 105 mg  $\text{Mo}_1\text{V}_{0.3}\text{Te}_{0.23}\text{Nb}_{0.12}\text{O}_x$  with 0.5 mL SiC were employed in order to keep the conversion of reactants low. The temperature was set to 350°C and molar feed gas ratio was propane (or propylene): $\text{O}_2$ : $\text{H}_2\text{O}$ :He = 4:2:4:5. The contact time was varied to reach different conversion levels.

The reaction pathways were also studied by feeding oxygenates that are possible intermediates in the propane oxidation pathway to the reactor. These reactions were conducted at lower temperatures (250°C or lower), since most of the oxygenates investigated here are highly reactive. 0.20 g VO-H-beta (0.5 mL) or 0.35 g  $\text{Mo}_1\text{V}_{0.3}\text{Te}_{0.23}\text{Nb}_{0.12}\text{O}_x$  (0.25 mL) were used for this study with a pretreatment at 350°C for one hour in He. For water-soluble oxygenates, the reactant input ratio used was oxygenate (10 mol% aqueous solution):  $\text{O}_2$ : He = 4:2:9. For water-insoluble oxygenates, the reactant input ratio was oxygenate (pure):  $\text{O}_2$ : He = 0.4:2:12.6. The contact time was varied between 0.25 s to 4 s.

## 4.3 RESULTS AND DISCUSSION

### 4.3.1 Partial Oxidation of Propane

#### 4.3.1.1 Propane Partial Oxidation Reaction Over VO-H-beta

The reaction products from propane oxidation over VO-H-beta were acetic acid, propylene, CO, CO<sub>2</sub>, and trace amounts of ethylene. At 350°C, the conversion of propane was 1.6%, the selectivity to acetic acid 21.1%, and the selectivity to propylene 20.9%. As the temperature was increased to 400°C, the conversion of propane increased to 4.3% and the selectivity to acetic acid decreased to 14%. The specific values of conversion and selectivity are summarized in Table 4.1.

The reactivity for propane oxidation over VO-H-beta is not high under the conditions investigated. The turnover frequency per vanadium atom (TOF) of propane consumption is  $7.4 \times 10^{-4} \text{ s}^{-1}$  for VO-H-beta at 350°C. Assuming an activation energy of 100 kJ/mole and first-order dependence on propane concentration, these data extrapolate to a propane consumption rate of  $2.3 \times 10^{-4} \text{ s}^{-1}$  at 333°C. This rate is comparable to results of previous studies on isolated monovanadate species by Khodakov and co-workers.<sup>27</sup>

#### 4.3.1.2 Propane Partial Oxidation Reaction over Mo<sub>1</sub>V<sub>0.3</sub>Te<sub>0.23</sub>Nb<sub>0.12</sub>O<sub>x</sub>

Mo<sub>1</sub>V<sub>0.3</sub>Te<sub>0.23</sub>Nb<sub>0.12</sub>O<sub>x</sub> is one of the best catalysts reported for the partial oxidation of propane to acrylic acid. The reaction results obtained here with Mo<sub>1</sub>V<sub>0.3</sub>Te<sub>0.23</sub>Nb<sub>0.12</sub>O<sub>x</sub> are compared to those reported in the patent literature in Table 4.2. The major products observed with the reaction conditions used in the patent are acrylic acid and CO<sub>x</sub>. At oxygen rich conditions like those reported in the patent literature, the conversion of propane was 58.3% and the selectivity to acrylic acid 39.2% at 400°C. This selectivity is

close to the results reported by Mitsubishi (propane conversion 75.3% and acrylic acid selectivity of 42.4%).<sup>25</sup>

The propane oxidation reaction was also performed in the presence of water with  $\text{Mo}_1\text{V}_{0.3}\text{Te}_{0.23}\text{Nb}_{0.12}\text{O}_x$  under reaction conditions similar to those used with VO-H-beta. At 350°C, the conversion of propane reached 27.2% and the selectivity to acrylic acid was 64.7%. Additionally, propane could be activated even at temperatures as low as 250°C (Table 4.2).

### 4.3.2 Reaction Pathways: Trends in Product Selectivities

The reaction pathways of propane oxidation over VO-H-beta and  $\text{Mo}_1\text{V}_{0.3}\text{Te}_{0.23}\text{Nb}_{0.12}\text{O}_x$  were first examined by analyzing product selectivities as a function of propane conversion, and the oxidation behavior of propylene at low conversions.

#### 4.3.2.1 Reaction Pathways for Propane Oxidation over VO-H-beta

The detected products from propane oxidation over VO-H-beta are propylene, acetic acid,  $\text{CO}_x$ , and trace amounts of acetone (less than 0.5% selectivity). At very low (<1%) propane conversion, the main product is propylene. With an increase in the conversion, the selectivity to propylene decreases while the selectivity to acetic acid increases (Fig. 4.1). In general, primary products of a given reaction can be discriminated from higher-order products by extrapolating product selectivities to zero conversion. Primary products have non-zero intercepts, while secondary and higher-order products have zero intercepts.<sup>5</sup> For the case of propane oxidation over VO-H-beta, the data (Fig. 4.1) do not conclusively distinguish between zero or very low selectivities

to acetic acid and  $\text{CO}_x$  at low conversion; however, it is clear that the dominant primary product is propylene, and the main routes to acetic acid and  $\text{CO}_x$  involve secondary oxidation of propylene.

Propylene oxidation over VO-H-beta was investigated in order to gain further insights into the formation of acetic acid. At 350°C, the main products are  $\text{CO}_x$ , acetic acid and acetone (Fig. 4.2).  $\text{CO}_x$  are the major products of propylene oxidation, with extrapolated selectivities to acetic acid and acetone of around 22% and 13%, respectively. At temperatures lower than 250°C, 2-propanol is the major product (Table 4.3). For example, the selectivity to 2-propanol is 88.3% at a propane conversion of 0.4% at 150°C. As the temperature is increased from 150°C to 350°C, the selectivity to 2-propanol decreases monotonically to zero, the selectivity to acetone first increases to a maximum (6.7% selectivity) and decreases thereafter, and the selectivity to acetic acid increases to 19.6% at a propylene conversion of 4.7%. Moro-oka and co-workers suggest that olefin oxidation over acidic metal oxides occurs through an oxyhydration mechanism in which olefins are first hydrated to corresponding alcohols on acid sites and then oxidatively dehydrogenated to form ketones.<sup>28</sup> The observations for propylene oxidation over VO-H-beta are consistent with this oxyhydration reaction pathway. A study of the oxidation of acetone (Section 3.3.1) indicates that acetic acid is a major product from acetone. Although no direct relationship between acetic acid and acetone is demonstrated from the data shown in Fig. 4.2, we suggest that acetone is an intermediate for the formation of acetic acid. Since the selectivity to acetone declines steeply with increasing contact time at 350°C (Fig. 4.2), some formation of  $\text{CO}_x$  directly from acetone is also possible.

Oxygenates other than acetic acid and acetone, such as acetaldehyde, propanal, propanoic acid, acrolein and traces of oligomer products, are observed from propylene oxidation. The selectivities to these oxygenates are very low, generally below 2% under the reaction conditions used here. Thus, the formation of acetic acid from these oxygenates is not likely important.

The results from the oxidation of both propane and propylene suggest that the reaction pathway for propane oxidation over VO-H-beta is that shown in Scheme 4.1. Propylene is the primary product of propane oxidation, and acetic acid is mainly produced by sequential oxidation of propylene, possibly through acetone. Intermediate oxygenates, such as acetone, can only survive at very low conversion. CO and CO<sub>2</sub> are major products of propylene oxidation.

#### 4.3.2.2 Reaction Pathways for Propane Oxidation over Mo<sub>1</sub>V<sub>0.3</sub>Te<sub>0.23</sub>Nb<sub>0.12</sub>O<sub>x</sub>

The products from the oxidation of propane in the presence of water over Mo<sub>1</sub>V<sub>0.3</sub>Te<sub>0.23</sub>Nb<sub>0.12</sub>O<sub>x</sub> at 350°C are acrylic acid, propylene, acetic acid, CO<sub>x</sub>, and small amounts of acetone and propanoic acid. The selectivity to propylene decreases while the selectivity of acrylic acid increases with increasing propane conversion (Fig. 4.3). For example, as propane conversion increases from 2.1% to 12.9%, the selectivity to propylene decreases from 73.4% to 20.9%, and the selectivity to acrylic acid increases from 22.1% to 60.0%. When extrapolating to zero propane conversion, the selectivity to propylene is 100% and the selectivities to other products are zero. Thus, propylene is the primary product of propane oxidation; acrylic acid and other oxygenates (acetic acid, trace amount of acetone and propanoic acid) are secondary or higher-order products. The rate of propane consumption at 350°C with C<sub>3</sub>H<sub>8</sub>:O<sub>2</sub>:H<sub>2</sub>O:He =4:2:4:5 at low conversions

is  $1.23 \times 10^{-4}$  mol/(gcat·min) and is approximately an order of magnitude higher than for VAPO-5 at the same conditions ( $1.9 \times 10^{-5}$  mol/(gcat·min)).

Propylene oxidation was also carried out over  $\text{Mo}_1\text{V}_{0.3}\text{Te}_{0.23}\text{Nb}_{0.12}\text{O}_x$  at 350°C to study the reaction pathways in going from propylene to oxygenates (since propylene is the only primary product of propane oxidation). The major products detected are acetone and acrylic acid. Smaller amounts of acrolein, acetic acid, propanoic acid, and  $\text{CO}_x$  are also observed (Fig. 4.4). The selectivities to acetone and acrylic acid do not vary significantly with propylene conversion. Upon extrapolating to zero propylene conversion, the selectivities to acrylic acid and acetone are 67% and 18%, respectively. The other compounds have small but non-zero selectivity at zero propylene conversion. Thus, it is reasonable to conclude that two major routes exist for propylene oxidation over  $\text{Mo}_1\text{V}_{0.3}\text{Te}_{0.23}\text{Nb}_{0.12}\text{O}_x$ : (1) propylene is oxidized to acrylic acid; (2) propylene is oxidized to acetone.

By combining the propylene and propane oxidation data, the main reaction pathways for propane oxidation are proposed in Scheme 4.2: propane is first oxidized to propylene which is then oxidized to acetone and acrylic acid.

It is interesting to note the differences in selectivities to acetone for propane and propylene oxidation. The selectivity to acetone is very low (<2% under all conditions tested) in the former case, while it is high (~19%) in the latter case. In a separate experiment, propane and propylene were simultaneously fed to the reactor at ratios varying from 0 to 0.75 ( $\text{C}_3\text{H}_8/\text{C}_3\text{H}_6$ ). The selectivity to acetone did not vary with the introduction of propane. Additionally, the rate of consumption for pure propane for low conversions at 350°C with  $\text{C}_3\text{H}_8:\text{O}_2:\text{H}_2\text{O}:\text{He}$  of 4:2:4:5 is approximately an order of

magnitude lower than the propylene consumption rate ( $C_3H_6:O_2:H_2O:He = 4:2:4:5$ ). These data suggest the presence of two different sites on  $Mo_1V_{0.3}Te_{0.23}Nb_{0.12}O_x$ ; one site is able to activate propane and propylene to acrylic acid, while the other converts only propylene to acetone.

### 4.3.3 Reaction Pathway Method II: Oxidation of Possible Oxygenates

#### 4.3.3.1 Oxidation of Individual Possible Intermediates

The oxidation of oxygenated species that are possibly involved in the propane oxidation reaction were investigated over VO-H-beta and  $Mo_1V_{0.3}Te_{0.23}Nb_{0.12}O_x$ . The oxygenated species chosen are those observed in the reaction results presented above. Acetic acid and trace amounts of acetone are observed in the propane oxidation over VO-H-beta (Table 4.1), while acrylic acid, acetic acid, acetone, and trace amounts of propanoic acid are obtained from propane oxidation over  $Mo_1V_{0.3}Te_{0.23}Nb_{0.12}O_x$  (Table 4.2). 2-Propanol is observed from propylene oxidation over VO-H-beta at temperatures under 250°C, and small amounts of propanal and acrolein are observed from propylene oxidation over  $Mo_1V_{0.3}Te_{0.23}Nb_{0.12}O_x$ . These compounds may also be involved in propane oxidation; however, they appear to be too reactive or in too low concentration to be detected under our reaction conditions. The detection of propanal and propanoic acid may indicate the presence of 1-propanol as an intermediate species. Hence, individual transformations of 2-propanol, 1-propanol, propanal, acrolein, acetone, acrylic acid, and acetic acid over VO-H-beta and  $Mo_1V_{0.3}Te_{0.23}Nb_{0.12}O_x$  were investigated.

### 2-propanol

Almost all the 2-propanol fed is consumed over both catalysts (> 99.5% conversion) at 250°C; however, the product distributions are quite different for these two catalysts. With VO-H-beta, the dehydration product, propylene, is dominant (more than 90% selectivity at contact time 2 s) at 250°C. Only small amounts of acetone, acetic acid, and CO<sub>x</sub> are observed at this temperature (Fig. 4.5). At 150°C, the product distribution is similar to that at 250°C, with the addition of the condensation product, diisopropyl ether.

For Mo<sub>1</sub>V<sub>0.3</sub>Te<sub>0.23</sub>Nb<sub>0.12</sub>O<sub>x</sub>, the major products are acetone, acrylic acid, propylene and acetic acid at 250°C (Fig. 4.5). At a contact time of 2 s, the selectivity to propylene is 11%, while the selectivities to acetone and acrylic acid are 41% and 25%, respectively. At 150°C, acetone and propylene are the major products with selectivities of 66% and 21%, respectively, at 50% 2-propanol conversion. No acrylic acid is observed at 150°C.

### 1-propanol

Similar to the case of 2-propanol, 1-propanol is almost completely consumed over both catalysts at 250°C (> 99.5% conversion) (Fig. 4.6). For VO-H-beta, the dehydration product, propylene, is the dominant product (selectivity higher than 95% under our test conditions). Small amounts of propanal are observed with a selectivity of 0.8% at 2 s contact time. Additionally, there are trace amounts of other products, such as acetone, acetic acid and acetaldehyde. These products each have selectivities less than 0.5% and may result from the oxidation of propylene. At 150°C, ether formation from intermolecular dehydration is the major product from 1-propanol.

For Mo<sub>1</sub>V<sub>0.3</sub>Te<sub>0.23</sub>Nb<sub>0.12</sub>O<sub>x</sub>, the dominant product is propanoic acid with a selectivity of 79.0% at 250°C (contact time of 2 s). Only small amounts of propylene are

observed (selectivity of 1.8%). No propanal is obtained at 250°C, while a large amount of propanal (selectivity of 38.7% at a conversion of 20.6%) is produced at 150°C. Thus, it is reasonable to consider propanal as an oxidation product of 1-propanol, and propanoic acid as a further oxidation product of propanal.

### Propanal

The detected products of propanal oxidation over VO-H-beta are propanoic acid, acetic acid, acetaldehyde, and large amounts of CO<sub>x</sub> (Fig. 4.7). The selectivity to propanoic acid is 19.5% (contact time 2 s and 250°C) at 60% conversion. The formation of propanoic acid from propanal indicates that VO-H-beta has oxidation capability for terminal HC=O. However, total oxidation products are dominant in propanal oxidation over this catalyst under the conditions tested here (selectivity to CO<sub>x</sub> is 54%).

High selectivity to propanoic acid and little CO<sub>x</sub> are observed for propanal oxidation over Mo<sub>1</sub>V<sub>0.3</sub>Te<sub>0.23</sub>Nb<sub>0.12</sub>O<sub>x</sub>. Even at complete consumption of propanal, the selectivity to propanoic acid at 250°C is 58% at a contact time of 2 s and 79% at a contact time of 1 s. At 150°C and a contact time of 1 s, the selectivity to propanoic acid increases to 91% with a propanal conversion of 44%.

### Acrolein

When acrolein is oxidized over VO-H-beta, only small amounts of acrylic acid (3.1% selectivity at a conversion of 7.8%) are observed at 250°C (contact time 2 s) and total oxidation products are dominant (Fig. 4.8). These results suggest that the oxidation of the double bond of acrolein is easier than the oxidation of HC=O at the allylic position.

Acrolein is very reactive over Mo<sub>1</sub>V<sub>0.3</sub>Te<sub>0.23</sub>Nb<sub>0.12</sub>O<sub>x</sub> and acrylic acid is the dominant product at 250°C (Fig. 4.8). When the contact time is 2 s, the conversion of

acrolein is 92% and the selectivity to acrylic acid is 94%. Thus, the double bond of acrolein is preserved. These results indicate that  $\text{Mo}_1\text{V}_{0.3}\text{Te}_{0.23}\text{Nb}_{0.12}\text{O}_x$  has superior allylic oxidation character.

Since acrylic acid is the dominant product of acrolein oxidation with  $\text{Mo}_1\text{V}_{0.3}\text{Te}_{0.23}\text{Nb}_{0.12}\text{O}_x$  and the oxidation of propylene yields a selectivity to acrolein that decreases significantly with increasing conversion of propylene (Fig. 4.4), it is likely that acrolein is an intermediate in the oxidation of propylene to acrylic acid.

### Acetone

The products of acetone oxidation over VO-H-beta are  $\text{CO}_x$ , acetic acid, and isobutene (Fig. 4.9). The selectivity to isobutene is 28% at 250°C at 20% conversion. The formation of isobutene is catalyzed by the acidity of VO-H-beta. The acetone conversion to isobutene can take place via acid-catalyzed aldolization and dehydration with subsequent cracking.<sup>29-31</sup> For the  $\text{Mo}_1\text{V}_{0.3}\text{Te}_{0.23}\text{Nb}_{0.12}\text{O}_x$  catalyst, acetic acid and  $\text{CO}_x$  are the only products formed, and no isobutene is observed. This suggests that  $\text{Mo}_1\text{V}_{0.3}\text{Te}_{0.23}\text{Nb}_{0.12}\text{O}_x$  has a lower acidity than VO-H-beta.

To confirm that acetic acid results from C-C(=O) cracking of acetone, the oxidation of 3-pentanone was performed over VO-H-beta and  $\text{Mo}_1\text{V}_{0.3}\text{Te}_{0.23}\text{Nb}_{0.12}\text{O}_x$ . As expected, propanoic acid, acetic acid, and acetaldehyde are the major oxidation products for both catalysts.

### Acids

Compared to alcohols and aldehydes, acrylic acid and acetic acid are very stable at 250°C over both VO-H-beta and  $\text{Mo}_1\text{V}_{0.3}\text{Te}_{0.23}\text{Nb}_{0.12}\text{O}_x$  catalysts. The conversions of acrylic acid over both VO-H-beta and  $\text{Mo}_1\text{V}_{0.3}\text{Te}_{0.23}\text{Nb}_{0.12}\text{O}_x$  are less than 6.5% at a

contact time of 2 s. However, much more total oxidation products are formed with VO-H-beta. The conversions of acetic acid over both VO-H-beta and  $\text{Mo}_1\text{V}_{0.3}\text{Te}_{0.23}\text{Nb}_{0.12}\text{O}_x$  are less than 5% at a contact time of 2 s and  $\text{CO}_x$  are the only products.

#### 4.3.3.2 Reaction Network and Catalytic Behavior of Propane Oxidation over $\text{Mo}_1\text{V}_{0.3}\text{Te}_{0.23}\text{Nb}_{0.12}\text{O}_x$

The exact reaction pathway of propane oxidation may vary from one catalyst to another. Broadly speaking, three major reaction routes are possible starting from propane (Scheme 4.3).<sup>32</sup> In the first route, propane is oxidized to 1-propanol, then to propanal and finally to propanoic acid. In the second route, propane forms propylene by oxidative dehydrogenation, that is oxidized to allyl alcohol, acrolein, and acrylic acid. In the third route, propane is oxidized to 2-propanol, and 2-propanol is oxidized to acetone and acetic acid. This reaction network may be further complicated by transformations between intermediates of different routes.

Based on the study of individual oxygenates (Section 3.3.1) and the trends in product selectivities as a function of conversion (Section 3.2), the reaction pathway described by route II (Scheme 4.3) is favored over routes III and I for propane oxidation over  $\text{Mo}_1\text{V}_{0.3}\text{Te}_{0.23}\text{Nb}_{0.12}\text{O}_x$ . A more detailed reaction network is shown in Scheme 4.4. Propane is first dehydrogenated to propylene and most of the formed propylene reacts further to acrolein and acrylic acid through allylic oxidation. Allyl alcohol may be an intermediate in the reaction of propylene to acrolein. Allyl alcohol injected to our GC system is completely converted to acrolein at temperatures under 200°C. Therefore, the collected liquid products were analyzed by  $^1\text{H}$  and  $^{13}\text{C}$  NMR. No evidence for allyl alcohol was obtained, suggesting that allyl alcohol, if formed, is too reactive to be

detected under our reaction conditions. A small amount of propylene is hydrated to 2-propanol and then oxidized to acetone. Trace amounts of observed propanal and propanoic acid may be from the oxidation of 1-propanol as shown in Section 3.3.1. However, since 1-propanol is not observed from propane and propylene oxidation, it is not clear whether the formation of propanal and propanoic acid is from oxidation of 1-propanol or from some other reaction pathway such as isomerization of allyl alcohol.<sup>33</sup>

The transformation of propane to acrylic acid requires two major oxidation steps: terminal oxygenation and dehydrogenation. As shown above, propylene is the primary product of propane oxidation. Acrylic acid is a dominant product when either propylene or acrolein is used as reactants, while no acrylic acid is produced when propanal is employed. These results suggest that the oxidation of propane to acrylic acid must first go through a dehydrogenation prior to terminal oxygenation, but not vice versa.

The formation of acrylic acid is favored at high temperatures, while the formation of acetone is observed at low temperatures. The allylic oxidation of propylene to acrylic acid over  $\text{Mo}_1\text{V}_{0.3}\text{Te}_{0.23}\text{Nb}_{0.12}\text{O}_x$  is found to occur at temperatures higher than 150°C; only trace amounts of acrylic acid are observed at 150°C where acetone is the major product. As the temperature is raised, the selectivity to acrylic acid increases, the selectivity to acetone decreases, and acrylic acid becomes the major product by 300°C. This trend also occurs for the oxidation of 2-propanol. When 2-propanol is injected to the reaction feed stream at 150°C, no acrylic acid is observed at all, while large amounts of acetone and propylene are formed. As the temperature is increased to 200°C and higher, acrylic acid is formed.

#### 4.3.3.3 Reaction Network and Catalytic Behavior of Propane Oxidation over VO-H-beta

The results of the oxidation of individual oxygenates over VO-H-beta (Section 3.3.1) are consistent with the reaction network for propane oxidation proposed in Scheme 4.1. Propane is first dehydrogenated to propylene and acetic acid is a further oxidation product of the propylene. Since acetic acid is one of the major products from oxidation of acetone, acetone could be an intermediate for the formation of acetic acid. Total oxidation products,  $\text{CO}_x$ , are the major direct products of propylene oxidation. No acrolein or acrylic acid is produced from propane oxidation over VO-H-beta. Scheme 4.5 shows the details of the reaction network proposed here.

The results from reacting individual oxygenates over VO-H-beta indicate that acidity plays a major role in catalysis. Dehydration is an important step over VO-H-beta when 1-propanol and 2-propanol are the reactants. This leads to high selectivity for propylene through intramolecular dehydration and formation of ether through intermolecular dehydration at lower temperature ( $150^\circ\text{C}$ ). The acidity also plays a critical role in the formation of isobutene from the oxidation of acetone over VO-H-beta. Large amounts of  $\text{CO}_x$  are observed in the oxidation of propanal and acrolein over VO-H-beta, with relatively little of their expected partial oxidation products, propanoic acid and acrylic acid, respectively.

#### 4.3.4 Comparison of Catalytic Behavior of Propane Oxidation over VO-H-beta and $\text{Mo}_1\text{V}_{0.3}\text{Te}_{0.23}\text{Nb}_{0.12}\text{O}_x$

By investigating the reactivity of individual oxygenates over VO-H-beta and  $\text{Mo}_1\text{V}_{0.3}\text{Te}_{0.23}\text{Nb}_{0.12}\text{O}_x$ , it is found that the main differences between these two catalysts are their acidity, capability for allylic oxidation, and the extent of total oxidation. As stated above, VO-H-beta has a much higher acidity than  $\text{Mo}_1\text{V}_{0.3}\text{Te}_{0.23}\text{Nb}_{0.12}\text{O}_x$ . Most reactions over VO-H-beta are acid-driven, while for  $\text{Mo}_1\text{V}_{0.3}\text{Te}_{0.23}\text{Nb}_{0.12}\text{O}_x$  oxidation is more important. Comparing 2-propanol and 1-propanol oxidation over VO-H-beta and  $\text{Mo}_1\text{V}_{0.3}\text{Te}_{0.23}\text{Nb}_{0.12}\text{O}_x$ , the dehydration products are almost the only products formed over VO-H-beta, while oxidation products (acetone and acrylic acid for 2-propanol, and propanal and propanoic acid for 1-propanol) are dominant products over  $\text{Mo}_1\text{V}_{0.3}\text{Te}_{0.23}\text{Nb}_{0.12}\text{O}_x$ .

The allylic oxidation capability of VO-H-beta is poor compared to the excellent performance of  $\text{Mo}_1\text{V}_{0.3}\text{Te}_{0.23}\text{Nb}_{0.12}\text{O}_x$ . For VO-H-beta, no acrylic acid is observed from propylene oxidation and only small amounts of acrylic acid are formed from the oxidation of acrolein. As allylic oxidation is an important step in the oxidation of propane to acrylic acid, this function needs to be greatly enhanced for further improvement of VO-H-beta.

Total oxidation is more severe over the zeolite-based catalyst compared to the bulk oxide catalyst. Besides deep oxidation from propane and propylene, large amounts of  $\text{CO}_x$  are observed in the oxidation of individual oxygenates over VO-H-beta. This could be due to factors such as acidity, high surface area, and long diffusion time in

contact with the catalytic active sites resulting from the microporous structure of zeolites. The behavior of VO-H-beta in oxidation of propanal and acrolein is particularly notable. These reactions involve oxidations of relatively weak C-H bonds and hence should be relatively facile; yet both exhibit relatively low activity and give little of the expected products, the respective carboxylic acids, compared to  $\text{Mo}_1\text{V}_{0.3}\text{Te}_{0.23}\text{Nb}_{0.12}\text{O}_x$  (Figs. 4.7 & 4.8). In contrast, for other apparently more difficult oxidations (e.g., C-C bond cleavage of acetone, Fig. 4.9) the VO-H-beta catalyst is as active or more so than  $\text{Mo}_1\text{V}_{0.3}\text{Te}_{0.23}\text{Nb}_{0.12}\text{O}_x$ . Such substrate-specific behavior is obviously crucial in determining successful catalysts for complex reactions, such as oxidation of propane to acrylic acid, and presumably is intimately connected with the detailed active site structure. Understanding these connections will be a major challenge for future research in the field.

#### 4.4 CONCLUSION

By investigating the trends in product selectivities as a function of propane and propylene conversion and the transformation of individual oxygenates, propylene is found to be the primary product for propane oxidation over VO-H-beta, and acetic acid is a sequential oxidation product of the formed propylene possibly through an acetone intermediate. With  $\text{Mo}_1\text{V}_{0.3}\text{Te}_{0.23}\text{Nb}_{0.12}\text{O}_x$ , propylene is the primary product for propane oxidation and the propylene thus formed oxidizes further to acrylic acid and acetone. Reaction of individual oxygenates also reveals the superior partial oxidation features of the mixed metal oxide catalyst relative to the zeolite-based catalyst.

**ACKNOWLEDGEMENTS**

Financial support for this work was provided by BP Amoco. L. L. thanks Dr. Masaki

Okamoto for useful discussions.

#### 4.5 REFERENCE

- 1)Grasselli, R. K. *J. Chem. Edu.* **63**, 216-221 (1986).
- 2)Hodnett, B. K. *Catal. Rev. Sci. Eng.* **27**, 373-424 (1985).
- 3)Centi, G.; Grasselli, R. K.; Trifiro, F. *Catal. Today* **13**, 661-666 (1992).
- 4)Chaar, M. A.; Patel, C.; Kung, H. H. *J. Catal.* **109**, 463-467 (1988).
- 5)Michaels, J. N.; Stern, D. L.; Grasselli, R. K. *Catal. Lett.* **42**, 135-137 (1996).
- 6)Hardman, H. F., US Patent 4,255,284, 1981.
- 7)Mazzocchia, C.; Aboumradi, C.; Diagne, C.; Tempesti, E.; Herrmann, J. M.; Thomas, G. *Catal. Lett.* **10**, 181-191 (1991).
- 8)Ai, M. *Catal. Today* **42**, 297-301 (1998).
- 9)Kim, Y. C.; Ueda, W.; Moro-oka, Y. *Chem. Lett.* **12**, 2173-2176 (1989).
- 10)Kim, Y. C.; Ueda, W.; Moro-oka, Y. *J. Chem. Soc. Chem. Commun.* **10**, 652-653 (1989).
- 11)Bartek, J. P.; Ebner, A. M.; Brazdil, J. F. , US Patent 5,198,580, 1993.
- 12)Li, W.; Oshihara, K.; Ueda, W. *Appl. Catal. A-Gen.* **182**, 357-363 (1999).
- 13)Misono, M.; Mizuno, N.; K., I.; Koyano, G.; Lu, X. *Stud. Surf. Sci. Catal.* **110**, 35-42 (1997).
- 14)Moffat, J. B. *Appl. Catal. A-Gen.* **146**, 65-86 (1996).
- 15)Centi, G.; Trifiro, F. *Appl. Catal. A-Gen.* **143**, 3-16 (1996).
- 16)Concepcion, P.; Lopez Nieto, J. M.; Perez-Pariente, J. *Catal. Lett.* **19**, 333-337 (1993).
- 17)Blasco, T.; Concepcion, P.; Lopez Nieto, J. M.; Perez-Pariente, J. *J. Catal.* **152**, 1-17 (1995).

- 18) Okamoto, M.; Luo, L.; Labinger, J. A.; Davis, M. E. *J. Catal.* **192**, 128-136 (2000).
- 19) Salem, G. F.; Besecker, C. J.; Kenzig, S. M.; Kowlaski, W. J.; Cirjak, L. M., US Patent 5,306,858, 1994.
- 20) Hathaway, P. E.; Davis, M. E. *J. Catal.* **116**, 263-178 (1989).
- 21) Hathaway, P. E.; Davis, M. E. *J. Catal.* **116**, 279-284 (1989).
- 22) Tsuji, H.; Yagi, F.; Hattori, H.; Kita, H. *Proc. 10th Int. Congr. Catal.*, pp 1171. Elsevier, Amsterdam, 1992.
- 23) Brownscombe, T. F. , US Patent 5,053,372, 1991.
- 24) Yoo, J. S. *Catal. Today* **41**, 409-432 (1998).
- 25) Ushikubo, T.; Nakamura, H.; Koyasu, Y.; Wajiki, S., EP 0608838A2, 1994.
- 26) Komorek, J.; Romotowski, T.; Serwicka, E. M.; Mastikhin, V. M. *Zeolites* **14**, 629-634 (1994).
- 27) Khodakov, A.; Olthaf, B.; Bell, A. T.; Iglesia, E. *J. Catal.* **181**, 205-216 (1999).
- 28) Moro-oka, Y. *Appl. Catal. A-Gen.* **181**, 323-329 (1999).
- 29) Hutchings, G. J.; Johnson, P.; Lee, D. F.; Williams, C. D. *Catal. Lett.* **21**, 49-53 (1993).
- 30) Hutchings, G. J.; Johnston, P.; Lee, D. F.; Williams, C. D.; Wilkinson, M. *J. Catal.* **147**, 177-185 (1994).
- 31) Kubelkova, L.; Cejka, J.; Novakova, J.; Bosacek, V.; Jirka, I.; Jiru, P. *Stud. Surf. Sci. Catal.* **49**, 1203-1212 (1989).
- 32) Bettahar, M. M.; Costentin, G.; Savary, L.; Lavalley, J. C. *Appl. Catal. A-Gen.* **145**, 1-8 (1996).
- 33) Hoang-Van, C.; Zegaoui, O. *Appl. Catal. A-Gen.* **164**, 91-103 (1997).

**Table 4.1** Propane oxidation over VO-H-beta.

Temp. (°C)	Conv. (%)		Sel. (%)				
	C <sub>3</sub> H <sub>8</sub>	O <sub>2</sub>	C <sub>3</sub> H <sub>6</sub>	C <sub>2</sub> H <sub>4</sub>	acetic acid	CO	CO <sub>2</sub>
350	1.62	9.12	20.9	0	21.1	28.3	29.7
400	4.27	25.4	13.6	1.2	13.9	38.0	33.4
450	13.0	83.3	11.1	1.5	8.12	45.4	33.9

Reaction condition: 0.20 g catalyst, molar feed ratio propane: O<sub>2</sub>: H<sub>2</sub>O: He = 4:2:4:5, and 15 mL/min total flow rate.

**Table 4.2** Propane oxidation over  $\text{Mo}_1\text{V}_{0.3}\text{Te}_{0.23}\text{Nb}_{0.12}\text{O}_x$ .

Temp. (°C)	Conv.(%)		Sel. (%)						
	$\text{C}_3\text{H}_8$	$\text{O}_2$	$\text{C}_3\text{H}_6$	acetone	acetic acid	propanoic acid	acrylic acid	CO	$\text{CO}_2$
250 <sup>a</sup>	4.00	12.2	27.9	7.3	10.8	2.6	43.4	5.0	3.2
300 <sup>a</sup>	12.3	44.9	19.8	3.2	12.6	1.7	51.0	6.1	5.6
350 <sup>a</sup>	27.2	79.8	9.30	0.8	15.2	1.4	64.7	4.4	4.3
400 <sup>b</sup>	58.3	63.3	3.16	0.0	4.6	0.0	39.2	26.2	26.6
400 <sup>c</sup>	75.3						42.4		

a) Reaction condition: 0.70 g catalyst, molar feed ratio propane:  $\text{O}_2$ :  $\text{H}_2\text{O}$ : He = 4:2:4:5, and 15 mL/min total flow rate.

b) Reaction condition: 1.75 g catalyst, molar feed ratio propane:  $\text{O}_2$ : He = 1:3.15:11.85 and 36.2 mL/min total flow rate.

c) Results reported by Mitsubishi,<sup>25</sup> with 0.37 g catalyst, a molar feed ratio propane:air = 1:15 at a space velocity of 1,734  $\text{hr}^{-1}$ .

**Table 4.3** Propylene oxidation over VO-H-beta.

Temp. °C	Conv. (%)		Sel. (%)				
	C <sub>3</sub> H <sub>6</sub>	O <sub>2</sub>	2-propanol	acetone	acetic acid	CO	CO <sub>2</sub>
150	0.41	0.33	88.3	0.41	0	8.32	2.97
200	0.67	1.87	59.3	5.10	6.91	16.0	12.7
250	1.05	5.71	10.5	6.66	17.0	22.0	43.8
350	4.65	38.6	0	3.92	19.6	19.3	51.6

Reaction condition: 0.20 g catalyst, molar feed ratio propylene: O<sub>2</sub>: H<sub>2</sub>O: He = 4:2:4:5, and 15 mL/min total flow rate. Trace amounts of acetaldehyde and propanal were observed.

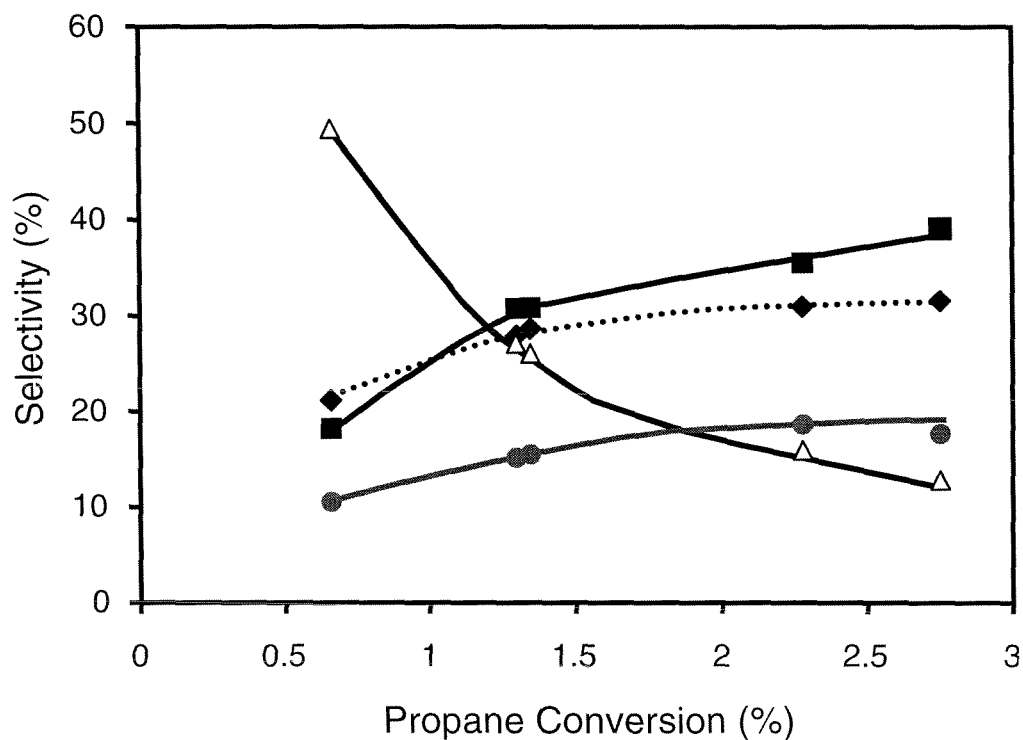


**Figure 4.1** Product selectivity profiles for propane oxidation over VO-H-beta. ( $\Delta$ ) propylene; ( $\bullet$ ) acetic acid; ( $\blacklozenge$ ) CO; ( $\blacksquare$ ) CO<sub>2</sub>. Reaction temperature was 350°C. The molar feed gas ratio was C<sub>3</sub>H<sub>8</sub>:O<sub>2</sub>:H<sub>2</sub>O:He = 4:2:4:5.

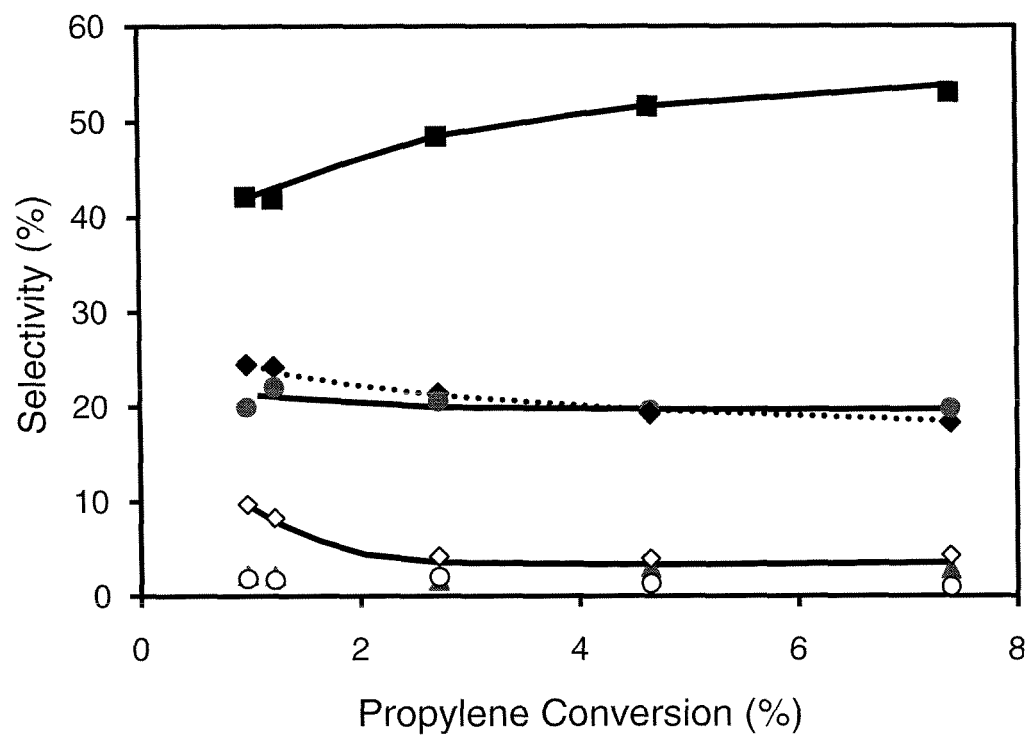


**Figure 4.2** Product selectivity profiles for propylene oxidation over VO-H-beta: (●) acetic acid; (▲) acetaldehyde; (◇) acetone; (○) propanal; (◆) CO; (■) CO<sub>2</sub>. Reaction temperature was 350°C. The molar feed gas ratio was C<sub>3</sub>H<sub>6</sub>:O<sub>2</sub>:H<sub>2</sub>O:He = 4:2:4:5.

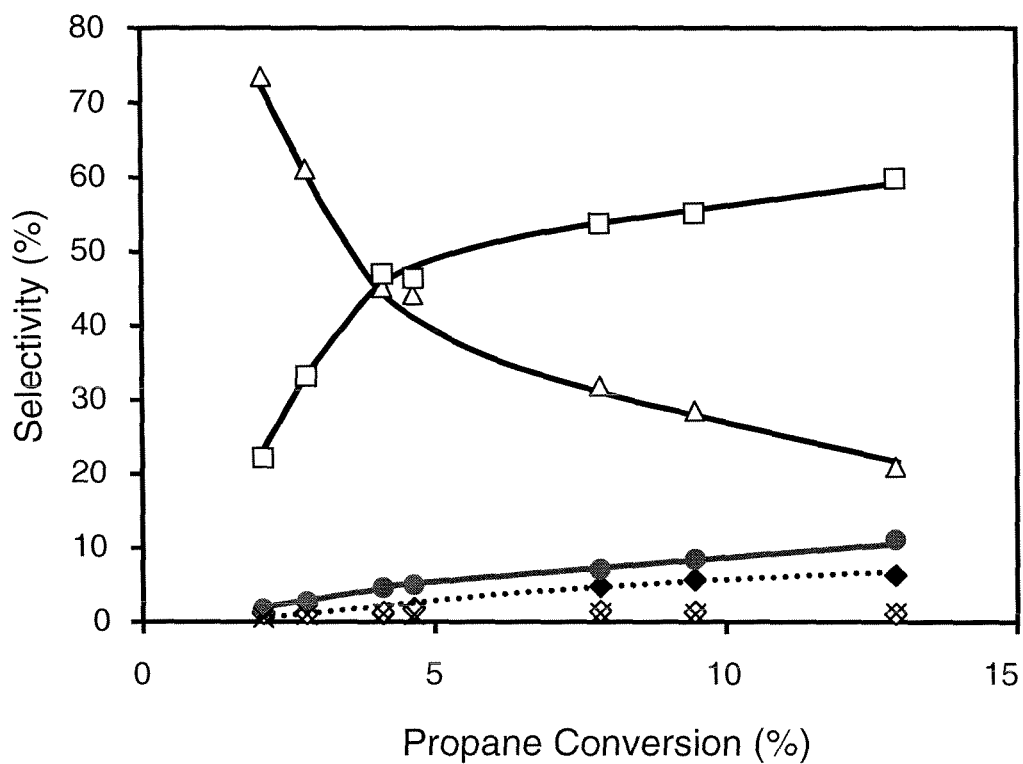


**Figure 4.3** Product selectivity profiles for propane oxidation over  $\text{Mo}_1\text{V}_{0.3}\text{Te}_{0.23}\text{Nb}_{0.12}\text{O}_x$ : ( $\Delta$ ) propylene; ( $\square$ ) acrylic acid; ( $\bullet$ ) acetic acid; ( $\diamond$ ) acetone; ( $\times$ ) propanoic acid; ( $\blacklozenge$ )  $\text{CO}_x$ . Reaction temperature was  $350^\circ\text{C}$ . The molar feed gas ratio was  $\text{C}_3\text{H}_8:\text{O}_2:\text{H}_2\text{O}:\text{He} = 4:2:4:5$ .

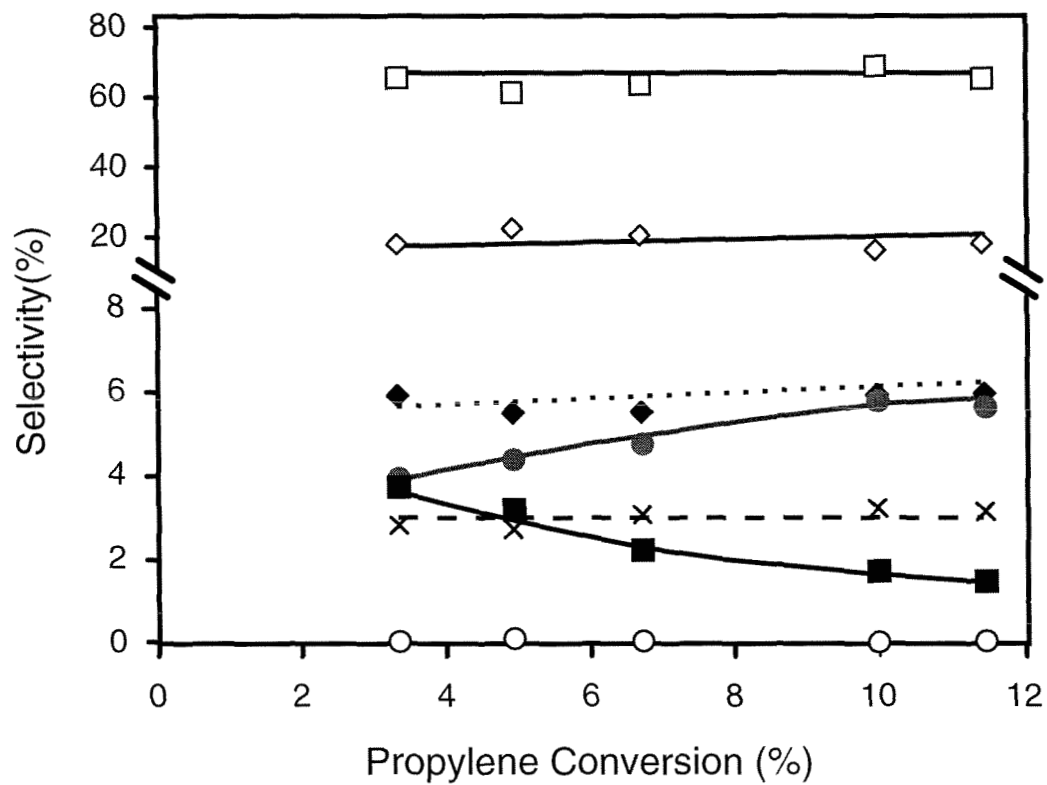


**Figure 4.4** Product selectivity profiles for propylene oxidation over  $\text{Mo}_1\text{V}_{0.3}\text{Te}_{0.23}\text{Nb}_{0.12}\text{O}_x$ : ( $\square$ ) acrylic acid; ( $\diamond$ ) acetone; ( $\blacksquare$ ) acrolein; ( $\times$ ) propanoic acid; ( $\circ$ ) propanal; ( $\bullet$ ) acetic acid; ( $\blacklozenge$ )  $\text{CO}_x$ . Reaction temperature was  $350^\circ\text{C}$ . The molar feed gas ratio was  $\text{C}_3\text{H}_6:\text{O}_2:\text{H}_2\text{O}:\text{He} = 4:2:4:5$ .

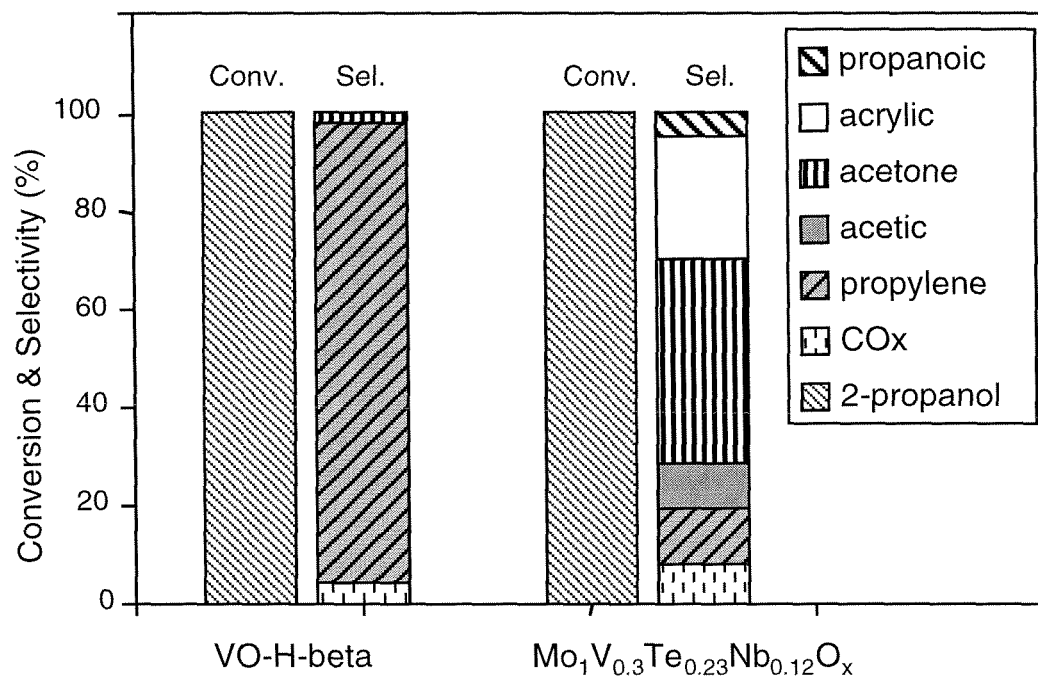


**Figure 4.5** Conversion and product distribution of 2-propanol oxidation over VO-H-beta and  $\text{Mo}_1\text{V}_{0.3}\text{Te}_{0.23}\text{Nb}_{0.12}\text{O}_x$  at 250°C and 2 s contact time with a molar feed gas ratio of 2-propanol:H<sub>2</sub>O:O<sub>2</sub>:He=0.4:3.6:2:9.

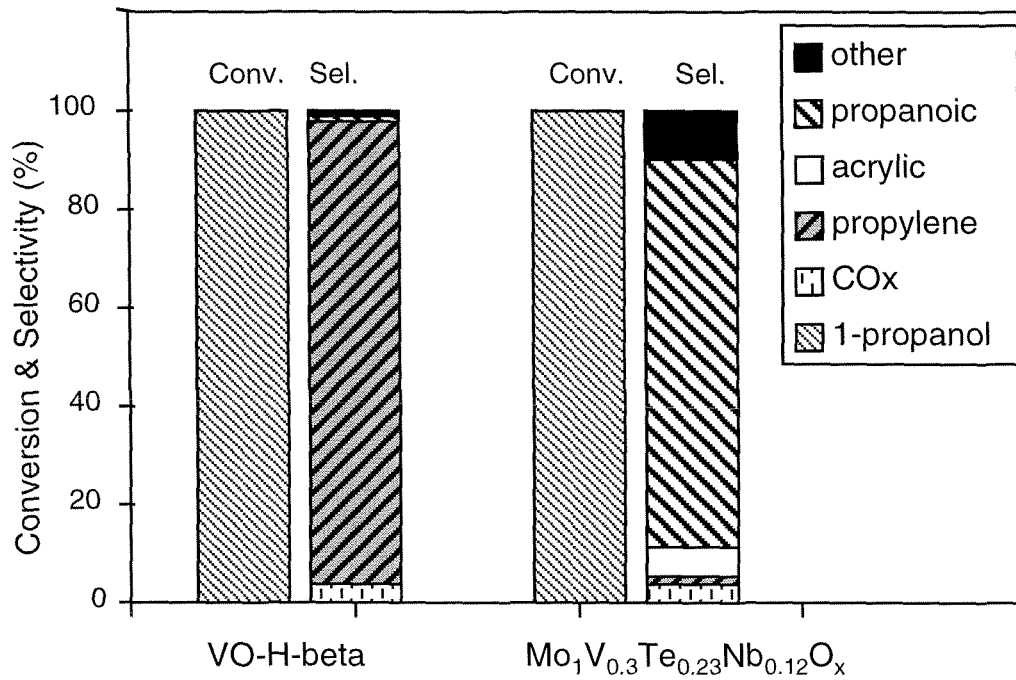


**Figure 4.6** Conversion and product distribution of 1-propanol oxidation over VO-H-beta and Mo<sub>1</sub>V<sub>0.3</sub>Te<sub>0.23</sub>Nb<sub>0.12</sub>O<sub>x</sub> at 250°C and 2 s contact time with a molar feed gas ratio of 1-propanol:H<sub>2</sub>O:O<sub>2</sub>:He=0.4:3.6:2:9. “Other” here refers to acetic acid, acetaldehyde and acetone.

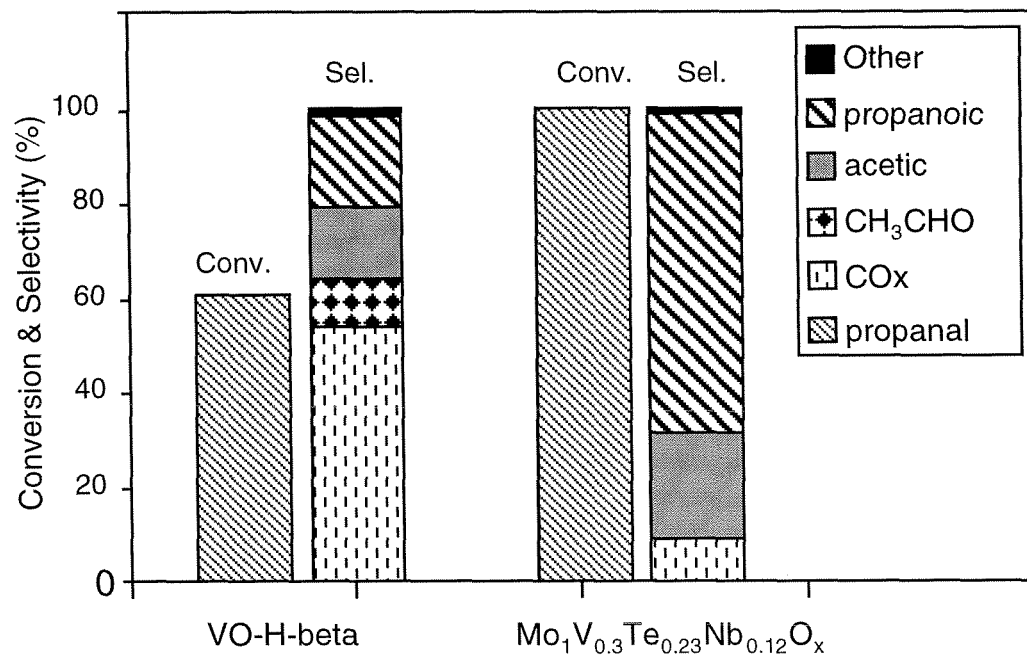


**Figure 4.7** Conversion and product distribution of propanal oxidation over VO-H-beta and Mo<sub>1</sub>V<sub>0.3</sub>Te<sub>0.23</sub>Nb<sub>0.12</sub>O<sub>x</sub> at 250°C and 2 s contact time with a molar feed gas ratio of propanal: O<sub>2</sub>:He=0.4:2:12.6.

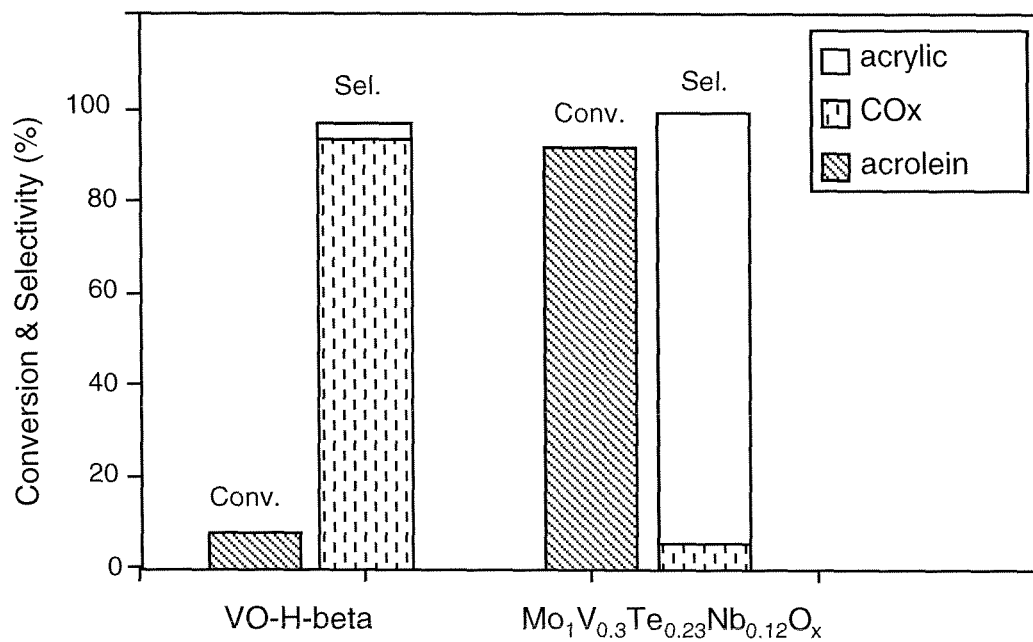


**Figure 4.8** Conversion and product distribution of acrolein oxidation over VO-H-beta and Mo<sub>1</sub>V<sub>0.3</sub>Te<sub>0.23</sub>Nb<sub>0.12</sub>O<sub>x</sub> at 250°C and 2 s contact time with a molar feed gas ratio of acrolein: O<sub>2</sub>:He=0.4:2:12.6. “Other” here refers to ethylene.

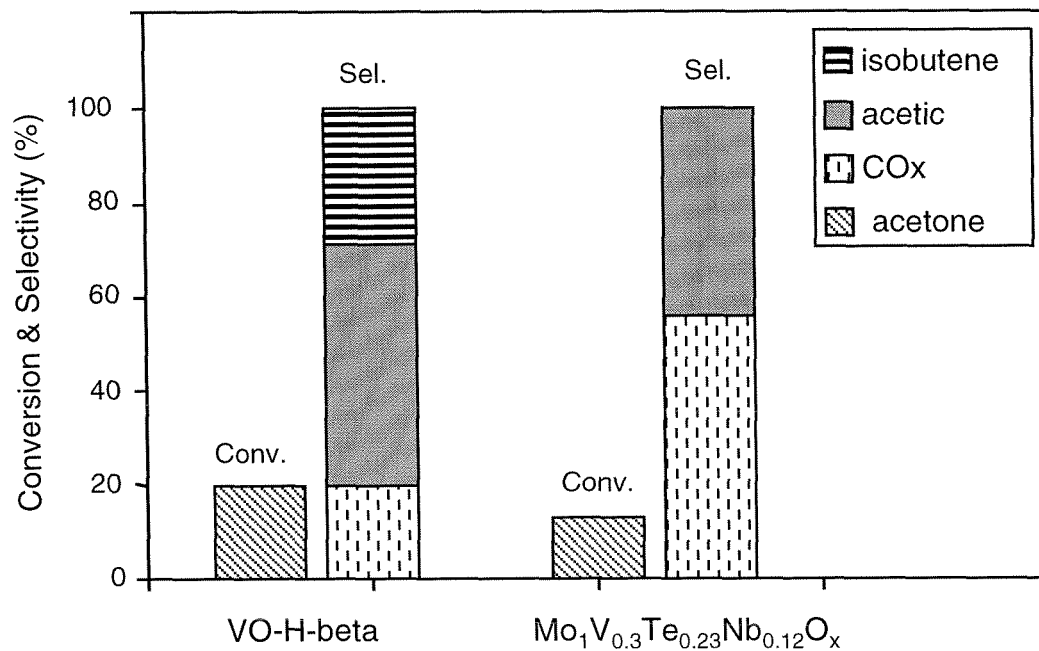
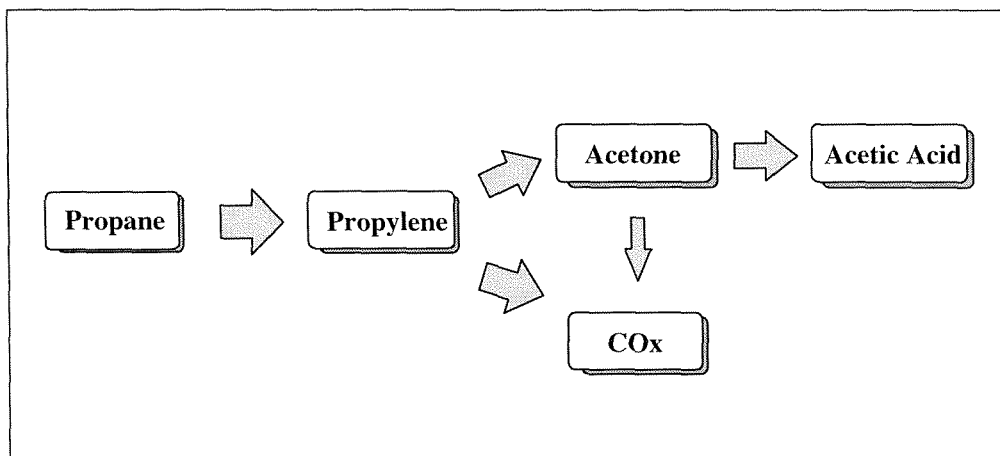
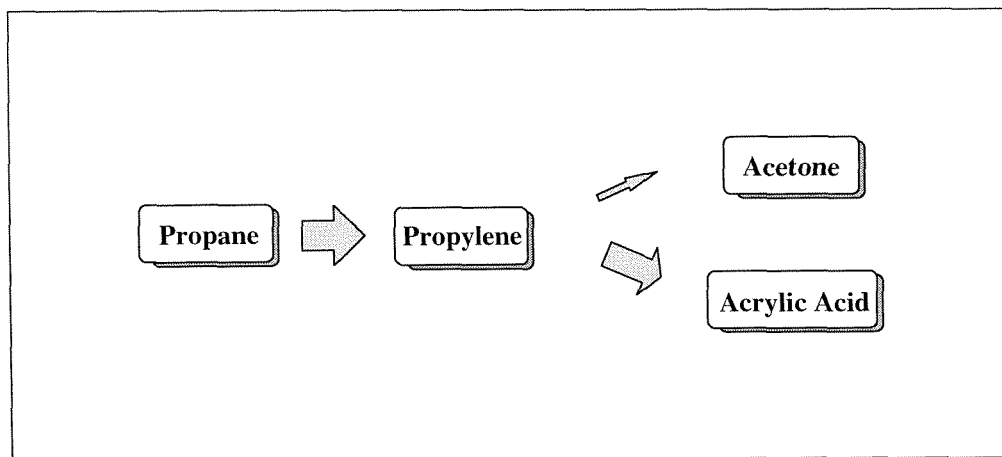


**Figure 4.9** Conversion and product distribution of acetone oxidation over VO-H-beta and Mo<sub>1</sub>V<sub>0.3</sub>Te<sub>0.23</sub>Nb<sub>0.12</sub>O<sub>x</sub> at 250°C and 2 s contact time with a molar feed gas ratio of acetone:H<sub>2</sub>O:O<sub>2</sub>:He=0.4:3.6:2:9.

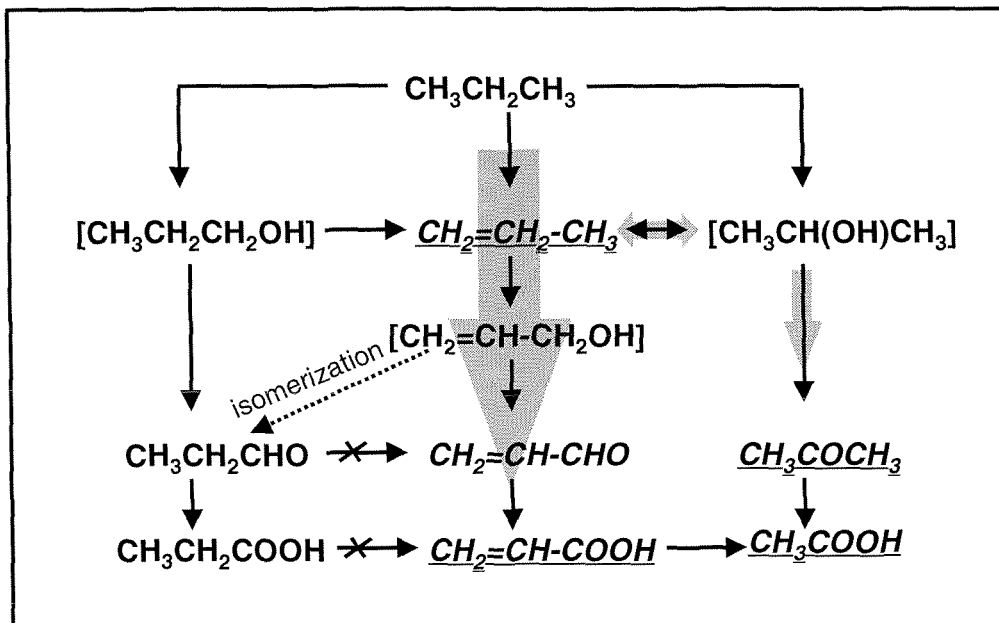


**Scheme 4.1** Main reaction pathways for propane oxidation over VO-H-beta.

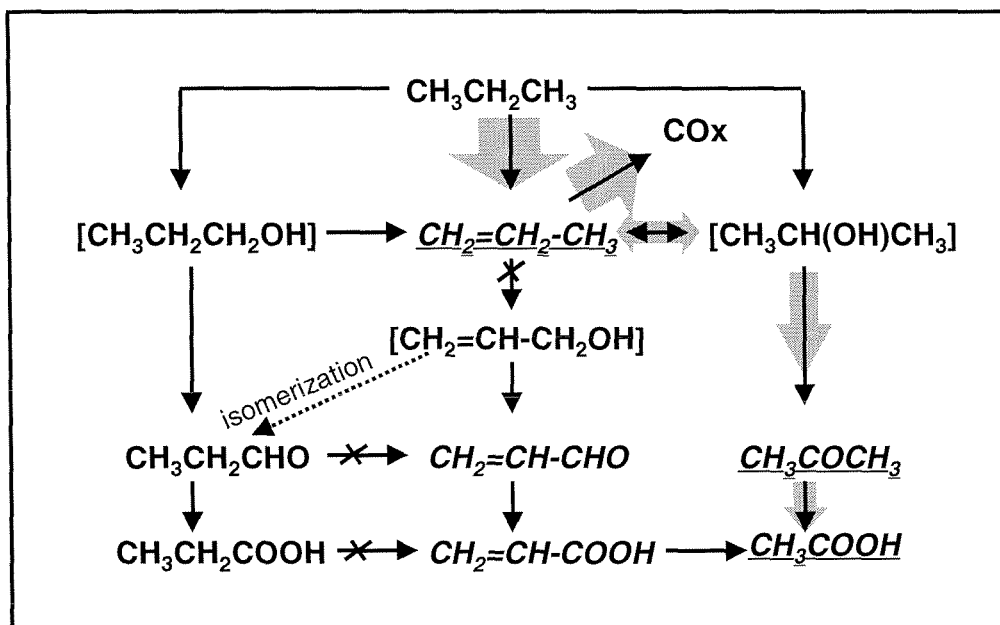


**Scheme 4.2** Main reaction pathway scheme for propane oxidation over  $\text{Mo}_1\text{V}_{0.3}\text{Te}_{0.23}\text{Nb}_{0.12}\text{O}_x$ .





**Scheme 4.4** Reaction network for propane oxidation over  $\text{Mo}_1\text{V}_{0.3}\text{Te}_{0.23}\text{Nb}_{0.12}\text{O}_x$ . Shaded arrow refers to main reaction pathway; compounds with underlines refer to the main products involved in propane and propylene oxidation reaction.



**Scheme 4.5** Reaction network for propane oxidation over VO-H-beta. Shaded arrow refers to main reaction pathway; compounds with underlines refer to the main products involved in propane and propylene oxidation reaction.

# **CHAPTER FIVE**

## **Summary**

Zeolite L was first chosen to be the support for vanadium oxide clusters because of its large pore system and small particle size. Metal oxide clusters are successfully formed inside zeolite L by an ion-exchange-hydrolysis method. The isolated metal atoms introduced to the zeolite charge-balancing sites agglomerate after hydrolysis and form larger occluded material inside zeolite pores. The resulting material does not show high activity for the partial oxidation of propane. As the hydrophilic framework of zeolite L that has high adsorption energies for the desired hydrophilic products could lead to their complete oxidation, I switched to a more hydrophobic framework, zeolite beta.

Metal oxide clusters inside zeolite beta are synthesized using ion-exchange-hydrolysis method. These catalysts show no significant catalytic activity improvements for propane oxidation over those obtained when using zeolite L. However, vanadyl ion-exchanged zeolite beta (VO-H-beta) is found to produce considerable amounts of acetic acid. This catalyst serves as a starting material for introducing a second metal by incipient wetness impregnation method. Most of the metals impregnated are located inside the zeolite pore system, and the interaction between different metals (V-Sb) has been observed by TPR. The effect of the second metal on propane oxidation is dependent on the loading. Addition of small amounts of the second metal (Mo or Sb) can increase the catalyst activity and propylene selectivity; however, when large amounts of the second metal are added, the catalyst activity decreases due to the blocking of access to some of the vanadium atoms.

Impregnation method is used to prepare catalysts to study the effects of acidity of the support on propane oxidation. The catalytic results show that acidity aids the formation of acetic acid, while basicity improves the formation of propylene. Catalysts

with basic supports require higher reduction temperatures, as indicated by TPR experiments.

Catalysts with vanadium inside the framework of zeolite beta are active for the oxidative dehydrogenation of propane. TPR shows no obvious difference in reducibility between catalysts with vanadium at framework or extraframework sites of the zeolite. The catalytic behavior of Vbeta (vanadium in the framework of zeolite beta) in propane oxidation is similar to that of vanadium impregnated Cs-beta (V/Cs-beta), however, different from that of vanadium impregnated H-beta (V/H-beta). These data suggest that the position of vanadium atoms is not as influential in propane oxidation as the acidity of the catalysts.

I have also studied catalysts with transition metals other than vanadium in the framework of zeolite beta. A combination of vanadium and titanium leads to the formation of small amounts of acrolein.

A hydrophobic framework is expected to help adsorption of propane and desorption of the desired hydrophilic products. As a consequence, a higher activity and higher selectivities to the desired products may be obtained. This idea is supported by the results from propane oxidation over pure-silica zeolite beta based catalysts with a highly hydrophobic framework. These catalysts are found to be much more active than the typical zeolite beta based catalyst. Thus, using highly hydrophobic matrix for partial oxidation could be a future direction for catalyst development.

Zeolite beta is not the only zeolite matrix active for propane oxidation, since vanadium impregnated SSZ-33 catalysts behave like the vanadium impregnated zeolite

beta catalysts. Acetic acid is found to be a general product for zeolite based catalysts with acidity.

By comparing metal oxide supported in zeolites with bulk metal oxides, metals supported in zeolites have lower reduction temperatures, mainly due to a better dispersion. The comparison of turnover frequency for propane oxidation of vanadium-containing zeolite beta catalysts and  $V_2O_5$  suggests that most of the zeolite-based catalysts are as active as  $V_2O_5$ .

As mentioned above, a considerable amount of acetic acid is produced with VO-H-beta during propane oxidation. It appeared that more valuable oxygenates, e.g., acrylic acid, may have been produced in the reaction and overoxidized to  $CO_x$ , since feeding acrylic acid into this reaction system at  $350^\circ C$  results in complete oxidation of the acid to  $CO_x$ . Motivated by these data, the reaction pathways for propane and propylene oxidation were investigated on this catalyst. For comparison, reaction pathways were also investigated for a "Mitsubishi" type catalyst,  $Mo_1V_{0.3}Te_{0.23}Nb_{0.12}O_x$ , one of the best catalysts for propane partial oxidation to acrylic acid. With VO-H-beta, propylene is the primary product of propane oxidation and acetic acid is a sequential oxidation product of the formed propylene possibly through an acetone intermediate.  $Mo_1V_{0.3}Te_{0.23}Nb_{0.12}O_x$  also gives propylene as the primary product of propane oxidation and the propylene thus formed oxidizes further to acrylic acid and acetone.

Based on the reactions of individual oxygenate compounds, the ability to perform allylic oxidation needs to be incorporated into the zeolite based catalysts. As observed from allylic oxidation of olefins, catalysts active for these reactions generally consist of multiple components. Therefore, a simple combination of V-Mo or V-Sb in bulk oxides

may not even possess good allylic oxidation capacity. A possible future direction for research in this area is to identify the phase in  $\text{Mo}_1\text{V}_{0.3}\text{Te}_{0.23}\text{Nb}_{0.12}\text{O}_x$  that provides for allylic oxidation and incorporate this composition into the zeolite.